SERDP

FINAL REPORT

3D Fuels: Hierarchically scaled datasets for three-dimensional wildland fuel characterization

Project lead: Susan J. Prichard, University of Washington (UW)
Federal PI: Adam Watts (current, USFS PNW) and Roger Ottmar (retired, USFS PNW)

Co-Is: Eric Rowell (Desert Research Institute), James Cronan (USFS PNW), Andy Hudak (USFS RMRS), Russ Parsons, USFS RMRS, Maureen Kennedy (UW), E. Louise Loudermilk (USFS SRS), Nicholas Skowronski (USFS NRS)

PhD students: Jonathan Batchelor and Gina Cova (UW), Michelle Bester (U West Virginia)

Analysis and data management: Ben Bright, Brian Drye, Paige Eagle, Deborah Nemens, Lauren Satterfield, and Jessie Thoreson

RC19-1064

August 2024

SERDP FINAL REPORT

Project: # RC19-1064

TABLE OF CONTENTS

Page

Executive Summary

Report

LIST OF TABLES

Page

ACRONYMS AND ABBREVIATIONS

2D – two dimensional
3D – three dimensional
ALS - Airborne laser scanning (LiDAR)
BD – Bulk density
BDMH – Bulk density of voxel fuels, estimated using the maximum height of fuels within the voxel frame
BDOV – Bulk density of voxel fuels, estimated using the occupied volume of voxel cells within the voxel frame
CW:H - crown width-to-height ratio
CFD – Computational fluid dynamics
Closing Gaps Project – RC20-1025 (PI Parsons): *Closing Gaps in Measurements and Understanding: Plume Characteristics, Live Fuel Moisture Dynamics, and Process-Based Modeling*
CWD – coarse woody debris (wood particles >7.6 cm in diameter)
DBH – tree stem diameter at breast height (cm)
DoD - Department of Defense
DoE – Department of Energy
FastFuels/QUIC-fire Project - RC23-7626 (PI Parsons): *FastFuels and QUIC-Fire: A Tool Suite Advancing DoD's Prescribed Fire Planning and Analysis Capabilities*
FCCS – Fuel Characteristics Classification System (https://www.fs.fed.us/pnw/fera/fft/fccsmodule.shtml)
FDS –Fire Dynamics Simulator (formerly WFDS – Wildland Urban Interface FDS)
FOFEM – First Order Fire Effects Model (https://www.firelab.org/project/fofem)
FIRETEC – An integrated set of computational fluid-dynamics and physics-based fire models' Full name: HIGHGRAD/FIRETEC
FWD – fine woody debris (wood particles < 7.6 cm in diameter)
FuelsCraft Project– ESTCP Project RC23-7779 (Prichard PI). *FuelsCraft: An Innovative Wildland Fuel Mapping Tool for Prescribed Fire Decision Support on Department of Defense Military Installations*
HPAD – horizontal projected area density (point cloud metric)
IFPL – Intrinsic fuel properties library (https://depts.washington.edu/fera/3dfuels/ifpl/)
LANL – Los Alamos National Laboratory (hosted two 3D fuels sites)
Lidar – Light detection and ranging
NRS – USFS Northern Research Station
Objects Project- RC-20-1346 (PI Hudak): *Object-Based Aggregation of Fuel Structures, Physics-Based Fire Behavior and Self-Organizing Smoke Plumes for Improved Fuel, Fire, and Smoke Management on Military Lands*
OV – occupied volume
PCM SA – point cloud metric surface area estimate
PCM Vol – point cloud metric volume estimate
PD – Particle density
PM2.5 – particulate matter < 2.5 microns
PNWRS – USFS Pacific Northwest Research Station
PS – phase shift TLS sensor (e.g., FARO unit)

PVC – polyvinyl chloride (piping)
QAQC – quality assurance and quality control
QSM – Quantitative structural modeling
RMRS – USFS Rocky Mountain Research Station
SE – Southeastern US
SfM – Structure for motion. A photogrammetric method that estimates 3D structure from sequences of 2D images
NRS – USFS Southern Research Station
STANDFIRE -
S:V – Surface-area-to-volume ratio
TLS – Terrestrial laser scanning (lidar)
TOF – time of flight TLS sensor (e.g., RIEGL unit)
TSF – time since fire
UAS – Unoccupied aerial systems
USFS – United States Forest Service
VPAD – vertical projected area density (point cloud metric)
WFSI – Wildland Fire Science Initiative (https://wfsi-data.org)

KEYWORDS

Computational fluid dynamics, fire behavior, longleaf pine, loblolly pine, ponderosa pine, prescribed fire, wildland fuels

ACKNOWLEDGEMENTS

This work was funded by the Department of Defense Strategic Environmental Research and Development Program through award RC19-1064. We thank the many host agencies for supporting our research sites, including the Center for Lands Management (Glacial Heritage and Tenalquot), Florida Forest Service (Blackwater and Tates Hell State Forests), Hitchiti Experimental Forest, Los Alamos National Laboratory (LANL Forest and Grassland), University of Montana (Lubrecht), Suwannee River Water Management District (Aucilla), US Department of Defense (Ft Stewart), US Forest Service (Osceola), Tall Timbers Research Station (Hannah Hammock), and Washington Department of Fish and Wildlife (Methow Wildlife Area). The Intrinsic Fuel Properties Library development was jointly funded by the Joint Fire Science Program (Project 20S013). Finally, we thank our field and laboratory crew members for their hard work and dedication, including Jessie Thoreson, Nick Tripodi, Lindsay Lascheck, Maddy Hallet, Teagan Darmody, Mason Patterson, Henry Gould, Kate Patronik, Grace Swan-Streepy, Jordan Hilton, Sophia Boyd, Jane Wynne, and Caitlyn Bell.

ABSTRACT

INTRODUCTION AND OBJECTIVES

The 3D Fuels project characterized the structure and composition of understory fuels common to prescribed burn programs within western US grasslands and pine-dominated forests of the southeastern and western US. Wildland fuels characterization is required for models of fire behavior and consumption, which are foundational for SERDP core fire science areas, including ecological fire effects, carbon accounting, smoke emissions and plume modeling. Traditional fuel characterization has been limited by 2D representations, including biomass, height and cover estimates per unit area. The objective of this study was to use a combination of airborne laser scanning (ALS), terrestrial laser scanning (TLS), and structure-from-motion photogrammetry (SfM) to create hierarchically scaled, 3D datasets of live and dead understory fuels to inform the scaled mapping of 3D fuels in forests that are commonly involved in prescribed burning programs. The overall goal of this project is to advance our understanding of 3D fuel characterization and provide evaluation datasets advance physics-based fire behavior, smoke and other fire effects models for operational use at scales relevant to Department of Defense (DoD) land managers.

TECHNICAL APPROACH

To inform models that parse 3D point cloud datasets and into segmented objects and metrics (e.g., height, cover, bulk density), we co-located intensively sampled 3D calibration plots across a total of 18 sites in the southeastern and western US (summarized on the 3D Fuels ArcGIS online site: https://arcg.is/1jTz9y0). We employed a hierarchical sampling design for mapping 3D surface and canopy fuels that relied on a combination of airborne and high-resolution TLS, SfM photogrammetry, and ground-based measures of physical fuel properties, including destructive sampling within a 3D grid (termed clip plot).

RESULTS

Deliverables include a hierarchically scaled, georeferenced dataset of remote sensing raw imagery, processed imagery, point cloud metrics, and field-based datasets of occupied volume, bulk density, height and fuel type. The datasets are documented with methods and geospatial locations to serve as a repository for machine learning and AI solutions for wildland fuel mapping and as inputs to computational fluid dynamics models of fire behavior and smoke. Several studies were conducted as part of the 3D Fuels project, including: 1) relationships between measured biomass and point cloud metrics developed from TLS and close range photogrammetry; 2) relationships between TLS reflectance and fuel moisture in common forest litter fuels, 3) quantitative structural modeling of common shrub species in southeastern pine forests, 4) relationships between forest floor properties and tree crowns, and 5) literature review and creation of an online intrinsic fuel properties library.

BENEFITS

The purpose of this study was to facilitate the production of 3D maps of surface and canopy fuels across a range of spatial scales and vegetation types that function as inputs for physics-based, coupled fire-atmosphere models and other models reliant on spatially explicit fuel characterization. The datasets will also serve as model training datasets for advanced modeling techniques to develop 3D maps of wildland fuels that can be used for prescribed fire operational mapping and fire behavior and smoke models. As such, the 3D Fuels dataset is now being used within the ESTCP-funded project RC23-7779, *FuelsCraft: An innovative wildland fuel mapping tool for prescribed fire decision support on Department of Defense military installations*.

EXECUTIVE SUMMARY

INTRODUCTION

The 3D Fuels project was designed to characterize the structure and composition of understory fuels common to prescribed burn programs within pine forests of the southeastern and western US and western grasslands. Traditional fuel characterization in these systems has been limited by 2D representations, including biomass, height and cover estimates per unit area. Over the past several decades, decision support tools for wildland fire management have shifted from models that primarily support wildfire suppression to those that support complex and highly interrelated objectives including prescribed burning, habitat restoration, smoke impacts, and carbon storage and sequestration. Operational models that were developed to support predictions of wildland fire spread and intensity of flaming fire fronts are not equipped to inform predictions of integrated fire behavior and effects, including fire-vegetation feedbacks, fire-atmosphere interactions, smoke, and impacts to wildlife habitat.

The objective of this study was to create hierarchically scaled datasets of live and dead understory fuels to inform the scaled mapping of 3D fuels across open forest types that are commonly involved in prescribed burning programs. As advancements are made to process-based computational fluid dynamics models of fire behavior and atmospheric interactions, wildland fuel complexes are recognized not only for their total fuel available for combustion but also for their structure and composition that influences fine- to coarse-scale wildland fire dynamics. Because prescribed burning operations are often conducted under prescription windows that minimize fire escapes and hazardous air impacts, they generally burn under mild weather conditions and contribute to low intensity understory fires. Within these fire environments, the composition and 3D structure of understory fuels – and gaps between them - strongly dictates the spread, intensity and duration of surface fires. Individual fuel elements such as tree boles, shrubs, and coarse wood can all act as barriers to fire flow with marked influence on fire and wind flow through prescribed burn units.

In this study, we evaluated methods to characterize forest understory and western grassland fuels as 3D complexes of live and dead vegetation, including organic soil (duff), litter, fine and coarse wood, grasses and shrubs. To inform models that parse 3D point cloud datasets into segmented objects and metrics (e.g., height, cover, bulk density), we co-located intensively sampled 3D calibration plots across a total of 18 sites in the southeastern and western US. Deliverables from this study include a hierarchically scaled, georeferenced dataset of remote sensing raw imagery, processed imagery, point cloud metrics, and field-based datasets of occupied volume, bulk density, height and fuel type.

OBJECTIVES

The goal of this project was to advance our understanding of 3D fuel characterization and provide evaluation datasets that advance physics-based fire behavior, smoke and other fire effects models for operational use at scales relevant to Department of Defense (DoD) land managers. In recognition of fire as an essential management tool on DoD installations, the 2014 DoD Fire Science Strategy (US Department of Defense 2014) prioritized research in core areas including fire behavior, ecological effects of fire, carbon accounting, emissions characterization, and fire plume dispersion. Wildland fuel characterization is therefore not only foundational for fire behavior and effects modeling but has cascading impacts on all SERDP core fire science areas. As such, a detailed understanding of 3D fuel structure and temporal dynamics is vital to advance these lines of research.

Current operational modeling systems such as Behave and Farsite require assignments of surface fire behavior fuel models that are used in Rothermel's (1972) surface fire spread model to calculate rate of spread and flame length. While convenient, fuel models fail to capture wildland fuel heterogeneity. To integrate fire behavior and effects predictions, a revised approach was developed called the Fuel Characteristic Classification System (FCCS, Ottmar et al. 2007). The FCCS accounts for all fuels with potential to burn, represents the geographic and structural diversity of wildland fuels, and provides a reference library of fuelbeds throughout the United States. These approaches provide generalized outputs useful for managers, but improvements are needed to advance fuel characterization to support physics-based fire and fuel consumption models for prescribed fire planning and implementation.

Over the past decade, the SERDP and ESTCP programs have supported a set of innovative and interrelated projects to advance fire science and related fields of fuel hazard carbon accounting and air pollution (**Figure E1**). With an objective to inform vegetation and fuels characterization for process-based fire behavior and effects modeling, the 3D Fuels project was developed and conducted in close collaborations with a number of SERDP and ESCTP-funded projects. Specifically, 3D fuels was designed to facilitate common definitions, methods, and data sharing with three SERDP-funded projects, including Objects (RC-20-1346 *Object-Based Aggregation of Fuel Structures, Physics-Based Fire Behavior and Self-Organizing Smoke Plumes for Improved Fuel, Fire, and Smoke Management on Military Lands*), Closing Gaps (RC20-1025 *Closing Gaps in Measurements and Understanding: Plume Characteristics, Live Fuel Moisture Dynamics, and Process-Based Modeling*), and RC19-1192 (*Characterizing Multiscale Feedbacks between Forest Structure, Fire Behavior and Effects: Integrating Measurements and Mechanistic Modeling for Improved Understanding of Pattern and Process*). Specifically, some 3D fuels sites are shared with the Objects project, and we collected field data to actively share with the Objects project to inform object-based mapping of fuel loads for smoke modeling. Similarly, the 3D fuels project was designed to lead to the active development of FuelsCraft (ESTCP Project RC23-7779 *FuelsCraft: An Innovative Wildland Fuel Mapping Tool for Prescribed Fire Decision Support on Department of Defense Military Installations*) and active collaborations with Russ Parsons and team on their Closing Gaps project and ESTCP-funded work on FastFuels (RC23-7626 *FastFuels and QUIC-Fire: A Tool Suite Advancing DoD's Prescribed Fire Planning and Analysis Capabilities*).

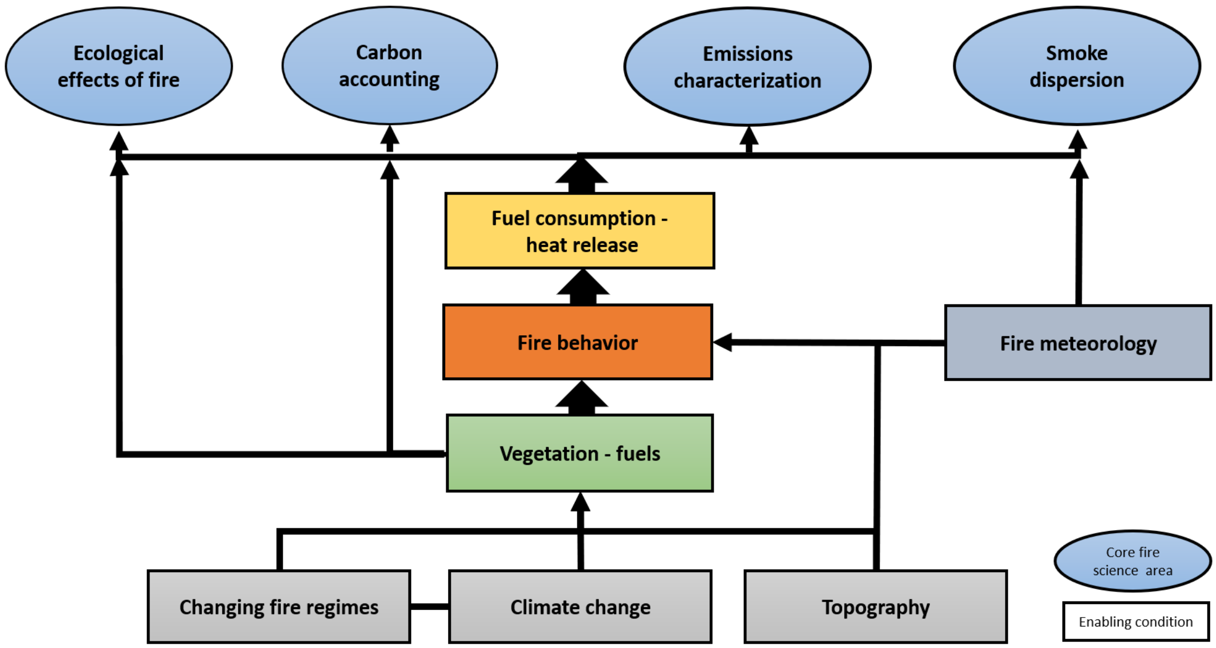

Figure E1: Core fire science areas outlined by the SERDP Fire Science Strategy (US Department of Defense 2014).

TECHNOLOGY APPROACH

We employed a hierarchical sampling design for mapping 3D surface and canopy fuels that relied on a combination of airborne and high-resolution TLS, SfM, and ground-based measures of physical fuel properties, including destructive sampling within a 3D grid (termed clip plot). The purpose of this sampling design was to facilitate the production of 3D maps of surface and canopy fuels across a range of spatial scales and vegetation types that function as inputs for physics-based, coupled fire-atmosphere models and other next-generation models reliant on spatially explicit fuels. The datasets also facilitated the use of advanced mathematical modeling techniques to develop quantitative models that assign measured properties of fuels, and in the case of highly intermixed fuels (e.g., complex arrangements of surface fuels including shrubs, herbaceous fuels and intermixed live and dead fuel), develop 3D models of functional plant groups to inform mapping assignments.

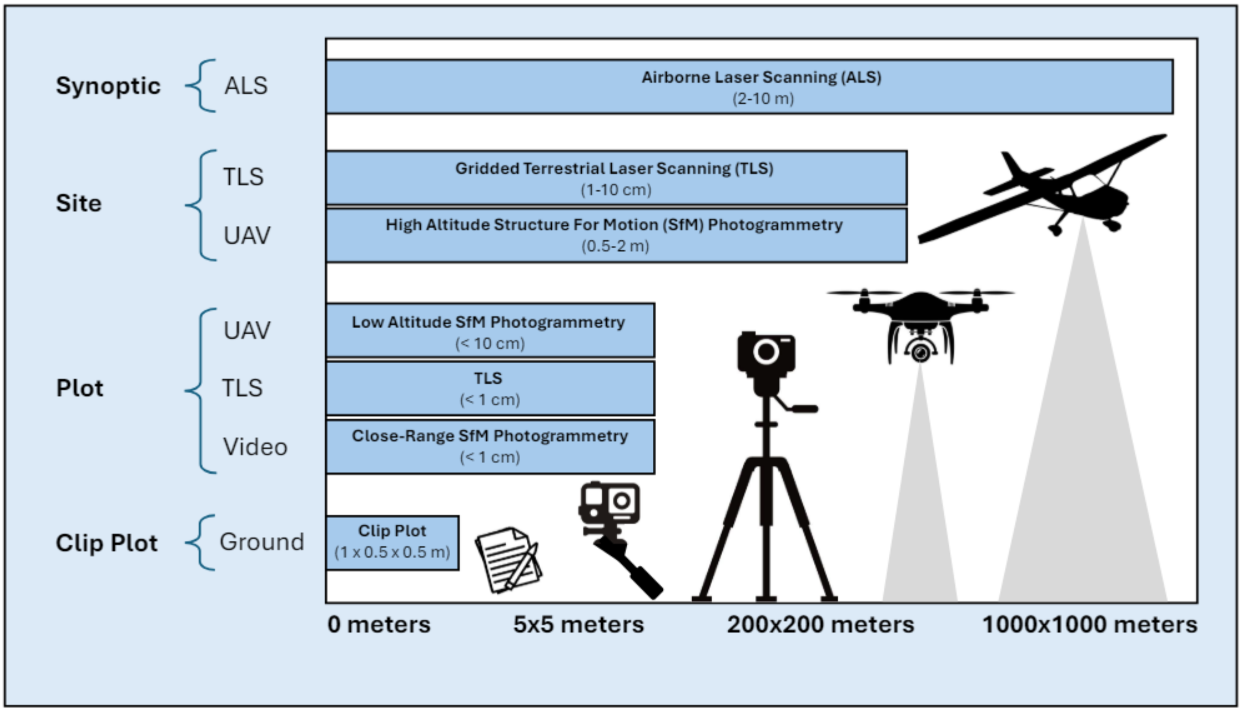

Figure E2. Hierarchical sampling design of the 3D Fuels project.

In addition to development of the 3D Fuels data repository, several studies were conducted as part of the project, including:

1) Predictive models of surface fuel biomass from TLS and close-range photogrammetry point cloud metrics;
2) Modeled relationships between forest floor properties and tree crowns;
3) Creation of an online intrinsic fuel properties library;
4) Evaluation of relationships between TLS reflectance and fuel moisture in common forest litter fuels; and
5) Quantitative structural modeling of common shrub species in southeastern pine forests.

RESULTS AND DISCUSSION

1. 3D Fuels data repository

The 3D Fuels project was designed to characterize the structure and composition of understory fuels common to prescribed burn programs within pine forests of the southeastern and western US. Traditional fuel characterization in these systems has been limited by 2D representations, including biomass, height and cover estimates per unit area. The objective of this study was to use a combination ALS, TLS, and SfM photogrammetry to create hierarchically scaled, 3D datasets of live and dead understory fuels to inform the scaled mapping of 3D fuels across open forest types that are commonly involved in prescribed burning programs. Forest understory fuels in this study are complexes of live and dead vegetation and were often characterized as fuel types, including organic soil (duff), litter, fine and coarse wood, grasses and shrubs. To inform models that parse 3D point cloud datasets and into segmented objects and metrics (e.g., height, cover, bulk density), we co-located intensively sampled 3D calibration plots across a total of 18 sites in the southeastern and western US. Deliverables from this study include a hierarchically scaled, georeferenced dataset of remote sensing raw imagery, processed imagery, point cloud metrics, and field-based datasets of occupied volume, bulk density, height and fuel type. All datasets and associated metadata that are being uploaded to the Wildland Fire Science Initiative (WFSI) data portal (https://wfsi-data.org).

2. Predictive models of biomass based on TLS and photogrammetry point cloud metrics

With recent developments in remote sensing technologies, including high-resolution terrestrial lidar scanning and close-range SfM photogrammetry, opportunities to characterize the 3D structure and composition of understory fuels are increasing. The field of understory characterization is still in its early stages, and methods for imagery collection and calibration for field development are still being tested. In this study, we evaluated predictive models of surface fuel biomass based on TLS- and photogrammetry point-cloud metrics. To our knowledge, this study represents the largest sample of image-based point clouds analyzed for understory fuel characterization, and the only study to evaluate predictive ability across different forest types. In addition to TLS scanning, we presented a novel, video-based approach for rapid data collection that demonstrates potential across multiple domains, and presented a suite of metrics that can be used to summarize point cloud models. Application of this technique has the potential to provide managers with an accessible option for inexpensive data collection and can lay the groundwork for rapid collection of input datasets to train landscape-scale fuel models.

Videos collected from a handheld GoPro camera produced SfM point clouds with reliable representations of fuel height and structure across our sites that had comparable performance with TLS (**Figure E3**). While previous studies that have assessed the applications of close-range SfM have largely relied on individually collected photographs to create point clouds (Bright et al., 2016; Piermattei et al., 2019; Wallace et al., 2022), the method presented here offers an efficient, affordable way to collect data with a single video taken in just under two minutes per plot. In this study, we used a combination of Python scripts and processing workflows in the commercial software Agisoft Metashape to produce point clouds for each sampling plot; this constituted a semi-automated approach that required manual input to define point cloud reference points and spatial scale. For wider adoption of this method, more automated approaches will be required. Rapid advances in machine learning and AI are catalyzing innovations in object detection and mapping from imagery, and we anticipate that the 3D fuels dataset will provide invaluable training data for these advancements. As the datasets are available for analysis in a cloud-hosted open-source code library, automated processing of videos to point clouds and ingestion-to-analysis workflows that provide a large library of outputs can be embedded into deep learning networks to improve coarser scale fuel mapping.

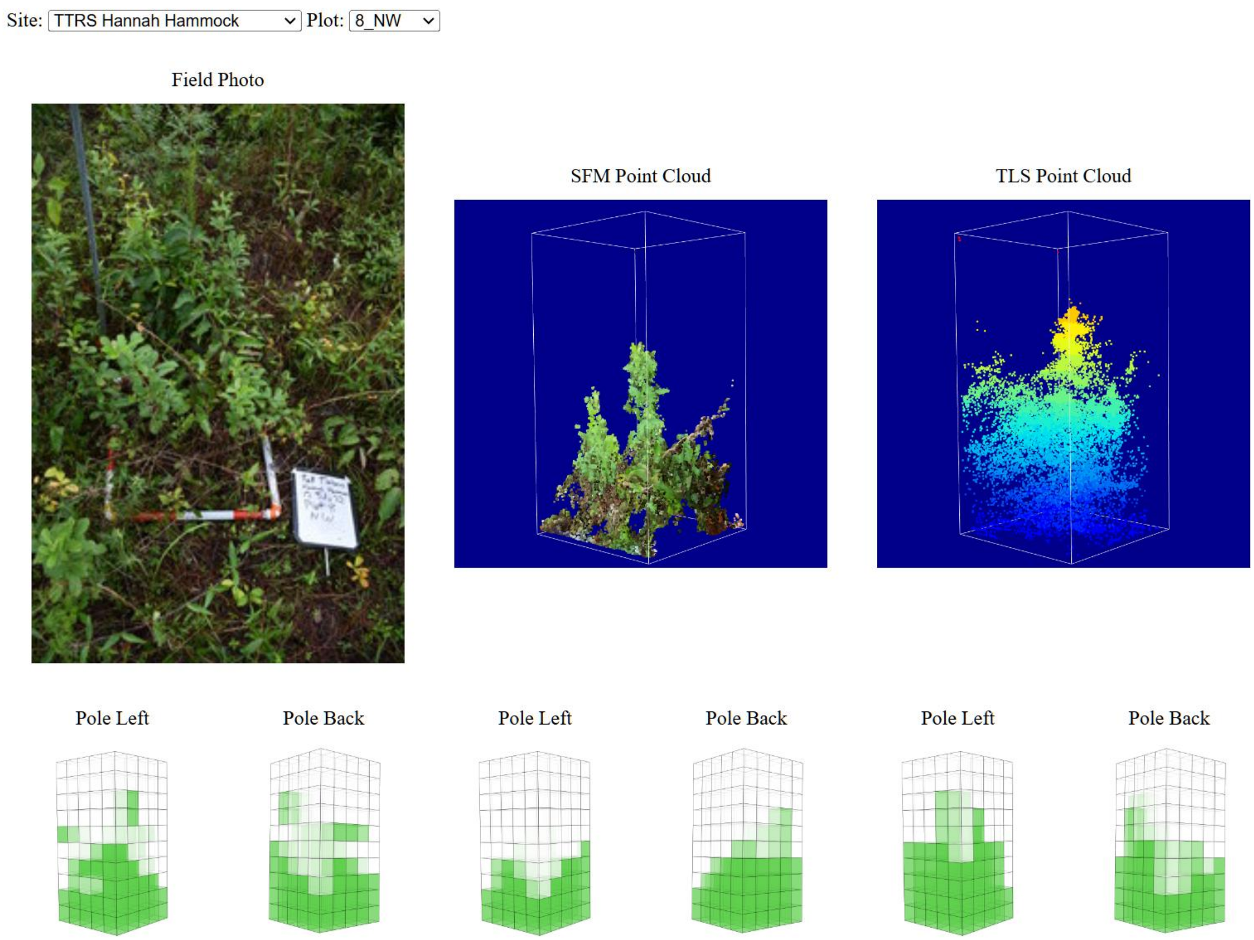

Figure E3. Sample comparison of TLS and SfM point clouds, comparing plot photo, point cloud visualizations, and voxelized imagery representing each clip plot.

3. Relationship of forest floor bulk density to tree crowns

As part of our larger effort to characterize the 3D structure and biomass of forest types common to prescribed burning programs in the southeastern and western US, study sites included southeastern pine flatwoods, loblolly-sweetgum plantations, and western ponderosa pine and mixed conifer forests. Our main objective was to evaluate if tree crowns, in combination with other site variables such as forest type and time since disturbance, can be used to inform local predictions of forest floor cover, depth and biomass. Within the three main forest types sampled in this study, we evaluated how forest floor layers vary across bole, inside tree crown drip line, and outside drip line positions. As anticipated, we found that litter and duff depth, biomass and bulk density were highly variable within and between sites with high reported standard deviations. Even with high reported variability, there were strong statistical differences across transect positions.

The SE flatwood and western pine sites both contained much greater accumulations of litter and duff next to tree boles than the inside drip line and outside drip line positions. In contrast, litter depth and biomass were not significantly different across transect positions in SE loblolly-sweetgum sites. The presence of the broadleaf deciduous tree, sweetgum, throughout loblolly pine understories likely distributed more uniform leaf litter across the sites and contributed to more even distributions of litter depth and biomass. However, accumulated duff layers were significantly greater next to tree boles than inside and outside transect positions in loblolly sweetgum forests.

4. Intrinsic fuel properties library

The objective of creating the Intrinsic Fuel Properties Library (IFPL) was to provide a central repository of fuel properties that can be used to refine fuel characterization for wildland fire behavior modeling (**Figure E4**; https://depts.washington.edu/fera/3dfuels/ifpl/). Computational fluid dynamics models of fire behavior rely on three-dimensional grids of wildland fuel structure, composition and properties. In this task, we compiled literature and created an online database that is the first of its kind. The IFPL currently supports values specific to North America but was designed to be expandable.

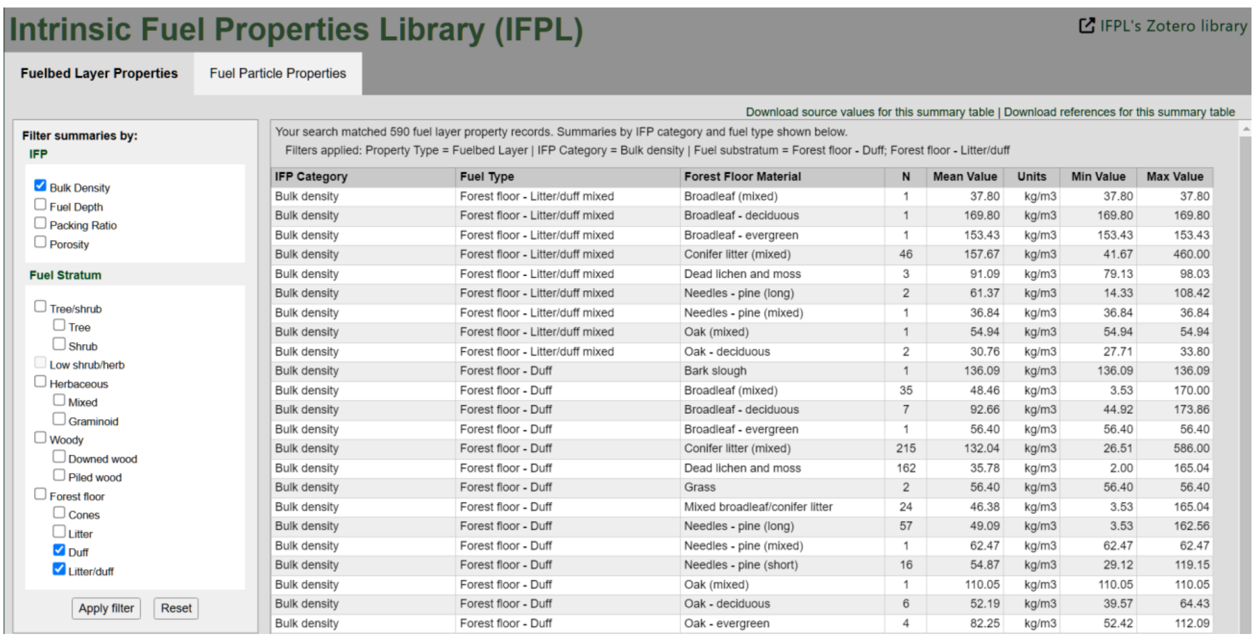

IFP Category	Fuel Type	Forest Floor Material	N	Mean Value	Units	Min Value	Max Value
Bulk density	Forest floor - Litter/duff mixed	Broadleaf (mixed)	1	37.80	kg/m3	37.80	37.80
Bulk density	Forest floor - Litter/duff mixed	Broadleaf - deciduous	1	169.80	kg/m3	169.80	169.80
Bulk density	Forest floor - Litter/duff mixed	Broadleaf - evergreen	1	153.43	kg/m3	153.43	153.43
Bulk density	Forest floor - Litter/duff mixed	Conifer litter (mixed)	46	157.67	kg/m3	41.67	460.00
Bulk density	Forest floor - Litter/duff mixed	Dead lichen and moss	3	91.09	kg/m3	79.13	98.03
Bulk density	Forest floor - Litter/duff mixed	Needles - pine (long)	2	61.37	kg/m3	14.33	108.42
Bulk density	Forest floor - Litter/duff mixed	Needles - pine (mixed)	1	36.84	kg/m3	36.84	36.84
Bulk density	Forest floor - Litter/duff mixed	Oak (mixed)	1	54.94	kg/m3	54.94	54.94
Bulk density	Forest floor - Litter/duff mixed	Oak - deciduous	2	30.76	kg/m3	27.71	33.80
Bulk density	Forest floor - Duff	Bark slough	1	136.09	kg/m3	136.09	136.09
Bulk density	Forest floor - Duff	Broadleaf (mixed)	35	48.46	kg/m3	3.53	170.00
Bulk density	Forest floor - Duff	Broadleaf - deciduous	7	92.66	kg/m3	44.92	173.86
Bulk density	Forest floor - Duff	Broadleaf - evergreen	1	56.40	kg/m3	56.40	56.40
Bulk density	Forest floor - Duff	Conifer litter (mixed)	215	132.04	kg/m3	26.51	586.00
Bulk density	Forest floor - Duff	Dead lichen and moss	162	35.78	kg/m3	2.00	165.04
Bulk density	Forest floor - Duff	Grass	2	56.40	kg/m3	56.40	56.40
Bulk density	Forest floor - Duff	Mixed broadleaf/conifer litter	24	46.38	kg/m3	3.53	165.04
Bulk density	Forest floor - Duff	Needles - pine (long)	57	49.09	kg/m3	3.53	162.56
Bulk density	Forest floor - Duff	Needles - pine (mixed)	1	62.47	kg/m3	62.47	62.47
Bulk density	Forest floor - Duff	Needles - pine (short)	16	54.87	kg/m3	29.12	119.15
Bulk density	Forest floor - Duff	Oak (mixed)	1	110.05	kg/m3	110.05	110.05
Bulk density	Forest floor - Duff	Oak - deciduous	6	52.19	kg/m3	39.57	64.43
Bulk density	Forest floor - Duff	Oak - evergreen	4	82.25	kg/m3	52.42	112.09

Figure E4. Fuelbed layer properties available within the IFPL, showing summary data for published bulk density value for litter and duff by fuel type and forest floor material.

5. Quantitative structural models of common southeastern US shrubs

Accurate characterization of shrub architecture is important for understanding how architectural traits affect ecosystem dynamics and processes. In this study, we investigated the accuracy of shrub architectural traits derived from quantitative structure models (QSMs), developed using TLS data. We used TreeQSM to model the shrub architecture of ten architecturally different shrubs at two-point cloud density levels (**Figure E5**). As a reference, we manually measured the shrub's architectural parameters and compared them to the QSM-derived parameters. The QSMs derived from both the low-density point clouds (QSM_L), and the high-density point clouds (QSM_H), showed a high agreement with reference shrub height measurements, with R^2 values of 0.98 and 0.99, respectively. QSM_H correctly modeled an average of 80% of branches, while QSM_L correctly modeled 56% of the branches. The accuracy of the models was similar across growth forms, but was strongly affected by architectural complexity and branch diameter size. The results of this study illustrate the potential of non-destructive lidar approaches for quantifying shrub architectural traits.

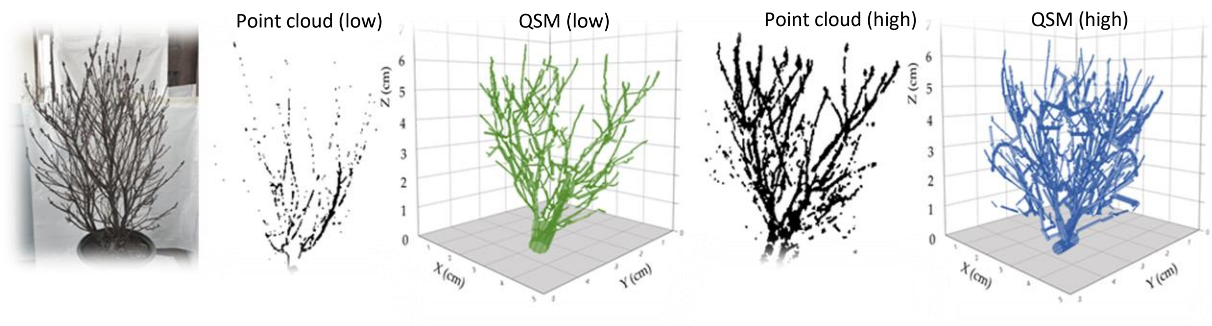

Figure E5: Example of a shrub with complex architecture, represented by a low density and high density point cloud.

6. TLS-based fuel moisture

Electromagnetic radiation at 1550 nm is highly absorbed by water and offers a novel way to collect fuel moisture data, along with 3D structure of wildland fuels/vegetation, using lidar. Two terrestrial laser scanning (TLS) units, representing a phase shift scanner (FARO s350) and time of flight (RIEGL vz-2000) scanner were assessed in a series of laboratory experiments to determine if lidar can be used to estimate moisture content of dead forest litter. Samples consisted of two control materials where angle and position could be manipulated (pine boards and cheesecloth), and four single-species forest litter types (Douglas-fir needles, ponderosa pine needles, longleaf pine needles, and southern red oak leaves). Sixteen sample trays of each material were soaked overnight, then allowed to air dry with scanning taking place at 1-hr, 2-hr, 4-hr, 8-hr, 12-hr and then in 12-hr increments until sample moisture reached ambient relative humidity. Samples were then oven dried for final scanning and weighing.

Spectral reflectance values of each material were also recorded over the same drying intervals using a field spectrometer. There was a strong correlation between the spectral reflectance at 1550 nm measured by the spectrometer, and the moisture content of all samples. There was also a strong correlation between the spectrometer measurements and the intensity of laser pulse returns measured by both the phase shift and time of flight lidar units. At fuel moisture contents greater than 100% moisture content, the correlation between the pulse intensity values recorded by both scanners and fuel moisture content was strongest. The relationship deteriorated with distance, with the TOF scanner maintaining a stronger relationship at distance than the PS scanner. Our results demonstrate that lidar can be used to detect and quantify fuel moisture across a range of forest litter types. Based on our findings, lidar may be used to quantify fuel moisture levels in near real time and could be used to create spatial maps of wildland fuel moisture content.

IMPLICATIONS FOR FUTURE RESEARCH AND BENEFITS

A synthesis of this project's contributions to science and management applications is provided in **Table 1**. Wildland fuel characterization is critical for prescribed burn support as it estimates the amount of live and dead biomass available for consumption and smoke production. To date, DoD managers have mostly relied on 2D raster maps of biomass for prescribed fire decision support tools including fire behavior modeling platforms such as FlamMap or FARSITE and smoke models such as BlueSky and Vsmoke (Prichard et al. 2019b). Pixel-based biomass values are typically assigned based on major vegetation types and recent history including forest management activities (i.e., timber harvest) or disturbances (i.e., fire) (https://www.landfire.gov/disturbance.php). To transition to more realistic representations of fuels, modeled relationships are needed between remotely sensed datasets such as lidar and SfM photogrammetry and the actual 3D structure and composition of wildland fuels (Calders et al. 2018, Silva et al. 2021, Cova et al. 2023).

Because prescribed burning programs cover large geographic areas and are challenging to fully represent through synoptic imagery, land managers will continue to rely on modeled relationships between remotely sensed imagery, disturbance history, and wildland fuels. The 3D Fuels library will offer invaluable datasets for the development of predictive models of common understory fuelbeds in southeastern and western pine-dominated forests. Recent advances in remote sensing and artificial intelligence (AI) offer innovative ways to better predict the composition and amount of wildland fuels in 3D. Computational fluid dynamics models of wildland fire behavior and smoke, including QUIC-fire/FIRETEC and WFDS, require 3D gridded fuel layers. One of the most promising approaches to generate gridded, 3D inputs to these models is through the use of AI for synthetic fuelbed development.

In the recently funded ESTCP technology demonstration, FuelsCraft, we are using the geospatially coordinated field and remotely sensed wildland fuel datasets of the 3D Fuels project, AI, and 3D visualization software, to generate synthetic fuelbed inputs to CFD models via FastFuels, that represent wildland fuels common to prescribed burning programs within DoD installations of the SE US. Within FuelsCraft synthetic fuels will be generated to model physical traits of individual fuel particles (e.g., needles, leaves, or branches) based on fitted distributions of these fuels built with site-specific measures of height, cover, bulk density, and spatial patterns. By assigning mesh and physical characteristics of the synthetic fuel objects, informed by empirical distributions of wildland fuels, fuel properties such as bulk density and surface area-to-volume ratio can be estimated at a particle or object scale, with improved accuracy over remote sensing alone (Prichard et al. 2022). Synthetic fuelbeds that include realistic understory and canopy fuels have the potential to supply physical models of wildland fuels that are both highly realistic and dynamic based on site-specific customization (Parsons et al. 2011, Pimont et al. 2016, Rowell et al 2016).

Table E1. Summary of project tasks, knowledge gained, applications and implications for future research and applications.

Project activity	Knowledge gained	Application	Future utility
3D fuels sampling	Generate a one of a kind comprehensive 3D Fuels field data repository	Multi-scale 3D distributions within frequently burned pine forests and grasslands of the SE and western US	Applicable to Machine Learning network models as highest quality labels
Intrinsic fuels properties library (IFPL)	Produce a first of its kind fuels library of critical fuels properties	With over 8,000 records, the database provides key parameters to CFD modelers	A key resource for Machine Learning estimates of parameters across landscapes
Hierarchical sampling	Integrate fine-scale fuels measurements to estimate unit and landscape characteristics and values	Provides improved surface fuels estimates for prescribed fire managers and CFD fire behavior modelers	Increased sample sizes across landscapes improve surface fuels for LANDFIRE and FastFuels
Terrestrial laser scanning (TLS)	Test a range of metrics to characterize surface and shrub fuels at a range of spatial scales	Generate a lattice of multi-scale fuels for improving characterization of DoD prescribed fire units	Serves as the lattice to ingest initial information for fuels simulations in FuelsCraft
Airborne laser scanning (ALS) and UAS-based photogrammetry	The integration lattice for all fine-scale data to larger landscape scales	Produces broad scale fuels maps that are critical capturing the current state of fire managed landscapes	Simulate changes of landscape fuels in tandem with prescribed fire prioritization tools
Data quality assurance	Disparate modes of data collection are difficult to compare without an extensive QA/QC process	A robust assessment and assurance for integrating complex data collections into useable and defensible products	Strong replicability of the methods through development of a standard automated approach
Quantitative structural modeling	Shrub and tree objects with internal architecture can be extracted from 3D point clouds	Libraries of these objects can be generated to represent mean traits and variation in patterns to represent features across landscapes	Tree and shrub libraries can be ported into developing digital twin and simulation platforms to improve estimates of lacunarity, bulk density,
Close range photogrammetry	Low-cost photo-based data collection exceeds expected performance over gold standard methods using TLS	Surrogate of TLS data sources for fuels characterization that also includes high resolution RGB data for fuel typing	Optimal mode of data collection to crowd source and improve CONUS scale fuels for FIA and LANDFIRE
TLS fuel moisture	Reflectance of NIR TLS data produces rational relationships with a gradient of fuel moistures	Laboratory based and controlled environments across ranges of fuel types build a library of relationships	Repeated scans in a prescribed fire setting can be used to build dynamic fuel moisture estimates for models
Tree objects and fuels	Trajectories of litter and duff amounts dependent on position related to tree objects.	Test the distributions of fuels as a function of overstory tree objects for implementation with TLS tree maps and objects	Integrate the relationships with tree objects to tie to simulations of litter and fine fuels deposition and accumulation

1.0 OBJECTIVES

The purpose of the 3D Fuels project was to advance our understanding of 3D fuel characterization and provide evaluation datasets advance physics-based fire behavior, smoke and other fire effects models for operational use at scales relevant to Department of Defense (DoD) land managers. The primary objective of this study was to use a combination of ALS, TLS, and SfM photogrammetry to create hierarchically scaled, 3D datasets of live and dead understory fuels to inform the scaled mapping of 3D fuels across open forest types that are commonly involved in prescribed burning programs.

This study used a hierarchical sampling approach to characterizing understory fuels in pine forests of the southeastern and western US. The forested sites are similar in structure with open forest canopies dominated by mature trees and fire-maintained forest understories. However, climate, productivity and the composition of vegetation markedly differ between southeastern and western sites and offer a way to evaluate how our sampling methods and fuel characterization can be used to characterize understory fuels across a range of fuel complexes from sites dominated by timber litter, grass to shrub fuels. Specifically, the southeastern sites are located within mesic flatwoods with a subtropical climate and high site productivity and shrub composition compared to western ponderosa pine sites with a semiarid climate and lower site productivity with a greater composition of timber-litter and grass fuel complexes.

Our study was guided by the following research questions:

1. What are the appropriate sampling resolutions of wildland fuels to model fire behavior and consumption, ranging from full physics-based modeling applications to operational models of fire behavior and consumption?
2. What are the critical fuelbeds and physical fuel properties required to advance physics-based fire behavior, smoke, and fire effects models for operational use on DoD installations? Specifically, is fine-scale heterogeneity in surface fuels critical to mapping and quantifying fuel consumption in sites commonly burned on DoD lands?
3. How can we most efficiently and accurately create gridded, 3D maps of surface fuel properties based on the integration of remotely sensed imagery and fuel properties informed from field-based and laboratory measurements?
4. What are the tradeoffs between input precision, model fidelity, and time to collect and integrate 3D datasets?

2.0 BACKGROUND

Models of wildland fire behavior and effects are widely used to plan and conduct prescribed fires and to inform wildland fire management decisions on unplanned or unintentional wildfires (Furman et al. 2018, Hiers et al. 2020). As highlighted by the SERDP Fire Science Strategy (2014), wildland fuel characterization is foundational to fire behavior, consumption, and smoke modeling with cascading impacts to post-fire vegetation dynamics, carbon, and air quality (**Figure 1**). While all operational fire behavior and effects models require inputs on wildland fuel characteristics, the detail and resolution at which fuels are represented have been typically generalized and coarse scale in nature (Hiers et al. 2009). Vegetation and fuels are difficult to quantify spatially, limited by the intensive ground sampling protocols and traditional remote sensing methods that often struggle to characterize key elements as litter depth or three-dimensional organization of fuel mass (Brown and Bevins 1986; Falk *et al.* 2007).

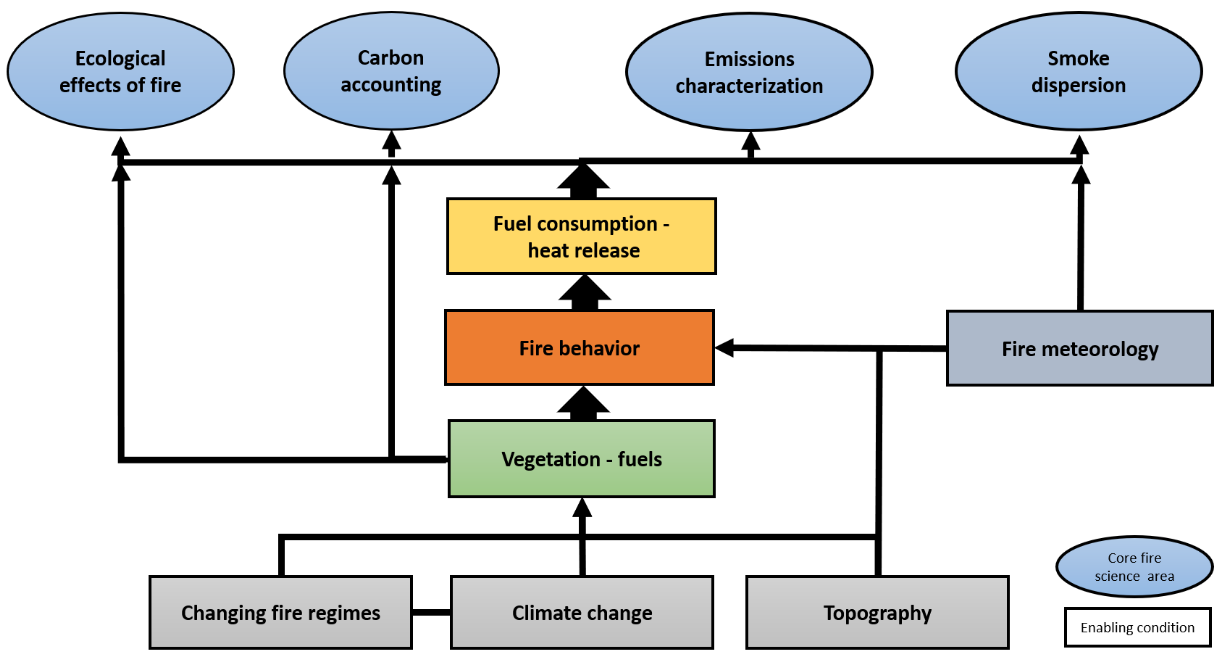

Figure 1: **Core fire science areas outlined by the SERDP Fire Science Strategy (US Department of Defense 2014).**

Operational models (e.g., Behave+, FSPro) in use today by wildland fire managers employ coarse two-dimensional (2D) resolution or simplified point estimates of fuels that enable rapid landscape assessments but do so at the expense of fine-scale spatial detail and mechanistic understanding (Dickman et al. 2022). The Rothermel surface fire spread model (Rothermel,1972) and operationalization of FARSITE and Fire Family Plus modeling frameworks leverage simplified fuels to give generalized rates and direction of spread (Sandberg et al. 2007, Finney et al. 2010, Bova et al. 2015). To meet these ends, the Anderson 13 Standard fuel models and the updated Scott and Burgan 40 fuel models were developed to represent easily interpretable characterizations of fuels and expected fire behavior, but lack realistic relationships to actual spatial distributions of fuels across North America (Anderson 1982, Scott and Burgan 2005). To adjust fuel models to better reflect expected fire behavior due to management treatments or inherent variability of fuels, fire modelers have customized fuels to produce rate of spread that represents observed or expected ROS or behavior. For prescribed fire decision support, the quantification of real fuels and their accurate spatial distribution is important to simulate fire and smoke production, the defining output of prescribed fire nationally (Parsons et al. 2011, Yedinak et al. 2018, Hudak et al. 2020, Loudermilk et al. 2022).

Current operational modeling systems such as Behave and Farsite require simple fuel characterizations summarized in surface fire behavior fuel models that are used in Rothermel's (1972) surface fire spread model to calculate rate of spread and flame length. While convenient, fuel models fail to capture wildland fuel heterogeneity. To integrate fire behavior and effects predictions, a revised approach was developed called the Fuel Characteristic Classification System (FCCS, Ottmar et al. 2007). The FCCS accounts for all fuels with potential to burn, represents the geographic and structural diversity of wildland fuels, and provides a reference library of fuelbeds throughout the United States. These approaches provide generalized outputs useful for managers, but improvements are needed to advance fuel characterization to support physics-based fire and fuel consumption models for prescribed fire planning and implementation.

Over the past decade, the SERDP and ESTCP programs have supported a set of innovative and interrelated projects to advance fire science and related fields of fuel hazard carbon accounting and air pollution. With an objective to inform vegetation and fuels characterization for process-based fire behavior and effects modeling, the 3D Fuels project was developed and conducted in close collaborations with a number of SERDP and ESCTP-funded projects. Specifically, 3D fuels was designed to facilitate common definitions, methods, and data sharing with three SERDP-funded projects, including Objects (RC-20-1346 *Object-Based Aggregation of Fuel Structures, Physics-Based Fire Behavior and Self-Organizing Smoke Plumes for Improved Fuel, Fire, and Smoke Management on Military Lands*), Closing Gaps (RC20-1025 *Closing Gaps in Measurements and Understanding: Plume Characteristics, Live Fuel Moisture Dynamics, and Process-Based Modeling*), and RC19-1192 (*Characterizing Multiscale Feedbacks between Forest Structure, Fire Behavior and Effects: Integrating Measurements and Mechanistic Modeling for Improved Understanding of Pattern and Process*). Specifically, some 3D fuels sites are shared with the Objects project, and we collected field data to actively share with the Objects project to inform object-based mapping of fuel loads for smoke modeling. Similarly, the 3D fuels project was designed to lead to the active development of FuelsCraft (ESTCP Project RC23-7779 *FuelsCraft: An Innovative Wildland Fuel Mapping Tool for Prescribed Fire Decision Support on Department of Defense Military Installations*) and active collaborations with Russ Parsons and team on their Closing Gaps project and ESTCP-funded work on FastFuels (RC23-7626 *FastFuels and QUIC-Fire: A Tool Suite Advancing DoD's Prescribed Fire Planning and Analysis Capabilities*).

Recent advances in remote sensing technologies have catalyzed novel methods for 3D characterization and mapping of wildland fuels as inputs to models of fire behavior and effects. Computational fluid dynamics (CFD) models such as FIRETEC (Linn et al. 2002, 2005) and the Fire Dynamics Simulator (Mell et al. 2007) simulate wildland fire behavior and fire-atmosphere interactions using gridded, 3D meshes of wildland fuel inputs including bulk density, heat content, fuel moisture, and other fuel properties. Although computationally intensive, CFD models can be used to evaluate how wildland fuel complexes contribute to fire spread, intensity, and duration. The model QUIC-fire was developed to more efficiently solve for turbulence and fire behavior than a full physics-based model using a cellular autonoma approach for fire behavior calculations that relies on gridded, 3D fuels inputs (Furman 2018, Linn et al. 2020). The 3D structure and composition of fuels not only contributes to heat release and fire propagation but also interacts with wind fields and can influence fire flow and duration. Next-generation models of fire behavior and smoke production rely on gridded, 3D inputs of wildland fuel complexes comprised of canopy and understory fuels (Hiers et al. 2009, Loudermilk et al. 2014). To date, much of the emphasis on 3D fuel characterization has been on improved understanding about how tree boles and crowns influence subcanopy wind fields and fire flow (Pimont et al. 2011, Hoffman et al. 2015, Atchley et al. 2021), but understory and surface fuels are critical drivers of fire behavior and smoke production (Ritter et al. 2020, Rowell et al. 2020). Relevant metrics of understory fuels for process-based models of fire behavior (i.e., QUICFire, FIRETEC and FDS) include fuel height (m), bulk density (kg/m3), surface area to volume ratio (m2/m3), fuel moisture, and other fuel particle properties. However, more work is needed to better understand how the scale and specificity of the 3D structure, composition, and resolution of understory fuels influence predicted fire behavior and effects (Loudermilk et al. 2022, Hutchings et al. 2024). Prescribed fire has been a prime motivation for improving fuels estimation, as these types of management activities generally occur on fuel moisture and weather margins where subtle changes in fuel mass and type may have substantial impacts on fire behavior, effects, and smoke production (Hiers et al. 2020). These factors are a strong motivation for developing fuels that encompass the inherent spatial and scale diversity that prescribed fire is applied. The shift to improved fuels characterization is driven by the development of a broad spectrum of physics-based and coupled atmospheric-parameterized fire models that operate at finer scales and require three-dimensional fuel inputs. Prescribed fire managers are increasingly tasked with improving the modeling and characterization of fire behavior and smoke and the ecological impacts of burning to fire-adapted ecosystems (Mitchell et al. 2006, O'Brien et al. 2018, Prichard et al. 2022). This study was designed to provide foundational fuels data to inform prescribed fire decision support.

To date, established methods do not exist that scale 3D fuels data from fine scale measurements in small locations to the larger landscape scales critical for decision making. This current disconnect between spatial scales poses a substantial barrier to informing next-generation modeling of wildland fire behavior and smoke. Recent advances in remote sensing and related technologies, suggest that new approaches can be developed to consistently map and attribute surface and canopy fuels to meet physics-based model requirements for 3D fuels at the landscape-level domain of land management decisions. Advances have been made in translating canopy fuel metrics into 3D inputs for computational fluid dynamics modeling of fire spread and turbulence (Mueller et al. 2014, Hoffman et al. 2015, Pimont et al. 2016, Silva et al. 2016, Parsons et al. 2018, Ritter et al. 2020, Atchley et al. 2021), but less work has been done to date on forest understory, shrubland and grassland fuels (but see Loudermilk et al. 2014. 2022).

The 3D Fuels project was designed to characterize the structure and composition of understory fuels common to prescribed burn programs within pine forests of the southeastern and western US. Traditional fuel characterization in these systems has been limited by 2D representations, including biomass, height and cover estimates per unit area. The objective of this study was to use a combination of ALS, TLS, and SfM photogrammetry to create hierarchically scaled, 3D datasets of live and dead understory fuels to inform the scaled mapping of 3D fuels across open forest types that are commonly involved in prescribed burning programs. Forest understory fuels in this study are complexes of live and dead vegetation and were often characterized as fuel types, including organic soil (duff), litter, fine and coarse wood, grasses and shrubs (Ottmar et al. 2007). To inform models that parse 3D point cloud datasets into segmented objects and metrics (e.g., height, cover, bulk density), we co-located intensively sampled 3D calibration plots across 18 sites in the southeastern and western US (**Table 1**).

Wildland fuel characterization is known to be incredibly challenging due to both the high heterogeneity of surface and canopy fuels across space and time (Keane 2015). This study represents an intensively sampled and hierarchically scaled dataset that can be used to train fine-scale models of relationships between field-based measurement and remote sensing dataset and broader scale mapping of wildland fuels for operational mapping and fire behavior and effects modeling. Our study was designed to evaluate and advance methods for 3D fuel characterization and to provide consistently scaled and labelled datasets to provide both a framework for additional studies as well as an evaluation dataset for model development and evaluation. More specifically, machine learning algorithms are currently being evaluated to assist the parsing of 3D point cloud datasets collected from ALS, TLS, and SfM photogrammetry. Based on calibration with field plots, our hierarchically scaled datasets can be used as the foundation for synthetic fuelbed mapping using statistical relationships developed from this study to inform probabilistic canopy and understory fuel assignments for wildland fire environments that are common to prescribed burning programs in southeastern and western pine forests. The study was guided by the following question: *How can we most efficiently and accurately create gridded, 3D maps of surface fuel properties based on the integration of remotely sensed imagery and fuel properties informed from field-based and laboratory measurements?*

Effective fuels management requires metrics that describe fuels in terms useful to managers. Before CFD models become operational, fire and fuels managers require interim metrics that translate lidar and other remotely sensed datasets to practical fuels management questions. At present, managers often use torching and crowning indices to evaluate crown fire potential and to assess fuel treatment effectiveness based on estimates of canopy height, height to live crown and surface fuel loadings (Van Wagner 1977, Heinsch and Andrews 2010). Our system of hierarchical fuels characterization and mapping provides opportunities to develop new metrics for 3D fuels useful interpretation and insights to managers, particularly with respect to fuel reduction treatments and prescribed burning programs. Leveraging the STANDFIRE prototype 3D fuel modeling platforms (Parsons et al. 2017), we can develop metrics to quantify fuel properties and spatial characteristics. In many cases, gaps between fuels may play as important a role in fire spread as their available biomass for combustion.

The 3D Fuels project contributes to wildland fuels research by integrating state-of-the-art fuel sampling techniques and quantitative fuels modeling with model sensitivity analyses to provide foundational methods and tools for both scientists and managers. At present, methods are still under development to map spatial fuels data at scales pertinent to operational wildland fires and for the application of the latest physics-based fire-atmosphere models (Keane 2015). Here we present new methods and metrics for 3D fuels that will provide useful interpretation of remotely sensed datasets and insights to fire and fuels managers, for fuels, fire, smoke and atmospheric modeling applications. Specifically, we created a 3D library of voxel fuels, intrinsic fuel properties and quantitative modeling scripts that partition point cloud data into voxels and create 3D input for existing and custom applications. With the expansion of machine learning and AI, these fully documented, and hierarchically scaled datasets will provide a foundation for parsing imagery to create 3D gridded inputs to next-generation operational models of fire behavior and effects.

3.0 METHODS

3.1 3D FUELS DATA REPOSITORY

We employed a hierarchical sampling design for mapping 3D surface and canopy fuels that relied on a combination of airborne and high-resolution lidar, SfM photogrammetry, and ground-based measures of physical fuel properties, including destructive sampling within a 3D grid (**Figure 2**). The purpose of this sampling design was to facilitate the production of 3D maps of surface and canopy fuels across a range of spatial scales and vegetation types that function as inputs for physics-based, coupled fire-atmosphere models and other next-generation models reliant on spatially explicit fuels. The datasets also facilitated the use of advanced mathematical modeling techniques to develop quantitative models that assign measured properties of fuels, and in the case of highly intermixed fuels (e.g., complex arrangements of surface fuels including shrubs, herbaceous fuels, and intermixed live and dead fuel), develop 3D models of functional plant groups to inform mapping assignments.

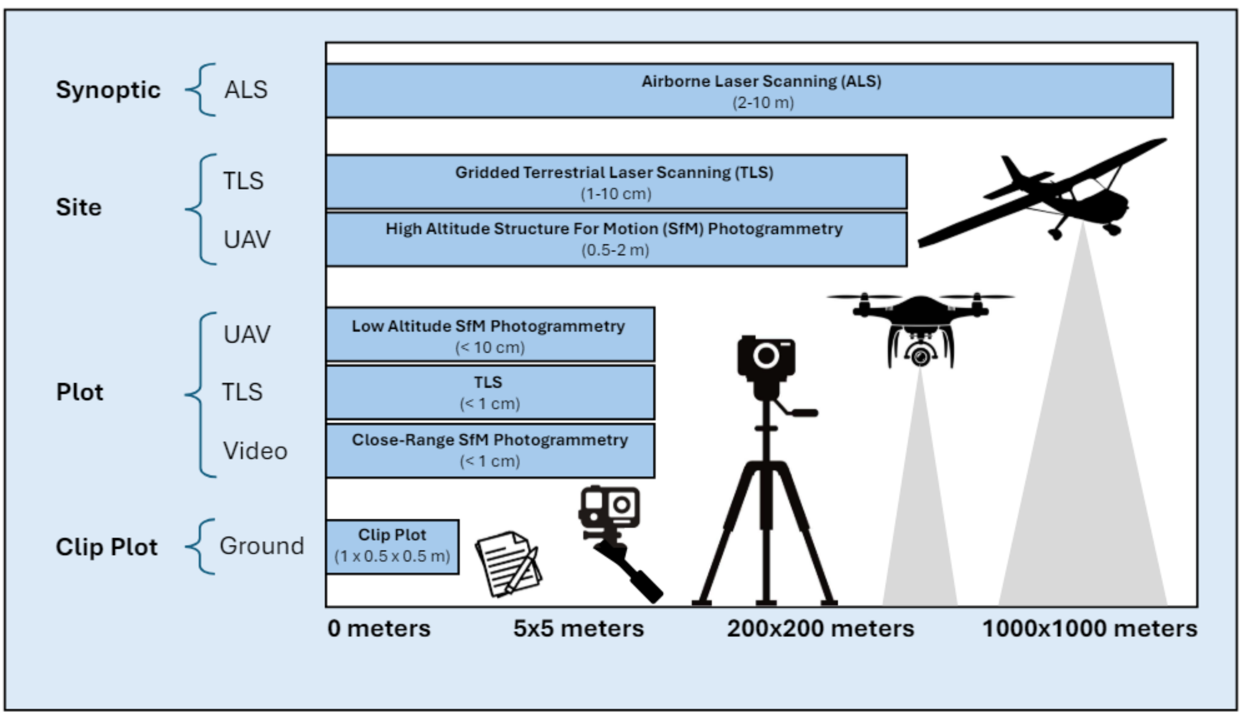

Figure 2. Hierarchical sampling design of the 3D fuels project.

3.1.1 3D Fuels study areas

The 3D Fuels dataset includes a total of 18 study sites to date, in 13 locations in southern pine forests of the southeastern US and 6 locations in pine forests and grasslands in the western US (**Figure 3, Table 1**). Forested sites had open pine-dominated canopies with understory fuel complexes that ranged from low to relatively higher biomass within each of three major forest types: southeastern pine forests (loblolly/longleaf) with flatwood understories, southeastern loblolly plantation forests with sweetgum understories, and semi-arid western ponderosa pine forests. Although geographically distinct and with markedly different climates, southeastern and western pine forests share structural similarities (e.g., single-story, open forests with grass/shrub/litter understories). Methods developed in this study to characterize canopy and understory can be broadly applied in mapping and to generate 3D model inputs. Specifically, we anticipate that because pine forests have similar structural characteristics, similar scripting algorithms can be used to interpret point-cloud imagery into gridded, 3D representations of both forest types. Intrinsic fuel properties and fuel moistures can then be tailored to be specific to southeastern and western fuel types.

Southern pine sites were selected to represent a range in understory biomass from low biomass (e.g., a 1-year rough) to high biomass (e.g., 4-5 year rough) (**Figures 4, 5**) whereas ponderosa pine forest and western grassland sites were selected to represent a range of productivity from lower to higher understory cover and biomass (**Figures 6, 7**). Selection criteria for all sites included availability of recent ALS, and relatively uniform ground surface on gradual slopes (< 30% gradient). Although the use of unoccupied aerial systems (UAS) was preferred for high- and low-altitude SfM photogrammetry, UAS flights were not permitted at all sites, particularly those sites located on US Department of Defense and some US Forest Service lands.

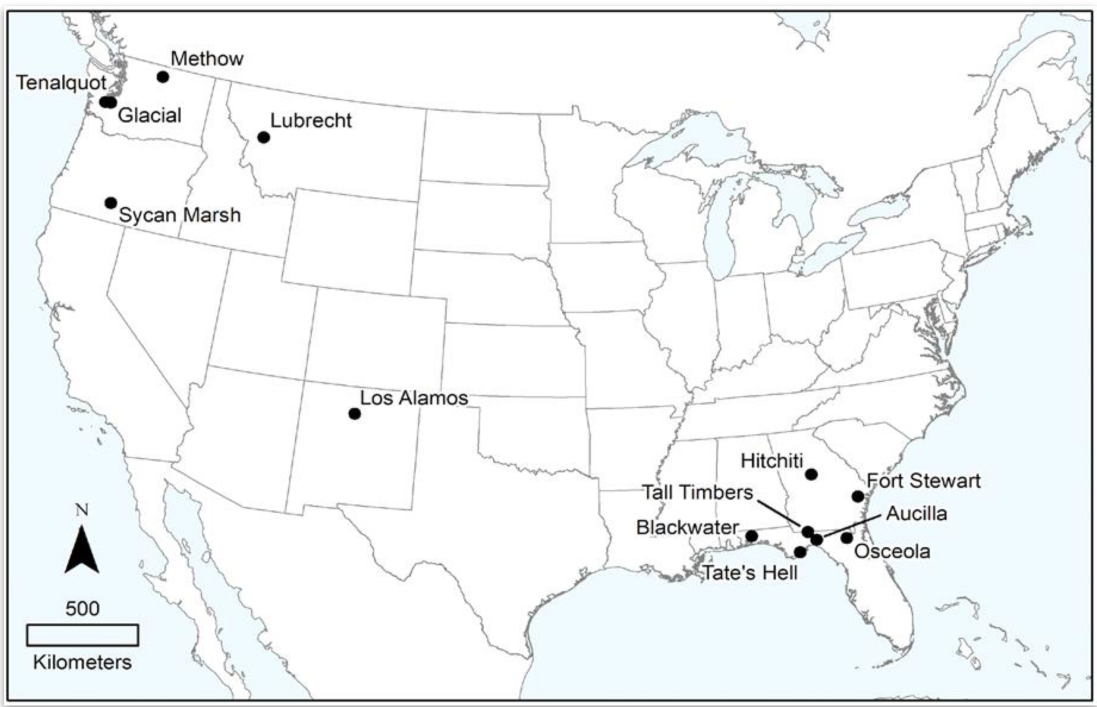

Figure 3. Study site locations. For an interactive map, visit our ArcGIS online site at: https://arcg.is/1jTz9y0

Southeastern flatwood forests

Aucilla

The site is a long-unburned forest sites (>5 years since fire) within the Middle Aucilla Conservation Area along the Aucilla River, roughly 6.5 miles south of the town of Lamont, Florida. The majority of the site is representative of mesic flatwood fuel types; portions of the eastern edge transitioned into bottomlands as the plot edge approached the river, and on the western edge as elevation decreased. The overstory is dominated by open canopy longleaf pine (*Pinus palustris*) with a developed understory of saw palmetto and ferns with some deciduous shrubs, oak sprouts, and grasses.

Blackwater

This site represents a 2-yr rough within the Blackwater State Forest, near Milton Florida (FL panhandle). The overstory is dominated by longleaf pine with a wiregrass (*Aristida stricta*) understory with scattered saw palmetto and other native shrubs. Sampling was coordinated with the FIREX-AQ campaign to sample plumes from summer prescribed burns at this site.

Fort Stewart

This site was sampled both pre- and post-burn as part of the SERDP-funded wildland fire science initiative experimental burns, which were conducted in March 2022. This specific site (Ft Stewart A) is on the western end of Fort Stewart 2022 burn unit F 6.4. The site is a flat, mesic flatwood forest that has not had any recent thinning but has been regularly burned every 2-3 years. The overstory is dominated by longleaf pine (*Pinus palustris*) and slash pine (*P. elliottii*) with occasional loblolly pine (*P. taeda*). A dense understory of low (less than 1 meter tall) evergreen shrubs and bunchgrass are dominant with occasional areas of taller vegetation. Duff is absent or nearly so due to frequent prescribed burns. This site was burned on March 2, 2022 with a low-intensity surface burn (prescribed fire) using aerial ignition. The fire consumed evenly at low severity throughout the understory with no unburned patches.

Oceola

This 3D Fuels site is located in Osceola National Forest east of Lake City, Florida and was sampled as part of a long-term fire study by the USFS Southern Research Station to measure the effects of fire at different burn intervals. Vegetation in the site consists of a longleaf pine (*Pinus palustris*) overstory with the understory dominated by saw palmetto (*Serenoa repens*) and gallberry (*Ilex spp.*) with some blueberry (*Vaccinium spp.*), wiregrass (*Aristida stricta*) and bunchgrasses. The sampling design was modified within this site to fit within a fuel consumption study coordinated by Louise Loudermilk and Christie Hawley (Ross et al. 2024).

Tate's Hell A and B

We established two separate sampling sites at Tate's Hell State Forest, located in the central panhandle of northern Florida. The first site, referred to as Tate's Hell A (THA), was sampled in late January 2020 and located in a mesic flatwood forest that was burned approximately one year prior to sampling. The overstory is dominated by open canopy slash pine (*P. elliottii*) with an understory dominated by saw palmetto (*Serenoa repens*) and gallberry (*Ilex glabra*), with some deciduous shrubs, oak seedlings, and grasses present in smaller abundance.

The second site, referred to as Tate's Hell B (THB) and sampled in early February 2020, was similarly located in a mesic flatwood forest dominated by open canopy slash pine, but was between two and three yr post-fire. As a result, the understory of THB contains similar species as THA (dominated by saw palmetto and gallberry) but with greater height and density.

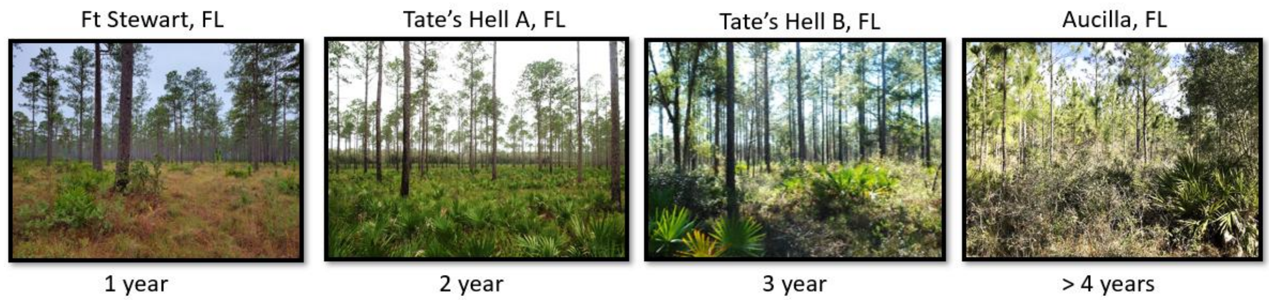

Figure 4. Representative photos of southeastern pine mesic flatwood sites, arranged by time since fire. The additional sites - Blackwater and Osceola are not pictured.

Additional mesic flatwood sites included Blackwater and Osceola.

Southeastern loblolly-sweetgum forests

Hitchiti A and B

Hitchiti A and B are located within the Hitchiti Experimental Forest, which is part of the Piedmont National Wildlife Refuge, GA, but managed by the US Forest Service. This experimental forest is part of the original Jarell Plantation and is dominated by loblolly and slash pine plantations with a sweetgum dominated understory. Hitchiti A represents a 2-3 year rough with moderate sweetgum cover. Hitchiti B is a 1-year rough with a dense sweetgum understory. These sites were sampled in February and March of 2022 before spring green up. Hitchiti A is bisected by a stream with a predominant S-facing exposure throughout. Hitchiti B is predominantly north facing with some steep topographic features; sampling grids were relocated to allow scanning and destructive sampling on relatively flat ground. Both units were previous cotton plantations, planted 70-80 years ago. They have been thinned in the past 10 years and have been regularly burned.

Tall Timbers - Hannah Hammock unit

This site is located in the Hannah Hammock unit of the Tall Timbers Research Station (FL) within a stand of pine forest that regenerated after a period of intensive agricultural land use, with no recent forest thinning. This area is burned regularly (every 2-3 years) by Tall Timbers staff. The overstory is primarily loblolly pine (*Pinus taeda*), although shortleaf pine (*Pinus echinata*) is common. Trees are widely spaced, and canopy gaps are present. Occasional understory trees include southern magnolia (Magnolia grandiflora) and a large (~½ acre) section of pine saplings in the middle of the site. Understory vegetation (excluding saplings) is 1-3 meters tall. Abundant understory species include winged sumac (*Rhus copallinum*), greenbriar (*Smilax spp.*), goldenrod (*Solidago canadensis*), American beautyberry (*Callicarpa americana*), various shrubby oak species (*Quercus* spp.), grasses (wiregrass is not present at this site), shortleaf pine seedlings, sweetgum (*Liquidamber styraciflua*) resprouts, Rubus spp., sweetbay (*Magnolia virginiana*), persimmon (*Diospyros virginiana*), grape (*Vitus* rotundifolia), and silkgrass (*Pityopsis graminifolia*). Litter is a mix of long and short-needle pine needles with broadleaf litter occasionally contributed by shrubs. Duff is present at this site despite frequent burning. Downed woody debris loading is light with only a few logs scattered throughout the site.

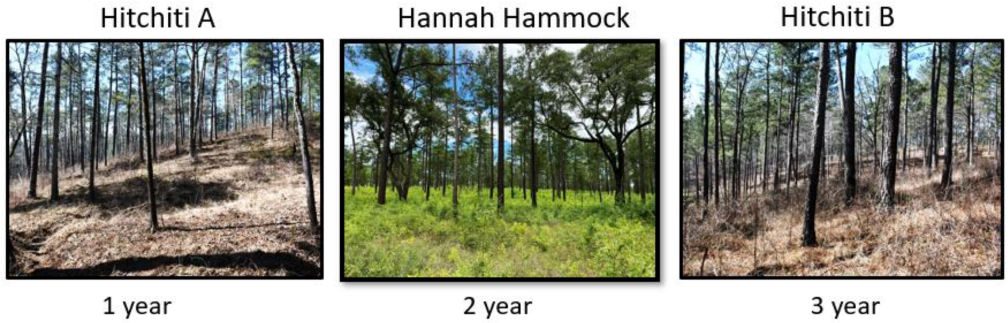

Figure 5. Representative photos of loblolly pine-sweetgum sites arranged by time since fire.

Western pine/mixed conifer forests

Los Alamos National Laboratory – forest site

The Los Alamos National Laboratory (LANL) forest site is a dry ponderosa pine site intermixed with Gambel oak and occasional southwestern white pine (*P. strobiformis*). The site is located on a generally south-facing slope with varied microtopography. A portion of the southern unit had a mastication treatment in the past, which was avoided during plot setup. The forest overstory is dominated by open-canopy ponderosa pine, and the understory is sparse, with scattered Gambel oak sprouts and grasses and occasional deciduous shrubs. The site is long unburned, with accumulated litter and duff around larger trees.

Sycan Marsh Preserve – forest sites

The Sycan Marsh Preserve spans over 12,000 hectares of mostly marsh and grassland in south central Oregon. Two forest sites were sampled within an upland forest in coordination with prescribed burning campaigns in the fall of 2019 and 2020, coordinated with the SERDP wildland fire science initiative. The forested site at the preserve (SMF) consists of an open canopy and uneven aged ponderosa pine forest, with evidence of past logging and thinning. The understory vegetation at SMF is dominated by scattered bitterbrush (*Purshia tridentata*) with some bunchgrasses, and surface fuels include fine wood (10-hr and 100-hr) with occasional rotten coarse woody debris. The site was thinned using an individual, clump, and openings prescription in 2019 and prescribed burned as part of our sampling campaign.

Methow Wildlife Area

The Methow unit is located in a young ponderosa pine forest on Washington Department of Fish and Wildlife land, approximately 7 miles NE of Winthrop. The unit is co-located with a pine thinning study that was conducted in the 1990s to thin naturally regenerated ponderosa pine forest. The unit is in a moderately open ponderosa pine forest with scattered bitterbrush understory. Bitterbrush is the dominant shrub species in the unit, with infrequent Pacific serviceberry (*Amelanchier alnifolia*). Dominant understory grass species are bluebunch wheatgrass (*Pseudoroegneria spicata*), Idaho fescue (*Festuca idahoensis*) and junegrass (*Koelaria* spp). Dominant forb species are arrowleaf balsamroot (*Balsamorhiza sagittata*) and yarrow (*Achillea millefolium*). Ground fuels are largely composed of pine needle cast and woody debris. Although nearby forests were burned in a recent prescribed burn and wildfires, this site has not been burned in over a decade.

Lubrecht Experimental Forest

Lubrecht Experimental Forest is located approximately 30 miles east of Missoula in the Blackfoot River drainage of western Montana. The overstory consists of predominantly ponderosa pine (*Pinus ponderosa*) and Douglas-fir (*Pseudotsuga menziesii*) with sparse understory vegetation dominated by scattered shrubs (*Vaccinium* spp.), kinnikinnick (*Arctostaphylos uva-ursi*), and timber litter. The site, which is part of the Fire and Fire Surrogates Project (Hood et al. 2024), was mechanically thinned during the winter of 2001, and last burned in the late spring of 2002.

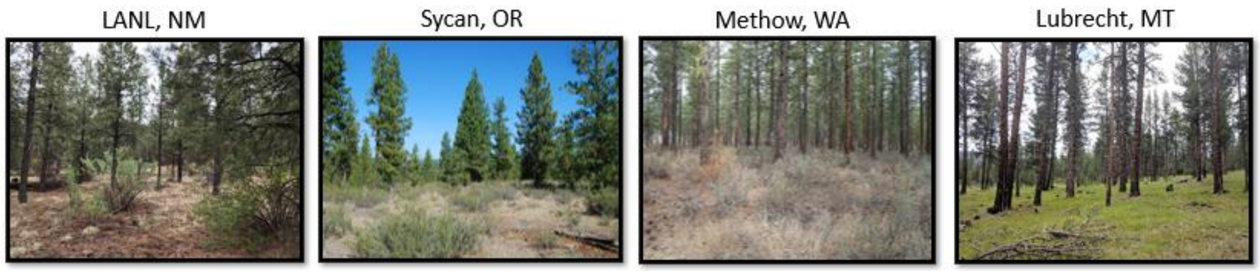

Figure 6. Representative photos of western pine/mixed conifer forests arranged by low to higher surface biomass (including forest floor layers).

Western grasslands

Los Alamos National Laboratory – grassland site

The grassland site is located just outside of the northern boundary of the Los Alamos National Laboratory, situated along the southern edge of Rendija road. The xeric site vegetation consists of invasive cheatgrass, eyebrow grass, and *Stipa* spp. as well as forbs, with deciduous and evergreen shrubs in lesser abundance. Scattered juniper (*Juniperus monosperma*) and Gambel oak occurred throughout the site with ponderosa pine lining the perimeter. The entire site is on flat terrain and has been highly disturbed by both humans and cattle, evidenced by the existence of garbage and animal dung distributed throughout the vicinity. Litter was sparse but present and found in the form of dead grass and shrub leaves. Duff was present, but less common than litter.

Sycan Marsh Preserve – grassland site

The Sycan Grass unit is located in the Sycan Marsh Preserve in south central Oregon. It is a dry, heavily grazed grassland with sparse bunchgrasses (*Festuca idahoensis, Poa secunda and/or pratensis, Koeleria macrantha, Danthonia californica*), forbs and other graminoids such as sedges and annual grasses. The site also contains some small patches of low sagebrush (*Artemesia arbuscula*). As with the Sycan forest site, sampling included pre- and post-burn remote sensing and field measurements.

Center for Natural Lands Management (CNLM) – Tenalquot and Glacial Heritage site

We sampled two grassland sites in the southern Puget Lowlands of western Washington state, located south of Olympia on CNLM prairie lands. The Tenalquot site is immediately adjacent to Joint-Base Lewis-McChord property, and is currently planned for late summer burning. This is a native bunchgrass prairie with a moderate level of invasive species. Dominant species include Idaho fescue (*Festuca idahoensis*), bentgrass (*Agrostis* spp.), oxeye daisy (*Leucanthemum vulgare*), bracken fern (*Pteridium aquilinum*), and hairy cat's ear (*Hypochaeris radicata*). Where scattered patches of kinnikinnick (*Arctostaphylos uva-ursi*) exist, there is a substantial moss/lichen layer.

The Glacial Heritage Preserve Site is typical of highly-invaded grasslands in the region. The site is dominated by invasive tall oatgrass (*Arrhenatherum elatius*) and oxeye daisy with occasional Douglas-fir trees, stumps, bracken fern, and scotch broom intermixed. The site is near the Mima Mounds Natural Area Preserve (WA Department of Natural Resources) and mounds are present throughout, which influenced plot placement. Shrubs are more prevalent on the crests of these mounds.

Figure 7. Representative photos of western grassland sites, arranged from low to higher total biomass.

Table 1. 3D Fuels study site description –location, time since fire or biomass range, vegetation type, sampling date, and available imagery from ALS, UAS-based SfM photogrammetry, and TLS across units and 5x5 plots. Sites with pre- and post-sampling in coordination with prescribed burning are noted with an (Rx).

Site	Location	TSF / biomass range	Vegetation type	Sample date	ALS date	specs	SfM UAS high	UAS low	close-range	TLS unit	5x5
Southeastern mesic flatwood forests											
Ft Stewart A	US DOD Ft Stewart, GA	2-3yr rough	Open longleaf/ loblolly pine forest - moderate load saw palmetto and gallberry	Jan-21	FASMEE/ DOD 2021	35 pts/m 26 GB laz	N	N	Y	Y	Y
Tate's Hell A	Tate's Hell State Forest, FL	1-2 yr rough	Slash pine plantation – low load saw palmetto and gallberry	Jan-20	2018 USGS	20 pts/m2 107 GB laz	Y	Y	Y	Y	Y
Tate's Hell B	Tate's Hell State Forest, FL	2-3 yr rough	Slash pine plantation – moderate load saw palmetto and gallberry	Jan-20	2018 USGS	20 pts/m2 107 GB laz	Y	Y	Y	Y	Y
Aucilla	Suwannee River Water Mgmt District, FL	>5 yr rough	Longleaf pine - high load saw palmetto and gallberry	Apr-21	2018 NWFL Water Management District	20 pts/m2 3 GB laz	Y	N	Y	Y	Y

Site	Location	TSF / biomass range	Vegetation type	Sample date	ALS date	specs	SfM UAS high	UAS low	close-range	TLS unit	5x5
Blackwater	Blackwater State Forest, FL	2 yr rough	Open longleaf pine forest - wiregrass understory	Aug-19	2018 USGS	20 pts/m2 108 GB laz	N	N	Y	Y	Y
Osceola (Rx)	Osceola NF, FL	1-2 yr rough	Open longleaf pine forest - low load palmetto and gallberry	Jan-20	2018 USGS	25 pts/m2 3.5 GB laz	Y	Y	Y	Y	Y
Southeastern loblolly sweetgum forests											
Hannah Hammock (FL)	Tall Timbers RS, FL	1-2 yr rough	Loblolly pine plantation with sweetgum understory	Jul-22	2020	20 pts/m2 1.6 GB laz	Y	N	Y	Y	Y
Hitchiti A	Hitchiti Exp. Forest (GA)	2-3 yr rough	Loblolly pine plantation with sweetgum understory	Feb-22	2021	30 pts/m2 101 GB laz	Y	Y	Y	Y	Y
Hitchiti B	Hitchiti Exp. Forest (GA)	1 yr rough	Loblolly pine plantation with sweetgum understory	Feb-22	2021	30 pts/m2 101 GB laz	Y	Y	Y	Y	Y
Western ponderosa pine forests											
LANL Forest	LANL, NM	Low	Open pine forest with sparse Gambel oak understory	Jun-21	2020 Tetra Tech	20 pts/m2 1.3 GB laz	Y	N	Y	Y	Y
Sycan Forest I (Rx)	Sycan Marsh Preserve, OR	Low	Open pine forest; sparse bitterbrush/ timber-litter understory	Sep-19	2018 Atlantic	20 pts/m2 2GB laz	Y	Y	Y	Y	Y
Sycan Forest II (Rx)	Sycan Marsh Preserve, OR	Low	Open pine forest; sparse bitterbrush/ timber-litter understory	Oct-21	2018 Atlantic	20 pts/m2 2GB laz	N	N	Y	Y	Y
Methow	Methow Wildlife Area, WA	Mod	Open pine forest with bitterbrush/timber-litter understory	Oct-20	2018 WA DNR	20 pts/m2 85GB laz	Y	N	Y	Y	Y
Lubrecht	Lubrecht Exp. Forest, MT	High	Open pine and mixed conifer forest with timber litter-shrub understory	Jul-19	2015 UM	20 pts/m2 35GB laz	Y	Y	Y	Y	Y

Site	Location	TSF / biomass range	Vegetation type	Sample date	ALS date	specs	SfM UAS high	UAS low	close-range	TLS unit	5x5
					Western grasslands						
LANL Grass	LANL, NM	Low	Sparse, dry grassland	Jun-21	2021 Tetra Tech	20 pts/m2 1 GB laz	Y	Y	Y	Y	Y
Sycan Grass (Rx)	Sycan Marsh Preserve, OR	Low	Sparse grassland with grazing	Sep-19	2018 Atlantic	20 pts/m2 2GB laz	Y	Y	Y	Y	Y
Tenalquot	Tenalquot Prairie Preserve, CNLM, WA	Mod	Native prairie grassland	Jul-20	2017 WA DNR	20 pts/m2 1 GB laz	Y	Y	Y	Y	Y
Glacial	Glacier Heritage Reserve, CNLM, WA	High	High biomass wWA nonnative grassland	Jul-20	2011 WA DNR	6 pts/m2 1 GB laz	Y	Y	Y	Y	Y

3.2 3D FUELS FIELD METHODS

Plots were installed along grid point spaced 50 m apart. The most common unit layout included points that were set on a 200 x 200 m grid, but grid shapes were adjusted to accommodate unit dimensions and avoid wetlands, streams, and steep slopes. Thirteen of the grid points were randomly selected for higher-resolution TLS scanning. Nine of these were selected for high-resolution scanning coupled with destructive biomass sampling, and a minimum of four were selected for high-resolution scanning alone. Plots were monumented using four 2-m metal conduit poles topped with a band of reflective tape, one in each corner of a 5 by 5 m plot. For destructive sampling plots, an additional 5 poles were used to mark interior points which served as the northwestern corners of 0.5 by 0.5 m destructive sampling plots, referred to as “clip plots” (**Figure 8**). Five clip plots were distributed in a grid formation within the larger plot, and labeled NW, NE, CTR, SW and SE for the cardinal pattern in which they were distributed. PVC squares measuring 0.5 m on each side were wrapped in reflective tape and used to mark boundaries of each clip plot on the ground. Reflective tape on poles and PVC squares allowed the location of clip plots in lidar and SfM imagery. Photos were taken of each clip plot prior to sampling.

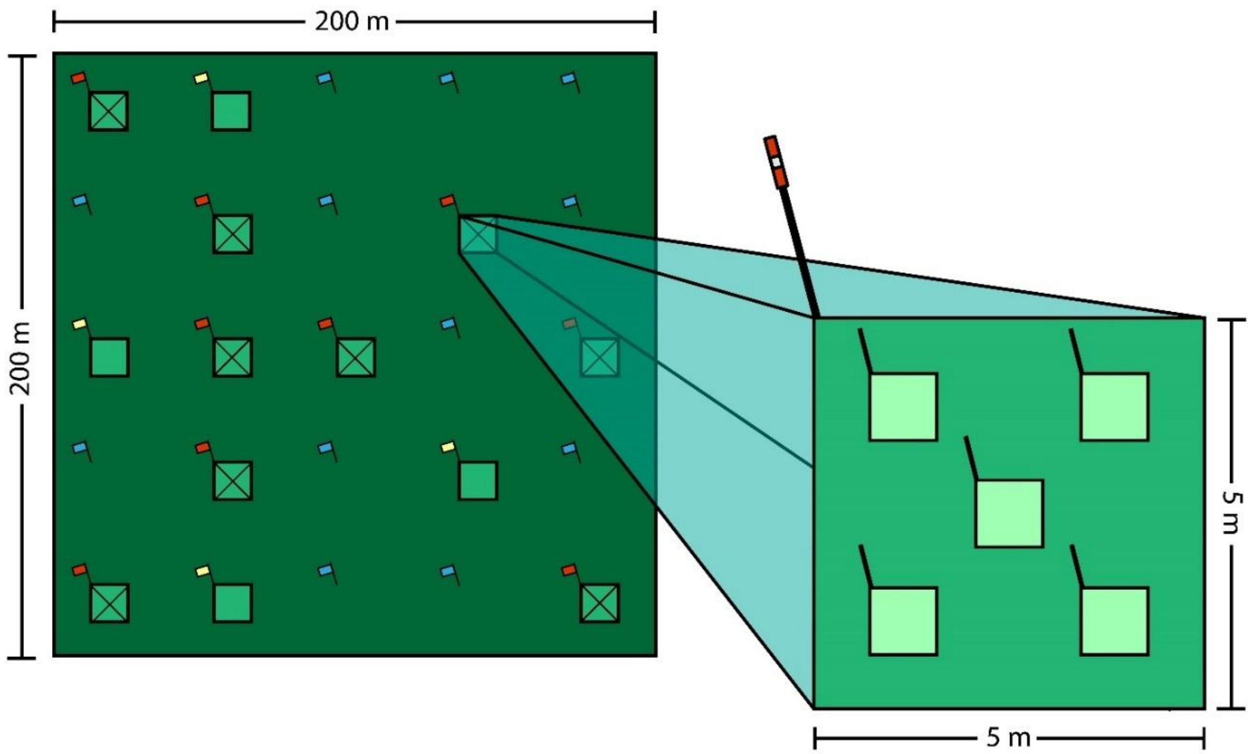

Figure 8. Schematic image of plot layout. 200x200 m grid with 9 5x5 m plots selected for destructive sampling (red flags) and four selected for intensive scanning (yellow flags). Blue flags represent the remaining grid points used for synoptic (single) scans. Five clip plots (0.5 x 0.5 m) are arranged in a grid pattern within each selected 5 x 5 m plot.

3.2.1 Terrestrial laser scanning

Terrestrial laser scanning was conducted using a RIEGL -VZ2000 (and RIEGL-VZ400i for a few sites) with 750 kHz for the laser sampling rate and vertical sampling density of 0.21 degrees, mounted on a tripod at a minimum height of 1.5 m. The REIGL has an integrated L1 GPS receiver, compass and inclination sensors that aid in geo-referencing point clouds. Each of the 13 plots designated for higher-resolution scanning received one 360° scan at each conduit pole marking the corner of the plot. Grid points that are not part of plots receive one 360° scan at each conduit pole location: these were later tiled to create a synoptic scan on the entire unit.

3.2.2 Photogrammetry

3.2.3 UAS-based photogrammetry

Unoccupied aerial systems (UAS) were used to collect videos at both low (plot-level capture) and high altitudes (entire 200 x 200 m unit capture) to be used in SfM modeling. Imagery was captured using a Zenmuse X3 optimal camera and a Micasense Red Edge 3 multispectral sensor mounted on a DJI Matrice 100 quadcopter. Flights were fully automated using Map Pilot Pro flight planning software. High-altitude flight parameters consisted of maintaining an altitude of 100m AGL, with 24 flightlines North-South (NS) and 26 East-West (EW) to ensure there was ~80% endlap and ~75% sidelap for the Micasense, the smaller of the two camera's footprints. Total image count for the X3 was 1295 files and 2749 for the Micasense. Ground control points were marked with coded black and white targets. Coordinates of these were recorded using an RTK/Differential GPS receiver/base combination. Ground control points were placed at the NW corners of plots in order to tie the high-altitude UAS acquisitions to the low-altitude acquisition. Low-altitude imagery was collected at an altitude of approximately 3m when tree density allowed.

Close-range photogrammetry

A handheld system was used to collect close-range photogrammetry (**Figure 9**). This included a GoPro Hero7 camera mounted on a Feiyu G6 gimbal which was then threaded onto a 36 inch lightweight rigid pole. A 1-2 minute video was filmed from a constant 1m elevation, maintaining a consistent snaking pattern above each clip plot. Camera resolution was set at 2700K, with a frame rate of 60 frames per second. A second snaking pattern was repeated at a 90° angle to the first, and finally the entire plot was circled with the camera at an oblique angle pointed inward to the plot. Cylindrical foam flotation devices and printed targets were placed around each plot for use as alignment markers in the imagery. A small whiteboard marked with the plot name, site and date was recorded in the initial 5 seconds of the video for plot identification purposes.

Figure 9. Close-range photogrammetry scan with a 2D frame representing the footprint of a clip plot, Lubrecht Experimental Forest.

3.2.4 Vegetation sampling

Occupied volume and fuel typing

A three-dimensional PVC frame was used to delineate 250 voxels in 3 dimensions for each clip plot (Hawley et al. 2018). Frames were cubes measuring 0.5m on each side and 1 m in height, with a sliding square that used to delineate a single stratum gridded with wire: each 10 cm of height was considered a stratum (e.g. 0-10 cm, 10-20 cm, 20-30 cm, etc., **Figure 10**). As the sliding square was placed at the level of a stratum, it was divided into 25 voxels using 0.5 m long rigid wires; voxels are numbered 1-25 on the lowest stratum and increase with each higher stratum, reaching 250 on the 90-100 stratum. Using a custom field form containing all voxel numbers, all fuels in the clip plot cube were marked as present or absent for each voxel, starting at the highest stratum containing vegetation and progressing downwards to the 0-10 cm stratum (voxels 1-25). If a trace amount of voxel space was occupied, presence in that voxel was not recorded. Plant

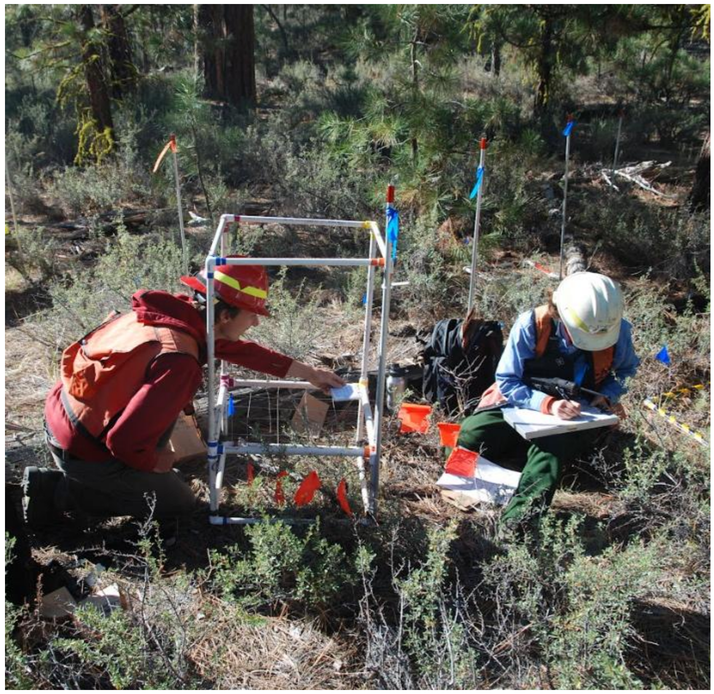

Figure 10. Ocular presence/absence sampling at Sycan Marsh Preserve, Oregon.

material was categorized into one of nineteen groups, termed fuel elements (**Table 2**). Some elements were further divided into subcategories where fuel properties differ widely within element groups, such as deciduous vs. evergreen shrubs.

Destructive biomass sampling

Biomass sampling was conducted once all scanning and documentation (photography, TLS and photogrammetry scanning) methods were complete (**Figure 11**). Vegetation was clipped for each stratum as presence/absence data was collected. The only exception was sites where prescribed burns were planned during the field campaign. At these locations, presence/absence data was collected from a random subset of plots without destructive sampling before the burn (pre-fire non-destructive plots), and the remainder was collected after the fire has passed through the area (post-fire destructive plots). For plots where biomass was sampled, vegetation was clipped beginning at the highest stratum where present, and was placed in an individual paper bag by stratum (for example, all material present in the 60-70 cm stratum was placed in a single bag), with the exception of "standing dead" material, which was placed in separate bags for transportation to the lab. If there was only a trace amount of biomass present in a voxel, it was collected as part of the stratum below. From the 0-10 cm stratum, 5 voxels were randomly selected to be sampled individually, and the remainder of the stratum was bagged as a unit. Duff, when present, was separated from litter in the field and bagged separately. Biomass collection continued until the mineral soil layer was exposed. All bags were labeled with the site name, clip plot name, date, stratum height, and fuel element if applicable.

Figure 11. Destructive sampling of vegetation in a clip plot.

Table 2. List of fuel elements used to categorize vegetation – several elements (e.g. woody leaves/litter) have sub-categories in order to allow finer distinctions (e.g. deciduous vs. evergreen). Fuel elements were grouped into broader fuel types for analysis of plot metrics based on dominant fuels, such as fine and coarse woody debris (FWD and CWD, respectively).

Fuel Element	Element sub-categories	Fuel type
Woody live shrubs/trees	Deciduous, Evergreen, Deciduous oak, Evergreen oak, Mixed oak, Mixed evergreen, Mixed deciduous, Mixed	Shrub & small tree
Woody leaves/litter	Deciduous, Evergreen, Deciduous oak, Evergreen oak, Mixed oak, Mixed evergreen, Mixed deciduous, Mixed	Forest floor
Woody standing dead shrubs/trees including conifers	NA	Shrub & small tree
Conifer live seedling/saplings	NA	Shrub & small tree
Vines (and vine litter)	NA	Shrub & small tree
Wiregrass/bunchgrass	Wiregrass, Bunchgrass, Mixed	Herbs
Other graminoids	NA	Herbs
Forbs (and forb litter)	NA	Herbs
1-hr fuel	NA	FWD
10-hr fuel	NA	FWD
100-hr fuel	NA	FWD
1000-hr + fuel	NA	CWD
Pinecone	NA	Forest floor
Conifer litter (bark flakes, pollen cones, other needles)	NA	Forest floor
Pine needles	Long, Short, Mixed	Forest floor
Duff (partially to fully decomposed litter)	NA	NA

3.2.5 Forest floor bulk density sampling

Within each of the forest sites, we randomly selected 9 overstory trees per site to evaluate how forest floor relates to crown position. Sampling transects originated at the bole of each tree and extended to outside of its projected crown (drip line). These datasets will be used to develop and evaluate models that predict forest floor biomass using tree stem and crown mapping (e.g., Sanchez et al. 2023). To randomly select overstory trees, we originated tree selection at the northwest corner of 5x5-m sample plots. To select a focus tree for each transect, we randomly set an azimuth and then located the first tree that met the following criteria (moving in a clockwise direction from the azimuth): trees had to be living and at least 15 cm DBH (**Figure 12**). Distance to the tree crown had to be within 15-30 m from each 5x5 m plot to ensure that the tree was within the TLS scanning area but far enough from the plot to avoid disturbance from foot traffic. Once a tree was located it was photographed, and GPS coordinates were collected from the base of the tree along with tree DBH (cm), height (m), height to live crown (m), and species.

Forest floor samples were measured and collected along each of two transects originating from the bole of the tree and extending in both north and south directions. Following a similar method to Banwell and Varner (2014), samples were positioned at 3 locations along each transect: 10 cm from base of the tree bole ("Bole"), half the distance between the bole and outer edge drip line of the crown ("Inside Drip Line"), and 2 m outside of the drip line of the tree being sampled ("Outside Drip Line", **Figure 13**). If tree crowns above the sampling area had a relatively closed canopy, an attempt was made to locate the third sample on a point along the transect that was outside of the drip lines of the focus tree as well as any nearby trees.

Prior to destructive sampling of forest floor layers, the sample plot was cleared of live vegetation, tree cones and downed wood, leaving litter and duff layers undisturbed. Embedded downed wood and cones were considered part of the forest floor and allowed to remain if the central axis of the material lay below the litter/duff boundary. Litter that was suspended in grass or other surface materials was not considered part of the forest floor and was excluded from the bulk density sample. A 25x25-cm sampling square was placed on the top of the litter layer, and material along the edges of the frame was carefully clipped to allow the frame to be inserted to the base of the organic soil layer (duff). Once the frame was in place, six nails (termed duff pin within our dataset) were equally spaced on a systematic grid such that the top of the pin was flush with the litter. If an obstruction such as a rock or root prevented this, we noted the distance between the top of the pin and the surface of the litter layer. Once pins were placed, the litter layer was carefully collected and stored in a labeled paper bag. At each pin location, we recorded the depth of the litter layer to the nearest mm along with the dominant litter type. Pins were then pushed further into the soil so that the top of each pin was flush with the duff layer. Duff was collected in a separate labeled paper bag, and depths were measured in the same manner.

Distinguishing between litter and duff layers can sometimes be challenging in the field. Duff is defined as partially to fully decomposed litter (Oe and Oa soil horizons) and depending on how dry and friable duff is during sampling, delineating boundaries between litter and duff can be challenging. Field crew members carefully calibrated definitions and collected material as duff where forest litter became highly fragmented with attached organic soil material, fungal hyphae, and/or evidence of decay.

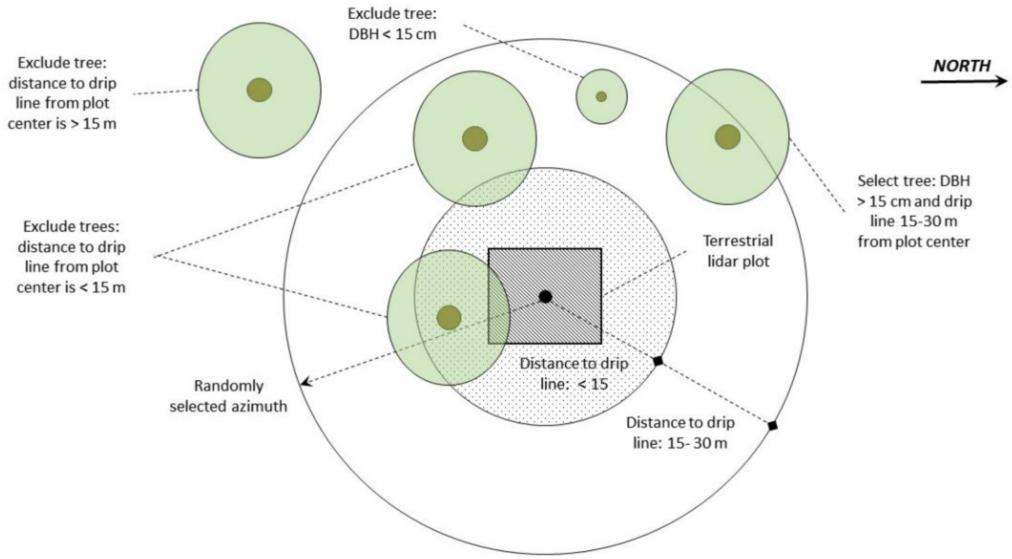

Figure 12. Tree selection for forest bulk density sampling. Trees were selected at each site by randomly selecting an azimuth at the NW corner of each 5x5 m scan plot and selecting the first tree that met our criteria.

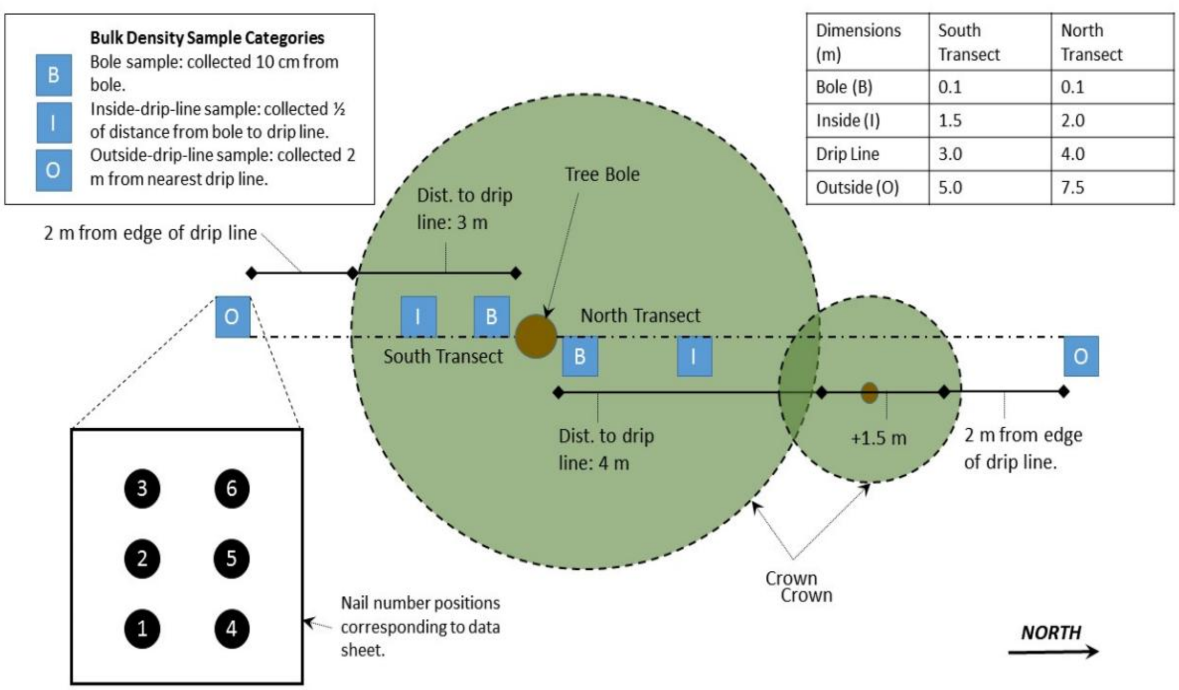

Dimensions (m)	South Transect	North Transect
Bole (B)	0.1	0.1
Inside (I)	1.5	2.0
Drip Line	3.0	4.0
Outside (O)	5.0	7.5

Figure 13. Plot layout for forest floor bulk density sampling. Samples were collected from 3 locations along two transects running to the N and S of sample trees.

3.3 3D FUELS LABORATORY METHODS

3.3.1 Airborne laser dataset acquisition

ALS data was acquired from appropriate sources depending on the site location (state database, landowner data, etc.). Tiles were merged, and the 200 x 200m site area was clipped so as to create a smaller point cloud (with a 50 m buffer) to be used in analysis. ALS point clouds were normalized using the LAStools version 230821 (https://rapidlasso.de; Gilching, Germany) lasground_new function, which classifies points as ground or non-ground, creating a bare-earth model. These files were then saved in a permanent repository.

3.3.2 Image processing and data analyses

Our workflow for image processing and calculation of point cloud metrics for TLS and close-range photogrammetry is provided in **Figure 14**. The clipping tool automatically segments plots using reflectance values and object orientation to generate spatial data and naming conventions that are based on the location of the object in the scan. These spatial data are used to clip TLS data (point clouds of field clip plots from 5x5 m scans), produce GIS layers for future clipping, and finally link GoPro-based close range photogrammetry to the proper geolocation. The laz formats are stored through cloud services, where analysis scripts process and store project deliverables.

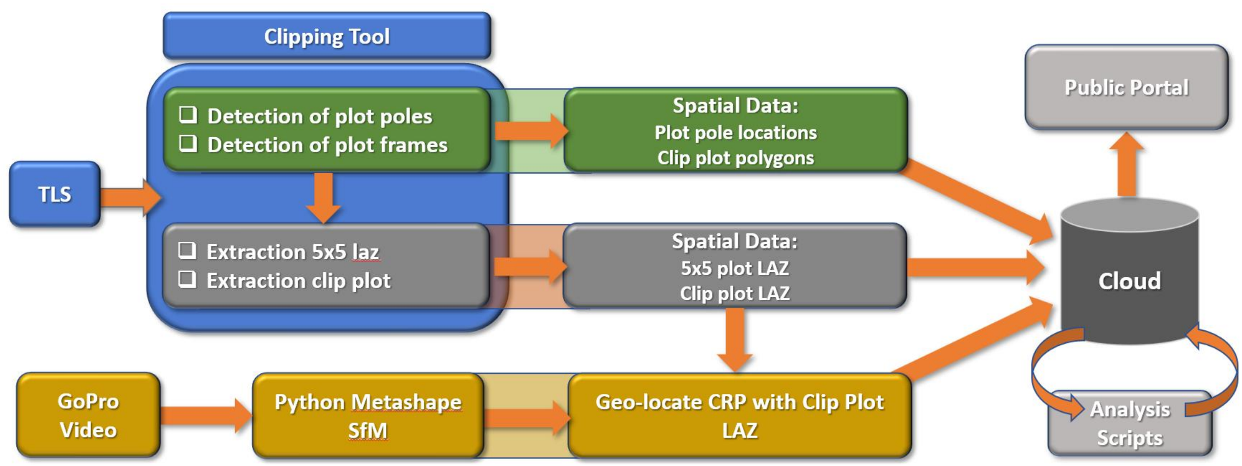

Figure 14. Image and point cloud processing workflow, where TLS data are processed through a purpose-built R tool using the Shiny package.

3.3.3 Terrestrial lidar point cloud processing

Synoptic lidar scans taken in the field were merged a single project for each site using RiSCAN PRO (www.riegl.com; Horn, Austria) the proprietary software for use with RIEGL scanners. All scans were registered and georeferenced using this software, then exported into laz files. Scans taken at the corner of each 5x5 plot were merged into a single laz of the 5x5 m area, clipped to include a 3m buffer. All scans were normalized using the LAStools version 230821 (https://rapidlasso.de; Gilching, Germany) *lasground_new* function, which classifies points as ground or non-ground, creating a bare-earth model and a digital representation of above-ground vegetation. Once point clouds were created from synoptic and plot-level scans, the files were saved with the site and plot names in a permanent data repository. Individual 0.5 x 0.5 x 1 m clip plots were clipped from the larger 5x5 point clouds using a custom-built R shiny application (R Core Team 2023). This semi-automated process uses the high reflectivity of the conduit poles and taped PVC frames in the point clouds to identify the clip plot boundaries and segment those points out of the larger point clouds. Following QAQC (see below), the shiny application was used to create both a laz file for each clip plot and a 2-dimensional shapefile of the clip plot location.

3.3.4 Photogrammetry point cloud processing

Both UAS-based and handheld photogrammetry data returns from the field in the form of high-resolution videos. We used a combination of python scripting and Agisoft Metashape Pro version 1.7.2 (www.agisoft.com) to create accurate 3-dimensional point clouds from the video formats. Python scripting was used to turn field-recorded videos into a series of still images, filtering out low-quality or irrelevant images. Once this step is completed, a technician reviews the still images to assure quality and relevance and proceeds to load the images into Agisoft. Using machine learning methods, this software tool combines ground control points, targets, and other objects visible in multiple frames as reference points to stitch together still frames taken at various angles into a 3-dimensional model of the sampled vegetation, generating a point cloud. In a last step, points inside of clip plot boundaries were segmented from the larger files using shapefiles of clip plot boundaries that were created using the custom shiny application detailed in the previous section. All point clouds were normalized using the LAStools version 230821 (https://rapidlasso.de; Gilching, Germany) *lasground_new* function, which classifies points as ground or non-ground, creating a bare-earth model a digital representation of above-ground vegetation.

3.3.5 Point cloud quality assurance

Several approaches were employed to ensure that voxel plot point clouds were correctly assigned plot names as surveyed and sampled during field data collection. Principally, this was done by comparing voxel occupancy of point clouds to visual occupancy measured in the field during sampling. This was accomplished by calculating percent occupancy for both datasets by stratum and comparing the resulting values using equivalence testing and linear modeling, pooled by 5x5 m plot. An additional visualization method was employed to ensure point clouds were correctly oriented, and no extraneous objects such as conduit poles (which could add error to models) were included in the point clouds. This method uses a custom-built R shiny application (https://depts.washington.edu/fft/plotviewer) that allows for a rapid comparison between clip plot photos, imagery derived from field presence/absence data, and both TLS and SfM point clouds (**Figure 15**).

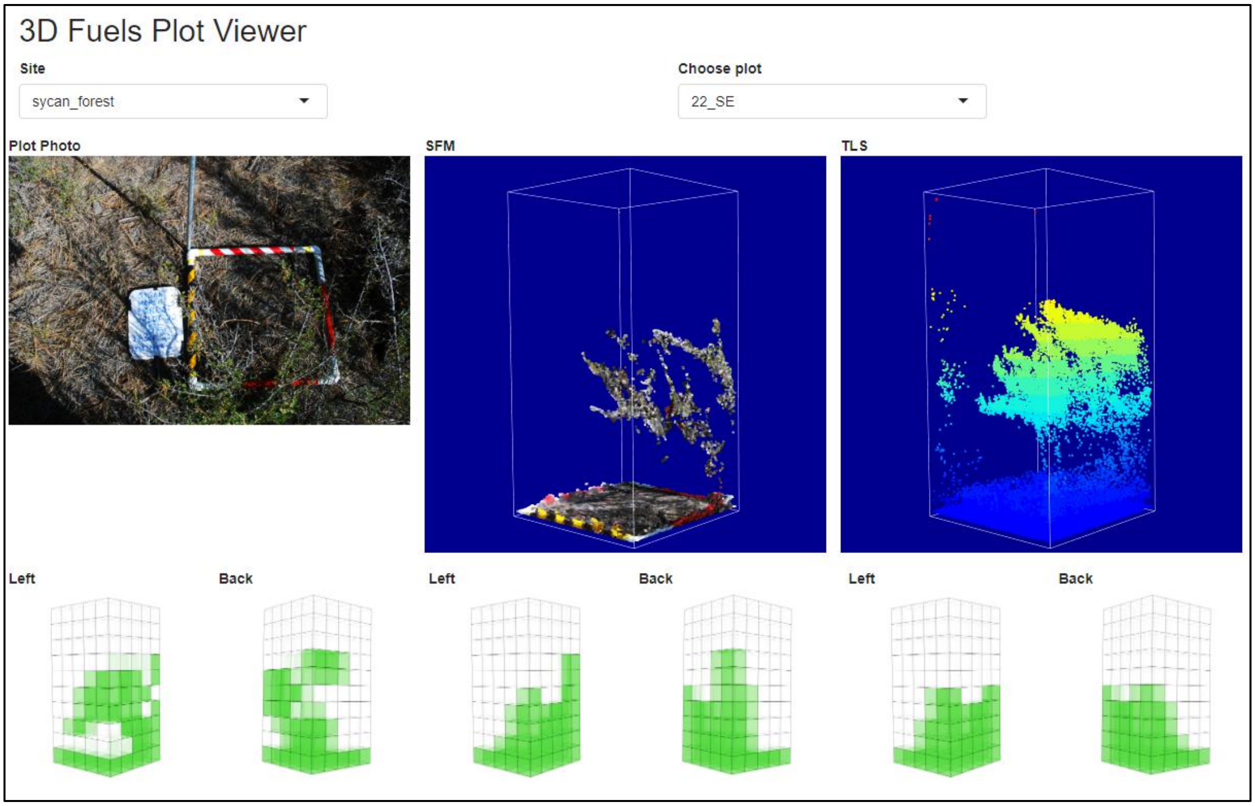

Figure 15. Image from viewing tool used for quality assurance of TLS and SfM point clouds, comparing plot photo, point cloud visualizations, and voxelized imagery representing each clip plot.

3.3.6 Biomass processing

Once received in the lab, biomass sample bags were placed on wire racks to facilitate drying. The contents of each bag were sorted into the component fuel elements, with each element placed into a labeled tin for oven-drying and subsequent weighing. Custom data sheets listing elements recorded in the field were populated from ocular presence/absence data for each clip plot to facilitate data entry. Missing elements were marked as such, as well as any new elements not recorded in the field if found in samples. Using mechanical convection ovens (Blue M 146 Series Inert Gas Mechanical Convection Oven, Thermal Product Solutions, White Deer, PA), fuels were dried at 70° C for 48-72 hours (or until its weight ceased to change), depending on fuel density (fine fuels were typically dried for 48 hours, 100-hour and 1000-hour time lag fuels and duff were typically dried for 72 hours). Calibrated balances (Ohaus Adventurer ARC120, Ohaus Corporation, Pine Brook, NJ) capable of accurately measuring weights down to 0.1 g were used for sample weighing. Samples were weighed immediately following removal from drying ovens (this prevents weight changes due to moisture absorption from ambient air). Dry biomass values from each sample were entered into custom datasheets by trained technicians.

3.3.7 Forest floor sample processing

Forest floor samples of litter and duff were treated much like litter and duff samples from clip plots, though litter samples were not sorted. Once received, samples were stored in paper bags on wire racks to facilitate air drying and reduce the risk of biomass loss due to decay. Litter samples were oven-dried at 70º C for 48 hours and weighed as a unit for calculation of dry biomass.

Following air drying, each duff sample was placed and dispersed within a 2mm mesh soil sieve, which was then gently tapped for 20-30 seconds to allow finer material to fall through, and visually inspected to remove any mineral soil aggregates or rocks. Portions of each sample that did not fall through the coarse sieve and contained no visible soil particles were deemed to be "pure" duff (uncontaminated by mineral soil) and was dried and weighed 70C for a minimum of 72 hrs. The remaining sample was sieved again with a finer (750µm to 1mm) sieve to remove loose mineral soil particles, which were disposed of. The remainder was a duff-soil mix, which was transferred to a pre-weighed tin and dried and weighed according to the protocols outlined above.

These contaminated samples required further processing to determine duff content, and were sent to the University of Washington Soil Analytics Lab for analysis. Each sample was then ground to ensure homogeneity, and a subsample was taken for analysis. Using an elemental analyzer (2400 Series II CHNS/O, PerkinElmer, Waltham, MA), the carbon fraction of each sample was determined; this was used to calculate the proportion of the sample mass that consisted of organic matter. This proportion was then applied to the dry weight of the original sample for a final calculated dry duff biomass value consisting of the "pure" sample and the pure duff fraction of the mixed sample. This value was entered into the same database that was used for biomass values of other samples collected in the field.

Litter and duff depths, sampled at the 6 pin locations, were averaged and then multiplied by the dimensions of the sampling square (0.25x0.25m) to estimate sampled volume for each litter and duff layer. Bulk density of litter and duff layers was then calculated as dry weight biomass per unit volume (kg m^{-3}).

3.3.8 Data entry quality assurance

Data entered from field-collected presence/absence data and biomass underwent a stringent quality control procedure to ensure data quality. All data quality assurance was conducted by a different team member than the person that initially entered the data. Electronic data entered into the database was compared to paper datasheets completed in the field. Biomass data (for which paper copies were not created) was checked for completeness and consistency with presence/absence data from field surveys.

3.4 3D FUELS DATA SUMMARIES AND STATISTICAL MODELING

3.4.1 Fuel typing

Using a combination of data-driven (using biomass values for 0-10 strata) and observational (using clip plot images) methods, each plot was assigned a dominant fuel type that described its vegetative composition. For the 0-10 strata, dominant fuels could be determined using biomass values for each fuel element, as that level of detail was available in the data. For strata above 10cm, where fuels were not sorted by element, high-resolution photographs were examined separately by two people for agreement on perceived dominant fuels. For fuel typing purposes, fuel elements were grouped into broader fuel types (e.g. shrub litter and needles were put into a larger "forest floor" category, **Table 2**).

3.4.2 Point cloud metrics

For image analysis and modeling, the 3D Fuels team calculated and evaluated a range of 3D Fuels metrics (**Table 3**) to relate structural metrics based on TLS and close-range photogrammetry point clouds. To model relationships between point cloud metrics and measured fuel biomass and bulk density, we first normalized TLS and close-range photogrammetry datasets to correct for terrain and then clipped point clouds to the 0.5x0.5x1.0 m voxel plot used for destructive sampling.

Voxel-based field data were summarized into two metrics including total occupied volume (Field OV) and field height. Field OV was defined as the number of voxels containing any of the inventoried fuel types divided by 250, the total number of voxels in the 3D sampling frame. Each plot was also attributed with a Field Height metric, determined by first taking the maximum occupied height as a function of stratum position of each vertical 'column' of voxels (voxels with the same x and y position), then taking the mean of the maximum heights across all 25 vertical voxel columns per plot. Biomass and bulk density were also summarized by each 10-cm stratum of the voxel sampling frame (e.g., 0-10cm, 10-20 cm, etc.). Point-cloud metrics included occupied volume, fuel height, horizontal and vertical projected area density, surface area and volume. Metrics shared between TLS and close-range photogrammetry point clouds are listed and defined in **Table 3** and described briefly here.

Porosity

Based on the intensity of laser returns, point cloud densities are much higher in TLS than close-range photogrammetry and can penetrate through more fuel complexes than structure-from-motion photogrammetry. As such, TLS metrics can also be developed to evaluate the relative porosity of fuels (e.g., Rowell et al. 2020). For example, sparse fuels are generally highly porous (e.g., grasses, scattered shrubs) whereas tree trunks, dense litter layers and mineral soil have low porosity. Porosity is basically calculated as an indexed ratio of the sum of occupied volume over the total volume. As a 3D metric, porosity can be directly related to the bulk density of vegetation and scaled to gridded inputs to QUICFire, FIRETEC and FDS. In our application, a porosity index is estimated for each 10x10x10cm voxel cell. The original porosity calculation developed at Pebble Hill, Georgia USA (Rowell et al. 2020) assumed interpolation of TLS points to a 1 cm voxel array capture both external volume and to a limited degree internal occupied volume of a segmented object per unit volume (Equation 1)

$$\boldsymbol{Porosity\ Index}\ (\lambda) = 1 - \frac{\sum OV_{1cm}}{Volume\ 10cm^3}[j] \qquad \text{Equation [1]}$$

Where porosity (λ) is the ratio of the sum of occupied 1cm voxels with the volume of a $10cm^3$ cube subtracted by one to calculate the amount of open space within the cube for voxel [j].

Sensitivity analyses in the 3D fuels project suggested high levels of point resolution variability from the TLS scans collected at the 3D Fuels sample sites and missing data within TLS sampled fuel objects that an alternative calculation was needed. The revised porosity calculation calculates occupied volume as a function of a mesh wrapped around points in 0.25 cm increments for the first strata of fuels (**Figure 16**). Strata include mesh wrapping for 0-0.25cm, 0.25-0.05 cm, and 0-0.10 cm. Discrete wrapping of the mesh per strata produces improved wrapping around points and maintains gaps and isolated points versus more smoothed representations of the mesh when all points are included.

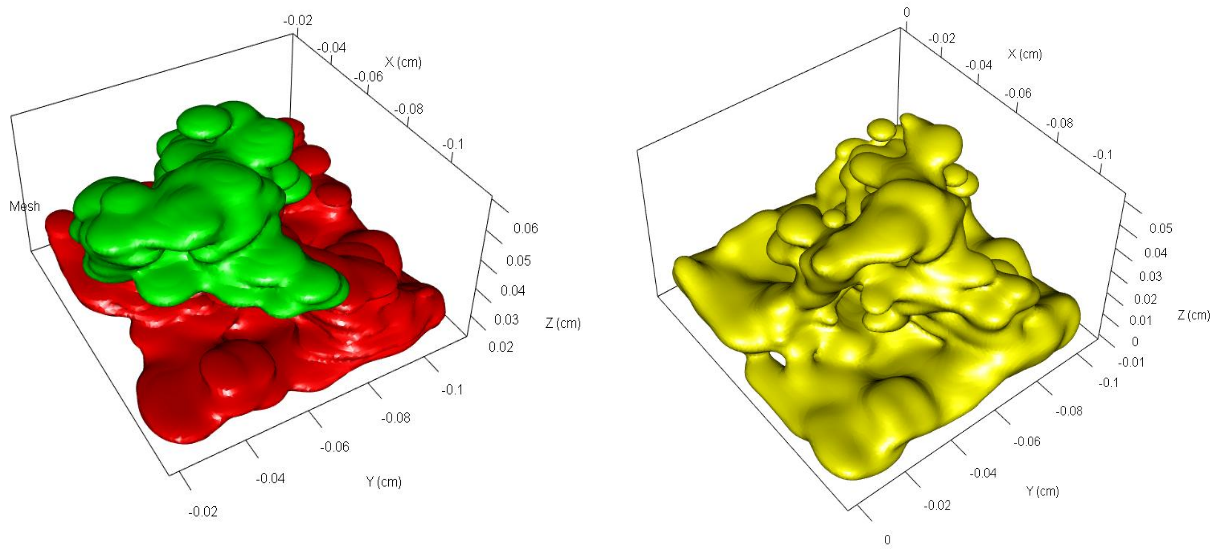

Figure 16. Implementation of the mesh algorithm for the revised porosity metric where discrete meshing of TLS data for multiple heights ensures fine-scale characterization of occupied and unoccupied space (left), versus more averaged representation using all points for the full 10cm^3 volume (right).

The revised porosity metric is described in Equation 2.

$$\boldsymbol{Porosity\ Index\ Rev}\ (\lambda) = 1 - \frac{MV}{V_s}[j] \qquad \text{Equation [2]}$$

Where porosity (λ) is the ratio of the mesh volume with the variable volume of a domain of 10cm^2 multiplied by 2.5, 5, and 10 cm subtracted by one to calculate the amount of open space within the domain for voxel [j].

Occupied Volume

Occupied volume calculated from point clouds has demonstrated moderate to strong relationships to biomass in previous studies (Wallace et al. 2017, Hudak et al. 2020, Rowell et al. 2020). To determine point-cloud based occupied volume (SfM OV) for each plot, we first used the voxR package in R to segment each point cloud into 10-cm^3 voxels. We chose this resolution to enable a direct comparison between point cloud and field-derived occupied volume, which was captured at the same resolution. Occupied volume for each point cloud was calculated by dividing the number of occupied voxels (voxels containing at least one point) by the total possible number of voxels (n = 250) for each plot.

Fuel Height

Height of vegetation is commonly used in field- and lidar-based allometric equations to aid in biomass estimation (Brown, 2002; Chave et al. 2005). We used voxelization from the occupied volume calculation as a basis to determine fuel height (PCM Height) for each of our plots. First, we subset each point cloud into 25 vertical voxel columns (voxels with the same *x* and *y* positions). For each column, we calculated the height of all points within that column, and determined the overall plot height by taking the mean of all column values. We used 99th percentile height rather than absolute maximum height for each column to avoid any potential outliers or artifacts caused by poor rendering of the models.

Horizontal and Vertical Projected Area Density

Horizontal projected area density (HPAD) is a metric similar to plant area density (Hosoi and Omasa, 2012) akin to a top-down view of each point cloud that measures plot occupancy based only on voxels in the *x* and *y* dimensions. Unlike PCM Height and PCM OV, which were calculated at a 10-cm voxel resolution to match field sampling, we calculated HPAD at a 1-cm voxel resolution to capture additional detail in point cloud models. Vertical projected area density (VPAD) is a similar concept to HPAD, but instead of flattening our plot in the *x* and *y,* we consider the occupancy of our plot as a 2D grid of voxels flattened in the *x* and *z.* As with PAD, PADV was calculated at a 1-cm voxel resolution using the voxR package in R.

Surface Area and Volume

We used the 'convhulln' function in the geometry package in R to generate a surface area (PCM SA) and volume (PCM Vol) metric for each plot. This function uses a convex hull approach to drape a minimum-bounding shell of facets over all points in each model and has shown promising relationships for biomass estimation in shrubs (Olsoy et al. 2014). To exclude ground points from surface area and volume calculations, we implemented a threshold so that only points at least 10 cm above the ground were considered in the calculation. Where no points at least 10 cm above the ground were present, as in timber litter dominated plots, surface area and volume values of 0 were returned.

Table 3. Structural metrics calculated from 3D TLS and close-range photogrammetry models and field-based voxel sampling data.

	Metric	Abbreviation	Description
Point Cloud Metric			
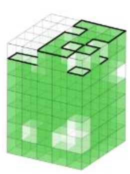	Fuel height	PCM Height	Mean value across the 99th percentile height of all points within each vertical voxel column (25 columns total, where each column is 10 cm in the horizontal *x* and *y* directions, 100 cm in the vertical *z*)

	Metric	Abbreviation	Description
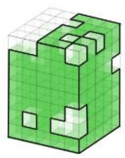	Occupied volume	PCM OV	Total *n* occupied 10 cm^3 voxels divided by total possible voxels (*N* = 250)
	Projected area density	PCM PAD	Total *n* occupied voxels when only voxelization in the *x* and *y* dimensions is considered; akin to a top-down view of each plot to assess horizontal continuity. Calculated at a 1 cm^3 resolution.
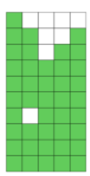	Projected area density - vertical	PCM PADV	Total *n* occupied voxels when only voxelization in the *x* and *z* is considered; akin to a side view of each plot to assess horizontal and vertical continuity. Calculated at a 1 cm^3 resolution.
	Surface area	PCM SA	Surface area of the smallest minimum-bounding shell (hull) of facets over all points greater than 10 cm in height
	Volume	PCM Vol	Volume of the interior 3D hull generated from surface area calculation
Field-Based Metric			
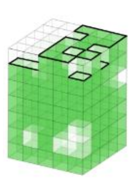	Fuel height	Field Height	Mean value of the maximum occupied height of each vertical voxel column (25 columns total, where each column is made of vertical stacks of 10

	Metric	Abbreviation	Description
			cm^3 voxels with the same *x* and *y* position)
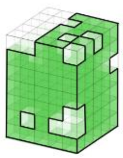	Occupied volume	Field OV	Total *n* occupied 10 cm^3 voxels divided by total possible voxels (*N* = 250)

3.4.3 Predicting surface fuel biomass from 3D point cloud metrics

The objective of this analysis was to use terrestrial lidar scanning (TLS) calibrated with destructive sampling to create fine-scale 3D maps of live and dead understory fuels in pine-dominated forests of the southeastern and western United States. Using calibration plots in which fuels were typed and destructively sampled in volumetric sampling cubes, called voxel plots, we first evaluated a number of TLS-based metrics to model bulk density (g m^{-3}) across major fuel types including timber-litter, grass, shrub, and complexes of understory fuels. We then applied models of TLS-based metrics to scan-only plots and synoptic scale TLS scans to compare the relationships between close range scanning and scans with increasingly oblique and lower point cloud densities. As TLS and SfM imagery becomes more widely accessible, relationships between metrics based on 3and fuel properties are needed in order to translate point clouds into 3D maps of fuels and properties relevant to fire behavior modeling including biomass/bulk density and surface area to volume ratios.

Traditionally, assessments of understory fuel structure to quantify biomass have been conducted in-field through visual estimation (https://depts.washington.edu/nwfire/dps/) or the use of point-intercept or transect sampling, which can be time consuming and error prone (Keane et al. 2013, Keane 2015). Although these methods have proven useful for coarse grain estimations and modeling, they are inherently abstractions of fuel conditions and largely fail to capture the fine-scale heterogeneity required for 3D fuel inputs to computational fluid dynamics modeling of fire behavior (Hiers et al. 2009; Loudermilk et al. 2009). As such, development of a more accessible, efficient, and reliable method to characterize fine-scale fuel structure and quantify biomass is needed. Satellite and airborne remote sensing methods – including airborne lidar, unoccupied aerial surveys (UAS), and UAS-derived photogrammetry – have been used extensively to quantify canopy fuels in 3D but are largely insufficient for understory fuel characterization due to canopy obstruction and inadequate spatial resolution (Bright et al. 2017)**.** Ground-based remote sensing methods such as terrestrial lidar scanning (TLS) have demonstrated accuracy in capturing understory fuel structure and have been used to quantify vegetation structure, biomass, and leaf area with high accuracy (Loudermilk et al. 2012, Greaves et al. 2015, Cooper et al. 2017, Calders et al. 2018, Rowell et al. 2020)**.** Despite this reliability and precision, TLS scanning instruments are high-cost, laborious to operate, and survey-grade instruments can be difficult to maneuver in rough or remote terrain (Liang et al. 2016).

SfM photogrammetry, in which overlapping images are arranged to create a 3D point cloud, has shown promise as an accessible alternative to field-based sampling and more expensive ground-based remote sensing techniques**.** Simple summary metrics of SfM point clouds such as height and occupied volume have been used to quantify 3D structure of fuels such as grasses, shrubs, fine woody debris, and tree diameter with moderate accuracy (Bright et al. 2016; Wallace et al. 2017, Piermattei et al. 2019). As an emerging approach for forest inventory analysis, previous methods used to generate SfM point clouds have relied on the collection of dozens of still photographs taken individually by a camera from multiple viewpoints at consistent distances over several minutes. While this approach provides an advancement over more time-consuming, traditional field-based sampling, evaluation and refinement to the SfM data collection technique itself are warranted.

In this study, we compared predictive models of surface fuel biomass from TLS and SfM point cloud metrics (detailed in 3.4.2) based on clipped point clouds representing each destructive voxel plot (0.5x0.5x1.0 m). Simple linear regression models were produced for all point cloud metrics to evaluate: 1) which point cloud metrics had the strongest relationship to surface fuel biomass, and 2) how point clouds performed for the entire voxel plots, including the 0-10cm stratum containing litter and duff layers compared to biomass contained within the 10-100cm strata, and 3) if stratifying fuels into dominant fuel types (i.e., shrubs, herbs, or timber-litter) improved model fit.

3.4.4 Predictive relationships between forest floor characteristics and tree crown position

We conducted an analysis to inform statistical models that relate overstory tree crown cover to forest floor characteristics, including litter and duff depth, biomass, and bulk density, in pine forests that are common to prescribed burning programs in the US. Existing literature demonstrates how variable litter and duff depth and biomass can be across all scales of inference – from high reported variables at submeter scales to high variability within forest patches (Hille and Stephens 2005, Kreye et al. 2014). A small number of studies have been conducted to measure relationships of forest floor depth, biomass and bulk density to tree crowns. Of these, Banwell and Varner (2014) have one of the most robust samples of accumulated duff in four long-unburned Jeffrey - white fir forest sites of Lake Tahoe Basin, California. A similar study was conducted to characterize accumulated litter and duff mounts around old sugar pine trees in the western Klamath of California (DiMario et al. 2018; Banwell and Varner 2014). In an earlier study, Hille and Stephens (2005) sampled pre-burn duff depth and post-burn consumption along systematic transects from focus pine trees in young, mixed conifer forests also within the Sierra Nevada range, CA. All studies reported statistical differences between forest floor accumulations and distance from tree crown.

This study was conducted within the larger 3D Fuels project an incremental step towards more comprehensive datasets on forest floor characteristics related to tree crown position - and one that will need more datasets to inform robust statistical inferences across forest types common within wildland fire management and smoke planning. Relationships between forest floor characteristics and transect position were evaluated using analysis of variance tests for significant mean differences between depth, biomass, and bulk density of litter and duff layers and transect position (bole, inside, and outside). Simple linear regression models were used to evaluate statistical relationships between depth and biomass for litter and duff layers.

3.5 QUANTITATIVE STRUCTURAL MODELING OF COMMON SHRUBS IN THE SOUTHEASTERN US

Accurate characterization of shrub architecture is important for understanding how architectural traits affect ecosystem dynamics and processes. In this study, conducted by M. Bester as part of her dissertation work (Bester 2022), we investigated the accuracy of shrub architectural traits derived from QSMs, developed using TLS data. The shrubs selected to investigate the QSM reconstructions came from a plant nursery in Pittsburgh, PA. We based our selections to ensure a wide variety of geometrical and architectural traits, choosing ten shrubs with different heights, complexities, branching patterns, and crown shapes.

3.5.1 Scanning

To prepare shrubs for scanning and measurement, we picked off all leaves from branches exposing the architectural form of each shrub. By only having the woody structure we can determine how well the QSM can delineate the shrub architecture, without it being occluded by leaves. We then manually measured the aboveground height of the leaf-off shrubs to the closest centimeter (cm). Additionally, we recorded the DBB (diameter before branching) of the main stem(s) and the diameter of shrub branches to the nearest millimeter using a digital Vernier Caliper.

We used a FARO® Focus S350 terrestrial laser scanner to acquire leaf-off scans of shrubs (FARO Technologies, Inc., www.faro.com). This scanner is compact, lightweight, and specifically designed for indoor and outdoor applications. The instrument's performance specifications include field of view of 300° vertical and 360° horizontal, wavelength of 1550 nm, beam divergence of 0.3 mrad (1/e), and ranging error of approximately 1 mm. In addition, the scanner has an integrated camera, which acquires high-resolution RGB images that can be coregistered post-scanning.

3.5.2 Quantitative structural modeling

The purpose of the shrub reconstruction is to reflect the architecture of the shrub, including its 3D geometry and topology. Our reconstruction procedure consisted of a multi-step process. First, we extracted the point cloud and converted it into a useable modeling format. We co-registered the four individual point cloud scans at each of the two resolutions (low and high) using FARO® Scene software (FARO® SCENE software) and created a bounding box around each individual shrub. We then extracted and exported low- and high-resolution point clouds for further analysis in CloudCompare (v 2.12). In CloudCompare, we removed features unrelated to the aboveground shrub biomass and then applied a noise and statistical outlier removal filter to create final point clouds.

We then applied the *TreeQSM* algorithm to the cleaned individual shrub point clouds to generate QSM representations of the high- (hereafter referred to as QSM_H) and low-resolution (hereafter referred to as QSM_L) datasets. *TreeQSM* is open-source code developed by Pasi Raumonen and available via Github (https://github.com/InverseTampere/TreeQSM, Raumonen and Åkerblom 2022). The algorithm is a semi-automatic script run within MATLAB software (*MATLAB*, 2018). The *TreeQSM* approach includes a random function, resulting in a slight variation each time the model is run, even when the parameters remain unchanged (Calders et al. 2015). Therefore, we ran the model twelve times for each shrub, and at each resolution, in order to characterize the distribution of results generated.

3.6 RELATIONSHIP BETWEEN TLS REFLECTANCE AND LITTER FUEL MOISTURE

3.6.1 Objectives

Intensity values of TLS sensors have been used to quantify many different variables of interest in live vegetation. Much the same as how vegetation spectral indices from images (such as NDVI) can be used to quantify vegetation health, leveraging relationships between different laser wavelengths of TLS units can also provide information on live leaf health and location. Lidar sensors of differing laser wavelengths can be used in conjunction with each other to provide an index based on intensity values to more easily separate out leaves from stems (Danson et al. 2014; Hancock et al. 2017). TLS intensity values have also been used to quantify the moisture content of live leaves, using a dual wavelength approach to account for energy loss due to distance traveled (Junttila et al. 2017, Elsherif et al. 2019). While TLS intensity values have been shown to be related to moisture content on many different levels, leveraging this relationship to quantify moisture gradients in dead forest litter from a single vantage point has yet to be fully explored (**Figure 16**).

For this study, which was conducted by J. Batchelor as part of their dissertation work (Batchelor 2023), we used 1550-nm wavelength terrestrial lidar scanners because of the sensitivity of that wavelength to moisture, and we also evaluated two types of TLS units: a time of flight (TOF) and phase-shift (PS; Raj et al. 2020). A TOF lidar unit sends out a discreet pulse of energy and records the time it takes for the pulse to be reflected off a surface. Using the known speed of light, the object distance is calculated (Raj et al. 2020). The advantage of TOF units is that multiple returns can be recorded for each pulse sent as a partial reflection of the energy that is still recorded. The disadvantages are that surfaces at proximity are often distorted and that each pulse must be returned before the next can be sent out. A PS lidar unit emits a laser beam with additional modulated wavelengths of light, and distance is calculated based on the sent and received waveform. PS tends to be faster with less distortion at close distances, but they tend to have a more limited range, mainly due to energy requirements. The different technologies produce slight differences in how intensity values are calculated (Calders et al. 2020, Suchocki, 2020).

TLS has been used extensively for fine-scale modeling of forest structural elements. Using TLS to quantify the location and amount of potential wildfire fuels is a topic that has seen extensive research (Loudermilk et al. 2009, Rowell et al. 2015). However, using TLS intensity returns for characterizing the condition of wildland fuels has not been fully explored. For a TLS unit using 1550 nm laser light, the amount of energy from a TLS pulse that is reflected off a surface should decrease by absorption of energy as surface moisture increases. Just as IR radiation at 1550 nm from the sun is absorbed, and not reflected, by water vapor and thin layers of water, the same principles hold true for IR radiation generated from a laser (Ponomarev et al. 2001). TLS has been used to detect moisture in building materials and mapping moisture movement in buildings by comparing relative changes in intensity values of returns (Suchocki et al. 2018). Phase-based TLS units have been successfully used to quantify surface moisture levels on a sandy beach (Jin et al. 2020).

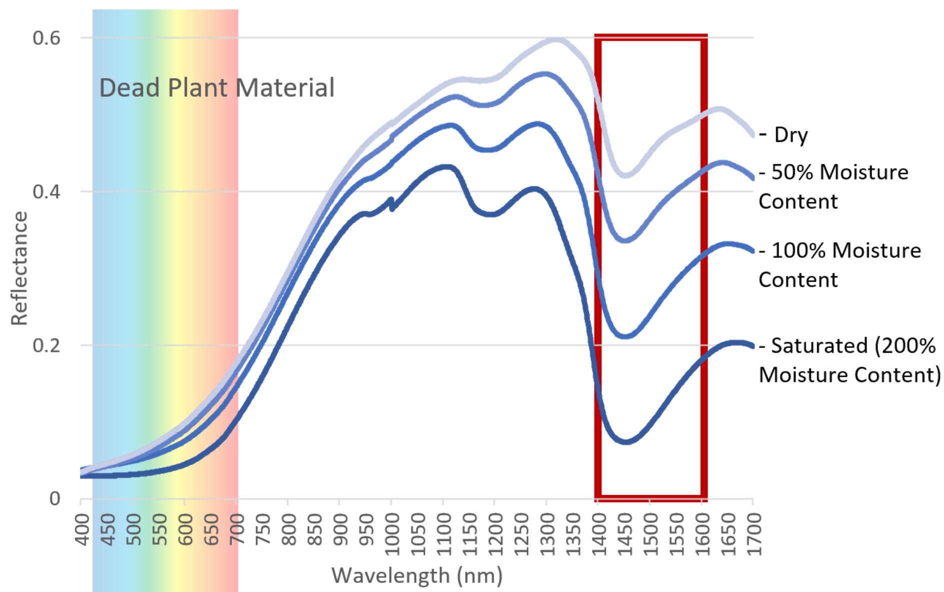

Figure 16. Conceptual diagram of the reflectance of dead vegetation when it is fully saturated with water to when it is dry. The red box is the section of the NIR electromagnetic spectrum that has the greatest change as vegetation dries (1400 – 1600nm).

3.6.2 Study design

Six unique materials were used to evaluate the relationship between lidar reflectance and fuel moisture, including four common forest litter types and two controls (**Table 4**). Litter beds were constructed from senesced needle and broad leaf material collected from forest locations in Washington and northern Florida. Litter types included Douglas-fir (*Pseudotsuga menziesii*) needles, longleaf pine (*Pinus palustris*) needles, southern red oak (*Quercus falcata*) leaves, and ponderosa pine (*Pinus ponderosa*) needles. Litter samples were air dried and sorted to remove any foreign particles. When assembling leaf litter trays, care was taken to ensure that the litter completely occluded the tray to ensure all point returns were plant material and not the underlying tray. Sample trays were constructed of a non-porous white plastic material measuring 30cm x 30cm x 5cm with a fine mesh screen as the base to allow for draining of water. Sixteen samples (trays) of each litter type and control material were assembled. The two controls, milled pine wood and fabric mesh, were used to assess the influence of scan angle on intensity of returns. The fabric mesh consisted of uniform layers of cotton cheese cloth (a gauze-like material) to mimic the porosity of forest litter. The other control material was milled, untreated pine board approximately 30 cm x 30 cm x 1.5 cm in size. Three of the sixteen Douglas-fir samples were removed from the analysis due to fine soil contamination that impacted reflectance values.

3.6.3 Laboratory scanning and analysis

The fuel moisture experiment was conducted at the Pacific Wildland Fire Sciences Laboratory in Seattle, WA. All samples were fully saturated by soaking them in water for a minimum of 24 hr in polyethylene bags. For scanning, samples were arranged in sets of four and placed at 3m, 6m, 9m, and 12m distance from the scanners (**Figure 17**). Samples were scanned simultaneously with PS and TOS units at 0 degrees (parallel to the ground) at each distance. Control surfaces were additionally scanned at 45 degrees and 90 degrees (perpendicular to the ground). The weight of each sample was recorded, then samples were rotated to the next defined distance and the process was repeated three times, such that each sample was scanned at all four scan locations.

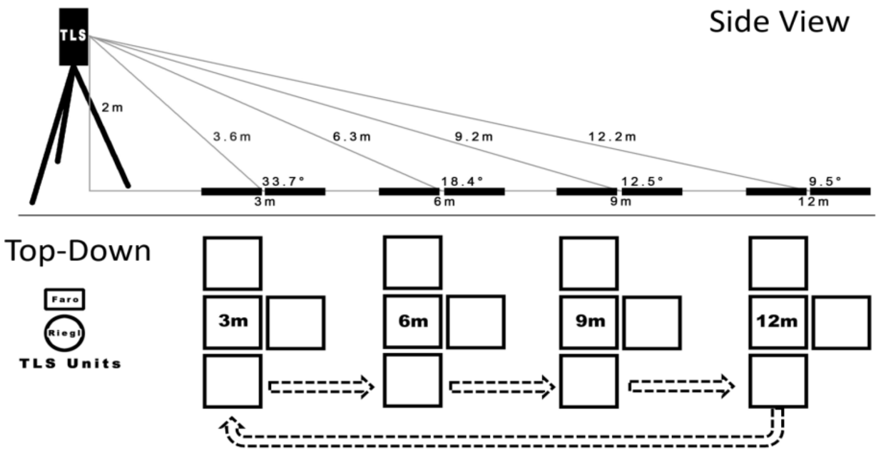

Figure 17. Layout of samples during scanning. Samples were moved in groups of 4. The arrow indicates the rotation direction used to scan every sample, at every location, at every time period. Sample orientation is referred to as 0 degrees which is perpendicular to the ground, but the angle to the scanner decreases as distance from scanner increases.

After the initial scan (hr 0), the process was repeated at the hourly time intervals of 1, 2, 4, 8, and 12 hr since removal from the water bath, and then repeated every 12 hours until samples reached equilibrium moisture content with the ambient relative humidity (i.e., their weight stabilized and was no longer decreasing due to water evaporation). Between scan times, samples were placed in a climate-controlled room with ~25% relative humidity to allow for gradual drying. Drying times varied by material type. Once samples reached a stable weight, they were placed in a drying oven set at 50˚C until samples achieved a constant weight (48 hr). A final set of scans was conducted immediately following the removal of samples from the oven, and then oven dry weights were collected. Sample moisture content was calculated by dividing the weight of the sample recorded during the drying process with the final oven dried weight.

An ASD-brand FieldSpec 4 Wide-Res Field Spectroradiometer with a spectral resolution of 30 nm at 1400 to 2100 nm was used to collect spectral information for each sample to compare with lidar-based reflectance values. The spectrometer lens was placed 33 cm above the tray at a perpendicular angle and an 8-degree lens was used to sample the approximate central 9 cm of each tray. The spectrometer was used when the samples were rotated through the 6 m distance location. It was logistically infeasible to collect spectral reflectance curves of every sample at every distance at each time interval. Sample trays were individually taken into a dark room dedicated for the spectrometer using a tungsten bulb as a light source (approximate wavelength range of 320 nm to 2400 nm). Samples were checked to ensure that there were no gaps exposing the tray bottom. The white material of the tray sides likely reflected non-sample light back into the spectrometer sensor; this reflective phenomenon was same for all trays, thus constant. Moreover, for this study we were only interested in the relative change in each sample as it dries, and not gaining a true and precise measurement of the spectral signature for each sample material. In maintaining a consistent sampling environment and procedure, relative change in spectral reflectance between samples was measured.

Table 4. Scanning intervals, starting with the time samples were removed from water bath (0). OD refers to oven dry. N is the total number of sample trays clipped from all lidar point clouds and the number of weights recorded. Only the controls were scanned at angles different than 0.

Sample type	Scan intervals	Angle	N*
Pine board (PB)	0, 2, 4, 8, 12, 24, 48, 72, 120, OD	0, 45, 90	3840 – lidar 1280 – weight
Fabric mesh (FM)	0, 2, 4, 8, 12, 24, 36, 48, OD	0, 45, 90	3456 – lidar 1152 – weight
Douglas-fir (DF)	0, 1, 2, 4, 8, 12, 24, 36, 48, OD	0	1280
Ponderosa pine (PP)	0, 1, 2, 4, 8, 12, 24, 36, 48,120, OD	0	1408
Longleaf pine (LLP)	0, 1, 2, 4, 8, 12, 24, 36, 48, OD	0	1280
Southern red oak (SRO)	0, 1, 2, 4, 8, 12, 24, 36, OD	0	1152

*Number of samples = Number of scans (4 distances) * number of trays (16) * scan intervals * 2 scanners (FARO and RIEGL) * 3 angles (PB and FM only)

Two 1550-nm wavelength TLS scanners including a time-of-flight RIEGL vz-2000 unit and phase-shift FARO s350 unit were used. The scanning resolution settings of the FARO and RIEGL were chosen to provide a scanning time of approximately 3.5 min. The FARO scanned at a lower resolution than the RIEGL. A short scan time was prioritized over matching scanning resolution to minimize the evaporation of water from the samples as they were rotated trough the 4 scanning locations of each time interval. The number of points per sample decreased as distance from the scanner increased in relation to the scan angle increment of each scanner (**Table 4**). The minimum number of points per sample tray was sampled at 12 m from the FARO unit (~900 points) and the maximum number of points per sample tray was sampled at 3 m from the RIEGL scanner (~103,000 points). The total area effectively sampled with each laser pulse also increased with distance as the laser footprint increased due to both the distance from the scanner as well as the angle of incidence. TLS units were placed as close as possible to each other (~20 cm) and were run simultaneously when scanning. This design was developed to balance the need to gather data rapidly (as the samples were actively losing moisture while TLS scanning was taking place) with the need to have sufficient replicants for statistical inference.

3.6.4 Image processing

The FARO software "Scene" (FARO, 2021) and RIEGL software "Riscan Pro" (Riegl, 2021) were used for the initial processing and conversion of the proprietary file formats into a las format. To ensure that all valid returns from the sample trays were preserved, point cloud filtering was not conducted. This inclusive processing method included some amount of noise from edge effects and errant reflected laser light. However, it was deemed better to use all point returns to ensure all valid returns were included rather than try to filter out noise and subsequently remove valid point returns.

RIEGL intensity values for points ranged from 0 to 50 and FARO intensity values ranged from 0 to 32,767 (scaled to a 15 bit radiometric resolution). After initial processing, the program "CloudCompare" ("CloudCompare," 2019) was used to crop out all points that were returns inside each sample tray. Care was taken to ensure that no points that no returns from the sample trays or tray bottoms were included. Intensity values were normalized between the FARO scans and the

RIEGL by dividing each intensity value by the maximum value present in each scan. The normalization process scaled the intensity values between 0 to 1 for easier comparison between the two scanners. The intensity metrics derived per sample were mean, median, 95th percentile, standard deviation (SD), variance, and skew.

An averaged spectral signature from the spectrometer sampling was created for each sample type at each sampling interval (e.g., the average value of each wavelength for all 16 ponderosa pine needle litter samples at the 2-hr scan time interval). The reflectance values for each sample at 1550 nm was determined and compared with the moisture content recorded for all samples at the 6-m distance. Simple ordinary least-squares (OLS) regression analysis was performed to determine if reflectance measured by the spectrometer (response) had a significant relationship with moisture content (predictor). Reflectance values recorded by the spectrometer were also compared with the TLS intensity metrics recorded for all samples at the 6-m distance. Simple regression analysis was performed to determine if there was a significant relationship between the spectrometer reflectance values and recorded mean TLS intensity.

Regression models compared the intensity mean, median, 95^{th} percentile, SD, variance, and skew of all points within each sample. Three regression forms were evaluated including a linear model, a first order polynomial transformation, and a linear broken stick model to determine what combination of the derived lidar intensity metrics performed best as predictor variables for the measured fuel moisture. Log and squared transformations were evaluated on the predictor variables, and a reduction in AIC. Finally, an analysis of covariance test was performed to determine if scan angle on the control samples significantly changed the coefficients between lidar intensity and moisture content, treating the scan angle as a simple factor.

4.0 RESULTS AND DISCUSSION

4.1 3D FUEL DATA REPOSITORY

Our hierarchical sampling design yielded detailed information on the structure and composition of canopy and surface fuels across southeastern pine, western pine and western grassland sites. The 3D Fuels repository is currently being archived with the SERDP-funded Wildland Fire Science Initiative data repository (https://wfsi-data.org). As part of our submission, we created project metadata, methods documentation and data libraries (**Figure 18**). Dataset and code libraries are documented in **Tables 5-7**. Internal datasets are still being used within a USFS Box library for further analysis with the plan to update WFSI output data and scripts as needed.

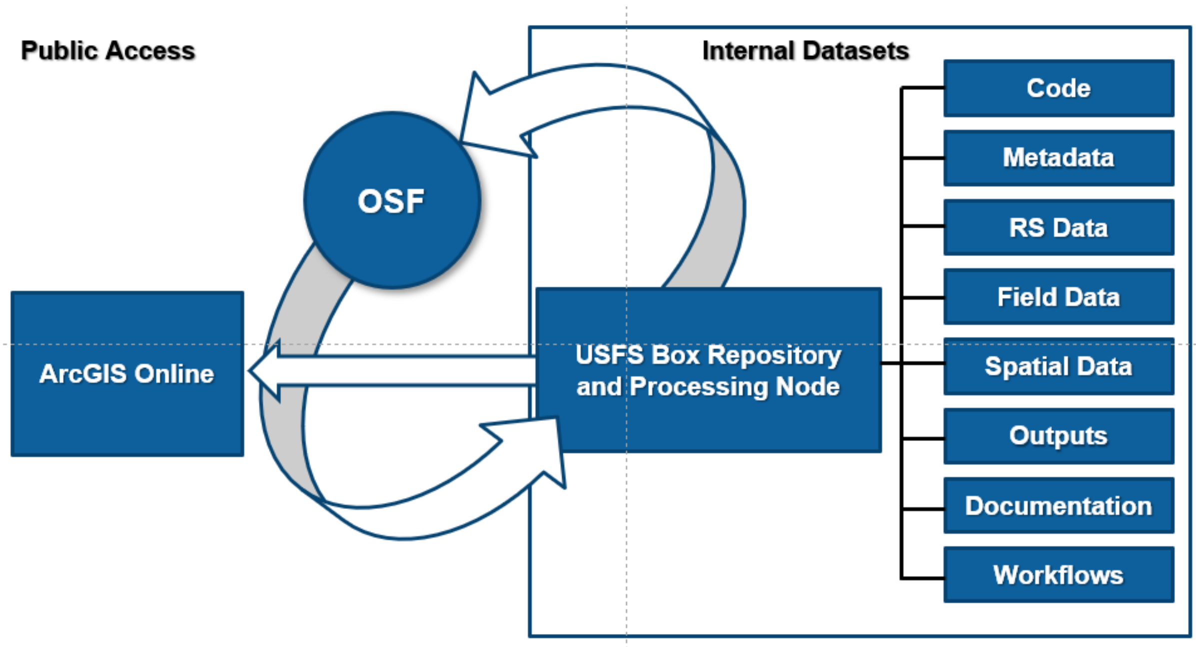

Figure 18. 3D Fuels data organization.

Table 5: 3D Fuels datasets for each site, including ALS, TLS, SfM photogrammetry, and field data.

Data type	Folder	Subfolder	Description
		ALS datasets	
Clipped			Normalized (& transformed if applicable) aerial lidar point clouds clipped to 200 x 200 m study area (with buffer)
DTM			Digital terrain model of site used for normalization
Metadata			Metadata from als vendor
Scan			Non-normalized als point clouds covering general area
		TLS datasets	
Plots	5x5 biomass plot	norm	TLS point clouds for destructive 5x5 plots normalized using LAStools - both Pre and Post files in same location, denoted with _PRE and _POST
	5x5 biomass plot	scan	Non-normalized tls point clouds for destructive 5x5 plots - both Pre and Post files in same location, denoted with _PRE and _POST
	5x5 scan plot	norm	TLS point clouds for scan-only 5x5 plots normalized using LAStools
	5x5 scan plot	scan	Non-normalized tls point clouds for scan-only 5x5 plots
	5x5 pole locations		CSV file of pole locations from point cloud clipping shiny app
	clipplot	biomass	Normalized and clipped destructively sampled 0.5x0.5 m clipplot point clouds - both Pre and Post files in same location, denoted with _PRE and _POST
	clipplot	non_destr	Normalized and clipped non-destructive 0.5x0.5 m clipplot point clouds
	clipplot	spatial	Shapefiles of .5x.5m subplots -- output from point cloud clipping shiny app
synoptic	norm		Normalized tls point clouds for grid points (synoptic scans)
	scan		Non-normalized tls point clouds for grid points (synoptic scans)
		Photogrammetry datasets	
dap	5x5	norm	Normalized point clouds of 5x5 plots taken with drone photogrammetry (dap, low altitude), add readme file where missing (many forested sites)
	5x5	scan	Non-normalized point clouds of 5x5 plots taken with drone photogrammetry (low altitude), add readme file where missing (many forested sites)
	synoptic	norm	Normalized point clouds of entire sites taken with drone photogrammetry (high altitude), add readme file where missing (several sites)
	synoptic	scan	Non-normalized point clouds of entire sites taken with drone photogrammetry (high altitude), add readme file where missing (several sites)
	metadata		Metadata from vendor or other collector of drone-based photogrammetry

Data type	Folder	Subfolder	Description
cr_sfm	norm		Normalized and rotated close-range photogrammetry point clouds created from handheld (close range) video photogrammetry
	scan		Non-normalized close-range 5x5 point clouds: Agisoft outputs
	video		Handheld GoPro videos of plots that were used to create close-range photogrammetry point clouds
Field data			
clipplot			Field data: biomass and presence_absence for clip plots
			Depths (measured from 10cm height to mineral soil) of 5 randomly selected voxels in 0-10 cm strata
			Presence-absence field survey data of sampled 0.5x0.5x1 m clip plots (both pre and post, denoted by _PRE and _POST in filenames)
			presence-absence field survey data of non-destructively sampled clip plots (there are no non-destructive post plots, all were clipped)
			Biomass data for destructively sampled clip plots (both pre and post-fire, denoted by _PRE and _POST)
bulk_dens			Field-collected forest floor bulk density dataset
	depth		Depths recorded at each forest floor sampling location
	trees		Data on focus tree around which bulk density plots were established
	weight		Net weight (g) of collected bulk density samples

Table 6: Summary of 3D Fuels python and R script libraries.

Folder	Description
ALS scripts	
Structural	Canopy and crown metric scripts adapted from Silva et al. (2023)
Structural	Canopy and crown metric scripts - Brian Drye modifications
Spatial	Scripts to create rasters, dtms and shapefiles from als point clouds
TLS scripts	
Processing	Shiny app "Clipper Tool" to clip 0.5x0.5m point clouds from larger (5x5 m) point clouds
Processing	QAQC comparison of TLS occupancy to field-measured occupancy
Analysis	TLS point cloud metrics
Analysis	Modeled relationships bet biomass and TLS point clouds, conduct regressions and plot results (adapted from Cova et al. 2023)
Close-range photogrammetry scripts	
Processing	Close-range photogrammetry point cloud metrics
Analysis	Close-range photogrammetry point cloud metrics
Analysis	Modeled relationships bet biomass and TLS point clouds, conduct regressions and plot results (adapted from Cova et al. 2023)

Table 7: Processed imagery datasets (output folders).

Folder	Subfolder	Description
		ALS outputs
Structural		Outputs of als metrics from Silva methodology (basics, canopy metrics, forest gaps, crown metrics, segmentation plots)
		TLS outputs
Clipplot_metrics		Outputs of tls clipplot (0.5x0.5) metrics
Syn_metrics		Outputs of tls synoptic metrics
5x5_metrics		Outputs of tls 5x5 metrics
		Close-range photogrammetry outputs
CR_sfm	clipplot_metrics	Outputs of close-range photogrammetry clipplot (0.5x0.5) metrics
Photo		Photos of subplots taken in field
Point_cloud	cr_sfm_image	Images of close-range structure from motion point clouds
Point_cloud	tls_image	Images of tls point clouds
Voxel	ocular_image	Voxelized images of field occupied volume from ocular survey data
Voxel	cr_sfm_image	Voxelized images of close-range structure from motion point cloud
Voxel	tls_image	Voxelized images of tls point cloud

4.1.1 Voxel-based field datasets and summary values

Based on destructive clip plot data (see Methods section 3.2.3), we characterized the surface fuels of each site by fuel type, calculating fuel height (**Figure 23**), biomass (**Tables 8, 9**) and bulk density (**Table 10**) values by dominant fuel type and region. Of the broad fuel types, forest floor dominated forested site biomass. Within our gridded sampling design, many voxel plots in forested systems fell on in locations lacking live vegetation, and the bulk of the biomass present was in the form of forest floor litter and pine needles. Even though western forests had aboveground live biomass in shrubs and grasses, the forest floor contributed most to overall mean plot biomass. In western grasslands, herbs were the most dominant, as these plots were largely covered in rhizomatous and bunchgrasses.

Bulk density values were estimated by dividing total dry biomass of a plot (using the biomass recorded from field data collection) and dividing by each of two volume metrics: 1) occupied volume of a plot approximated by using the maximum height of vegetation in that plot, and 2) total occupied volume of a plot as measured by the number of occupied voxels (out of a possible 250) recorded in presence/absence surveys in the field for that plot. Using maximum height to represent occupied plot volume resulted in much lower bulk density values than the method using volume by voxels marked as occupied in the field, as many more voxels that lack vegetation are included in the former method. Plots dominated by fine woody debris tended to have higher bulk density values in forested sites, though differences were small. Grassland plots had very low bulk density values unless dominated by shrubs.

Forest floor biomass values were also summarized by dominant fuel type and region, using the detailed information collected in the 0-10 cm stratum of each clip plot in the field and laboratory (**Table 10)**. High density fuels such as coarse woody debris and forest floor (which included duff as well as litter) constituted the bulk of the biomass collected within 0-10 cm stratum of forest plots. In grassland plots, biomass was nearly equally divided into forest floor, herb and shrub fuel types.

Comparisons of maximum height distributions revealed major differences in estimated height between field measures of occupied volume within voxel plots, close-range photogrammetry, and TLS. Although field measurements would normally be considered the most reliable estimate, installation of voxel frames may have inadvertently compressed or displaced some upper fuelbed layers such as grass inflorescences or shrub branches compared to close-range photogrammetry and TLS scans, which were conducted prior to the installation of voxel frames. Even so, the maximum height metric for TLS point clouds is likely biased by noise, suggesting that a different metric that removes the potential bias of outlier points may be advisable.

Of the variables collected by the 3D Fuels project, estimated bulk density and height distributions are among the most important to inform gridded, 3D inputs for CFD modeling. Table 11 summarizes measured bulk density by major vegetation and dominant fuel. Individual voxel plots are also classified into dominant fuel types and shrub or grass species, where applicable. We anticipate that these well-labelled datasets will be useful to both provide estimates of bulk density and fuel heights for these common vegetation types but also as inputs to machine learning algorithms that can be developed to predict distributed surface fuel cover, height and bulk density distributions based on canopy and site variables such as disturbance history, vegetation type, and forest age.

Table 8. Summary of measured biomass for entire voxel plots (total) and by 10-100cm, which excludes forest floor layers. Time since fire (TSF) is listed for SE sites, and western sites are classified as low, moderate, and high biomass. Mean field-measured fuel height and standard deviation (SD) are summarized by site.

			Total Voxel Plot Biomass (0-100cm)					**Biomass (10-100 cm)**			
Site	**TSF / biomass**	**Mean (SD) height (cm)**	**Mean (g)**	**SD (g)**	**Min (g)**	**Max (g)**		**Mean (g)**	**SD (g)**	**Min (g)**	**Max (g)**
	SE mesic pine flatwood forests										
Tates Hell A	1-2 yr	61.6 (23.2)	277.5	134.4	91.4	705.1		69.6	55.3	5.9	329.8
Osceola	1-2 yr	69.9 (23)	363.1	361.4	0.0	1165.5		100.2	124.5	0.0	533.7
Blackwater	2 yr	66.1 (23)	201.2	61.2	89.8	302.1		57.2	41.0	4.0	135.6
Fort Stewart	2-3 yr	49 (22.7)	425.3	834.9	0.0	7056.5		19.5	41.8	0.0	256.4
Tates Hell B	2-3 yr	69.1 (27.8)	492.8	262.3	69.0	1723.5		75.7	52.1	0.6	214.8
Aucilla	> 5 yr	73.6 (22)	336.6	219.2	81.3	1031.3		80.9	109.6	0.2	474.4
	SE loblolly pine sweetgum forests										
Hannah Hammock	1-2 yr	94 (9.9)	286.3	114.0	124.9	587.9		89.8	72.6	13.1	343.4
Hitchiti B	1-2 yr	84.9 (21.5)	448.3	250.9	148.5	1581.2		36.4	43.2	0.0	167.1
Hitchiti A	2-3 yr	66 (31.3)	509.1	251.5	159.6	1720.2		23.3	48.3	0.0	279.5
	W ponderosa pine forests										
Lubrecht	Low	41.8 (21.7)	435.1	283.2	41.3	1696.8		14.8	36.5	0.0	193.1
LANL F	Low	51.5 (32.8)	500.0	503.7	25.1	2738.2		33.3	74.3	0.0	329.4
Sycan F	Mod	54.4 (28)	682.4	1584.8	0.0	10085.8		20.9	63.7	0.0	326.2
Sycan F2	Mod	46.7 (22.2)	879.1	1886.7	46.4	9356.3		29.5	46.8	0.0	133.5
Methow	Mod	60.9 (27.9)	950.8	579.9	161.7	2411.8		47.7	108.2	0.0	667.7
	W grasslands										

			Total Voxel Plot Biomass (0-100cm)					Biomass (10-100 cm)			
Site	TSF / biomass	Mean (SD) height (cm)	Mean (g)	SD (g)	Min (g)	Max (g)		Mean (g)	SD (g)	Min (g)	Max (g)
Sycan G	Low	31.2 (9.5)	87.1	187.8	0.0	1220.3		7.4	37.1	0.0	249.4
LANL G	Low	28.6 (13.4)	121.8	99.7	10.9	408.1		3.9	8.5	0.0	40.6
Tenalquot	Mod	46.2 (12.1)	305.2	237.6	17.5	964.7		21.8	23.3	2.9	145.9
Glacial Heritage	High	54 (12.3)	170.1	62.6	81.4	432.5		21.1	12.3	6.6	76.8

Table 9: Summary biomass values in the 0-10 cm stratum for each vegetation type, categorized by fuel type.

Vegetation type	Fuel type	n	Total biomass (g)	Mean biomass	Min biomass	Max biomass	SD
Loblolly-sweetgum		530	32,960.75	62.19	-	1,315.20	95.52
	CWD	3	234.77	78.26	-	205.57	111.22
	Forest floor	135	20,596.15	152.56	12.44	476.39	93.59
	FWD	122	4,888.37	40.07	1.44	377.32	53.36
	Herbs	135	3,427.96	25.39	1.05	138.99	25.18
	Other	1	1.4	1.4	1.4	1.4	-
	Shrubs & small trees	134	3,812.10	28.45	0.44	1,315.20	112.94
SE Flatwoods		1128	60,348.33	53.5	-	3,144.90	116.34
	CWD	9	4,629.05	514.34	-	3,144.90	1,033.42
	Forest floor	313	36,286.26	115.93	8.21	357.63	74.41
	FWD	246	8,598.72	34.95	-	335.42	47.08
	Herbs	257	6,703.24	26.08	-	249.59	43.28
	Other	26	31.29	1.2	-	7.74	2.23
	Shrubs & small trees	277	4,099.77	14.8	0.01	97.84	15.46
Western grassland		505	24,039.44	47.6	-	451.6	59.04
	Forest floor	80	3,708.67	46.36	-	368.51	70.09
	FWD	66	1,539.49	23.33	0.06	451.6	58.87
	Herbs	173	9,714.96	56.16	0.04	161.19	34.17
	Other	120	5,889.99	49.08	0.06	299.08	59.92
	Shrubs & small trees	66	3,186.33	48.28	-	364.46	84.45
Western ponderosa pine		733	61,023.95	83.25	-	4,667.95	224.59
	CWD	7	7,812.93	1,116.13	-	4,667.95	1,832.05
	Forest floor	195	30,496.36	156.39	6.39	1,089.92	129.41

Vegetation type	Fuel type	n	Total biomass (g)	Mean biomass	Min biomass	Max biomass	SD
	FWD	187	16,296.18	87.15	-	905.94	130.57
	Herbs	168	3,174.35	18.89	0.01	307.38	32.36
	Other	62	342.56	5.53	-	28.88	7.09
	Shrubs & small trees	114	2,901.58	25.45	-	270.78	44.14

Table 10. Mean, standard deviation (SD), minimum (min), and maximum (max) bulk density values (BD, kg/m3) summarized by dominant fuel type. Bulk density is calculated as the biomass per volume estimated using maximum fuel height within voxel plots (BD-MH) and as the biomass per unit volume of occupied voxels (BD – OV).

Vegetation type	Dominant fuel	n	BD – MH Mean	Min	Max	SD	BD – OV Mean	Min	Max	SD
SE mesic pine flatwoods		313	0.031	0.002	0.555	0.035	0.299	0.016	7.44	0.463
	Forest floor	176	0.03	0.005	0.169	0.022	0.28	0.032	2.211	0.248
	FWD	2	0.041	0.033	0.048	0.011	0.404	0.265	0.542	0.196
	Herbs	108	0.032	0.002	0.555	0.053	0.335	0.016	7.44	0.718
	Shrubs & small trees	27	0.027	0.011	0.057	0.013	0.272	0.091	0.656	0.172
SE loblolly-sweetgum		135	0.039	0.01	0.239	0.026	0.407	0.084	2.64	0.292
	Forest floor	80	0.044	0.014	0.239	0.029	0.457	0.132	2.64	0.334
	FWD	1	0.048	0.048	0.048	-	0.527	0.527	0.527	-
	Herbs	46	0.031	0.01	0.083	0.016	0.329	0.084	0.932	0.196
	Shrubs & small trees	8	0.029	0.016	0.058	0.017	0.345	0.166	0.721	0.224
Western grassland		173	0.022	0.001	0.119	0.02	0.22	0.002	1.899	0.337
	Forest floor	16	0.019	0.004	0.038	0.011	0.144	0.022	0.485	0.121
	Herbs	143	0.018	0.001	0.096	0.015	0.137	0.002	0.942	0.177
	Shrubs & small trees	14	0.067	0.049	0.119	0.019	1.151	0.576	1.899	0.357
Western ponderosa pine		195	0.05	0.004	0.807	0.07	0.471	0.016	6.315	0.716
	Forest floor	143	0.052	0.004	0.807	0.081	0.443	0.016	6.315	0.795
	FWD	4	0.064	0.044	0.094	0.021	0.597	0.276	1.339	0.497
	Herbs	40	0.042	0.012	0.131	0.027	0.518	0.065	1.829	0.448
	Shrubs & small trees	8	0.049	0.009	0.08	0.023	0.673	0.207	1.158	0.3

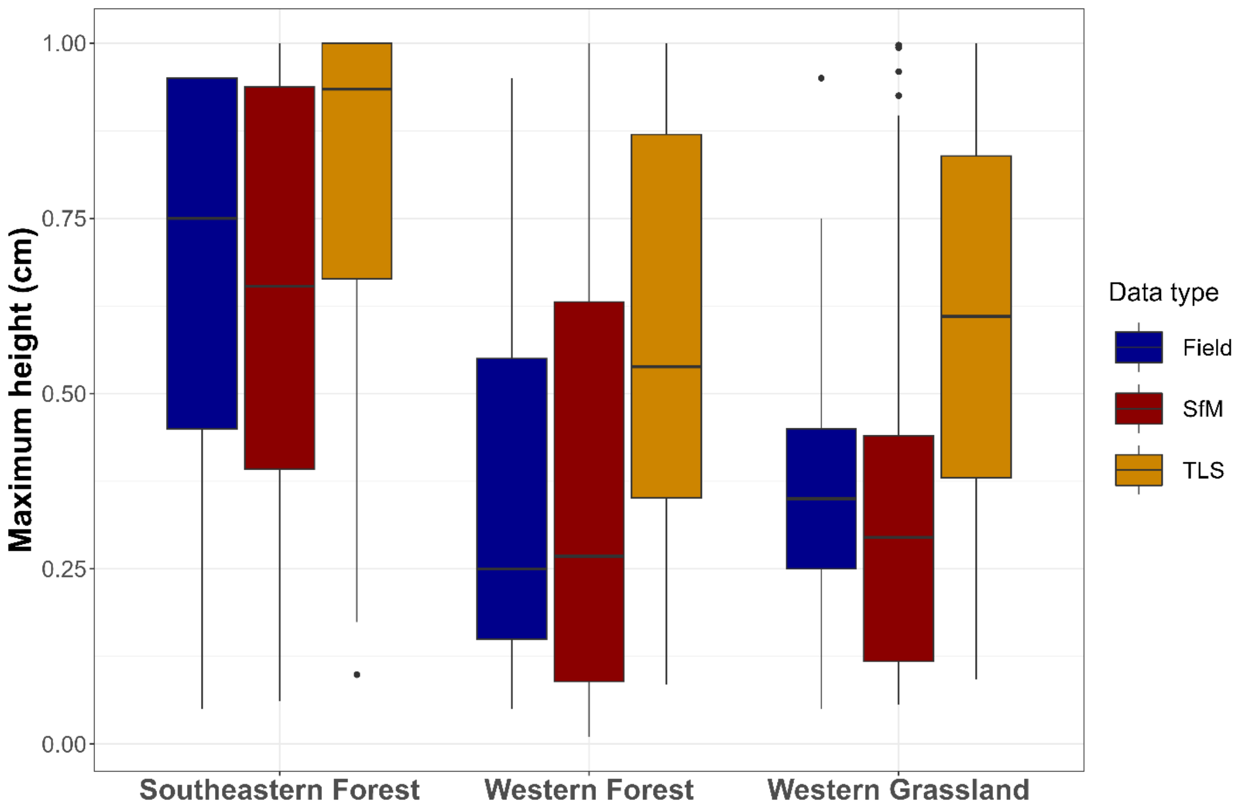

Figure 19: Distributions of measured maximum height by voxel plot from field data, close-range photogrammetry (SfM) and terrestrial laser scanning (TLS).

4.2 PREDICTIVE MODELS OF UNDERSTORY BIOMASS WITH POINT CLOUD METRICS

Background and objectives

Through increased availability of lidar and photogrammetry, methods for 3D characterization and mapping of wildland fuels are rapidly advancing. ALS is now widely used for forest canopy mapping, including stem detection, tree height, height to live crown, canopy cover and crown bulk density metrics (Silva et al. 2016, Donager et al. 2021). Modeled relationships between ALS point cloud densities and fuel bulk density are used to translate point clouds into gridded meshes of volumetric pixels termed voxels (e.g., Rocha et al. 2023). SfM photogrammetry is also used to create true-color and multi-spectral photogrammetric point clouds that can be classified into live and dead biomass and vegetation types.

With recent developments in remote sensing technologies, including high-resolution TLS (Calders et al. 2020) and close-range SfM photogrammetry (Bright et al. 2016), opportunities to characterize the 3D structure and composition of understory fuels are increasing. The field of understory characterization is still in early stages, and methods for imagery collection and calibration for field development are still being tested (Bright et al. 2016, Rowell et al. 2020, Hudak et al. 2020, Loudermilk et al. 2023). Evaluation of CFD models and their sensitivity to variability in surface fuels is also in early stages (Mueller et al. 2021, Linn et al. 2020, Loudermilk et al. 2022). Although several evaluations of CFD models of fire behavior have been conducted, surface fuels are commonly represented as homogenous layers (e.g., Mueller et al. 2021, Ritter et al. 2022).

To our knowledge, this study represents the largest sample of image-based point clouds analyzed for understory fuel characterization, and the only study to evaluate predictive ability across different forest types. In addition to TLS scanning, we presented a novel, video-based approach for rapid data collection that demonstrates potential across multiple domains, and presented a suite of metrics that can be used to summarize point cloud models. Application of this technique has the potential to provide managers with an accessible option for inexpensive data collection and can lay the groundwork for rapid collection of input datasets to train landscape-scale fuel models.

Videos collected from a handheld GoPro camera produced SfM point clouds with reliable representations of fuel height and structure across our sites. While previous studies that have assessed the applications of close-range SfM have largely relied on individually collected photographs to create point clouds (Bright et al. 2016; Piermattei et al. 2019; Wallace et al. 2022), the method presented here offers an efficient, affordable way to collect data with a single video taken in just under two minutes per plot. In this study, we used a combination of Python scripts and processing workflows in the commercial software Agisoft Metashape to produce point clouds for each sampling plot; this constituted a semi-automated approach that required manual input to define point cloud reference points and spatial scale. For wider adoption of this method, more automated approaches will be required. Rapid advances in machine learning and AI are catalyzing innovations in object detection and mapping from imagery, and we anticipate that the 3D Fuels dataset will provide invaluable training data for these advancements. As the datasets are available for analysis in a cloud-hosted open source code library, automated processing of videos to point clouds and ingestion-to-analysis workflows that provide a large library of outputs can be embedded into deep learning networks to improve coarser scale fuel mapping.

We found weak relationships between point cloud metrics and biomass 0 to 10 cm in height. In models that excluded the 0-10 cm stratum and associated litter and duff layers, we found that fuel height and VPAD, a novel metric to measure the vertical profile of vegetation produced the strongest relationships to biomass across different fuel types. Point cloud metrics performed best in shrub-dominated and grass/forb dominated plots across all sites. Modeled relationships between point clouds and biomass performed most poorly in litter-dominated plots, as TLS and photogrammetry-based point clouds were unable to adequately characterize the 0-10 cm fuel stratum due to occlusion.

Because TLS point clouds have greater resolution and can penetrate more deeply into complex vegetation, we anticipated that models based on TLS point cloud metrics would outperform close-range photogrammetry. Overall, the close-range photogrammetry models had comparable relationships with biomass, which was somewhat surprising because TLS is generally more accurate. However, for TLS, each set of 5 voxel plots were scanned collectively within 5x5 scan plots based on four scan positions adjacent to each side of the 5x5 plots. In contrast, close-range photogrammetry videos were taken above each voxel plot and ultimately had better coverage of the voxel plots and overall less occlusion than the TLS scans. These findings suggest that low-altitude close-range photogrammetry scanning either with hand-held devices or UAVs may provide a cheaper and more efficient scanning technique than existing TLS technologies. However, TLS is also rapidly developing to be available in backpacks and as payloads on UAVs and may be coordinated with true-color or hyperspectral video to allow for merged, high-resolution point clouds in the future.

In predictive models of shrub biomass, height was the best point cloud predictor of shrub biomass based on either TLS or SfM close-range photogrammetry dataset (**Figure 20**). Herb models varied considerably, with stronger model fits in SE Forests and Western grasslands with relatively weaker model performance in western forests (**Figure 21**). Regardless of point cloud metric, models of litter biomass all demonstrated weak relationships between TLS and SfM metrics and biomass (**Figure 22**).

Relative to other studies of TLS and SfM point cloud performance for estimating surface fuel biomass, our study had somewhat weaker overall performance. For example, recent studies of relationships between TLS metrics and biomass reported much higher coefficients of determination (Greaves et al. 2015, Rowell et al. 2016, Wallace et al. 2016). Even so, our findings suggest that fuel type is an important consideration in biomass estimation. Although we were able to broadly classify voxel biomass into dominant fuel types, in reality they were highly variable mixtures of litter, downed wood, herb, and shrub biomass. To capture the inherent variability of these fuel complexes, we would have needed much higher sampling intensity. An alternative method for future studies is to stratify fuel in the field and sample dominant fuel types that represent much more uniform fuelbeds and development of mixed models based on established biomass relationships for complex fuels.

Overall, our study findings suggest that passive sensing through ALS, TLS and structure-from-photogrammetry are promising for mapping where fuels are in 3D space. However, imagery alone is insufficient for estimating the total aboveground biomass available to burn within wildland fire events. For model applications such as inputs to QUIC-Fire and other process-based models of fire behavior and effects, a combination of approaches will be required. Specifically, TLS and close-range photogrammetry can be used to estimate the height, cover and type of understory vegetation. However, object-based modeling of litter and fine wood deposition is likely required to estimate litter and duff accumulations under live vegetation. The 3D Fuels project was able to highlight some of the uncertainty in wildland fuel estimation, and the hierarchically scaled fuels dataset will be invaluable as a model training dataset for machine learning and AI applications of predictive wildland fuel estimation and mapping.

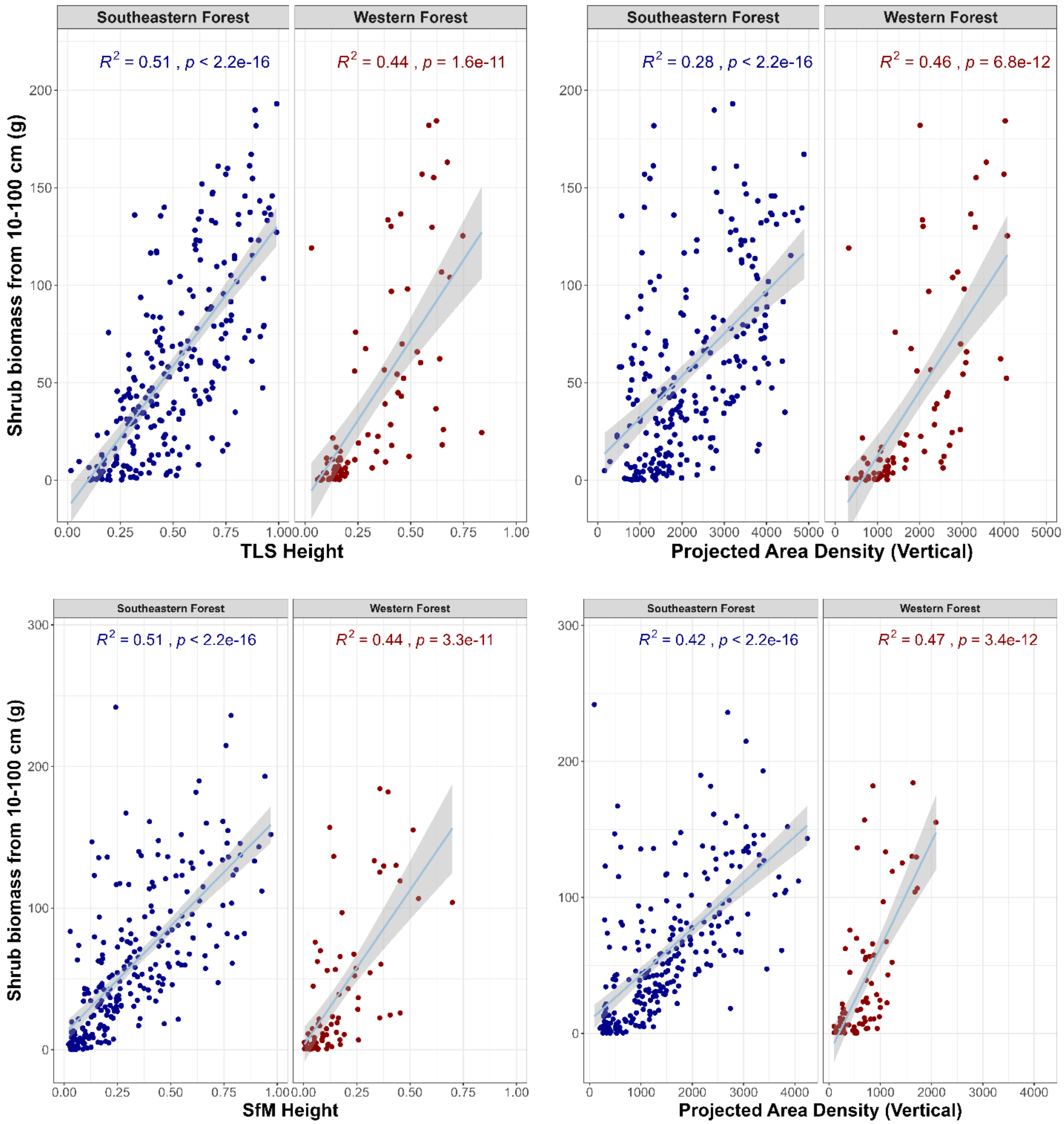

Figure 20: Shrub biomass models. Scatter plot and fitted linear regression models for shrub biomass based on TLS and SfM close range photogrammetry (SfM) height and projected area density – vertical point cloud metrics.

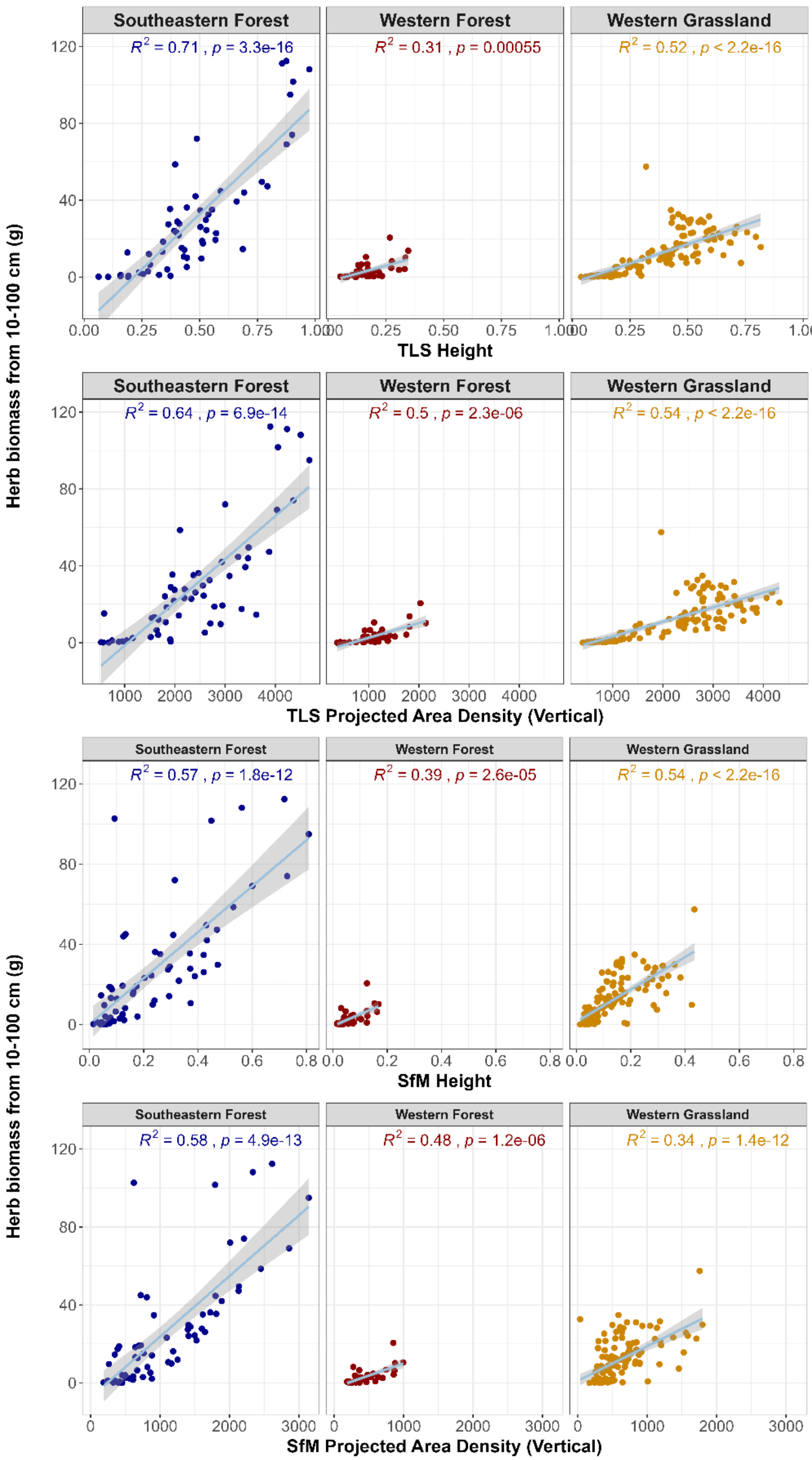

Figure 21: Herb biomass models based on height and PADV point cloud metrics.

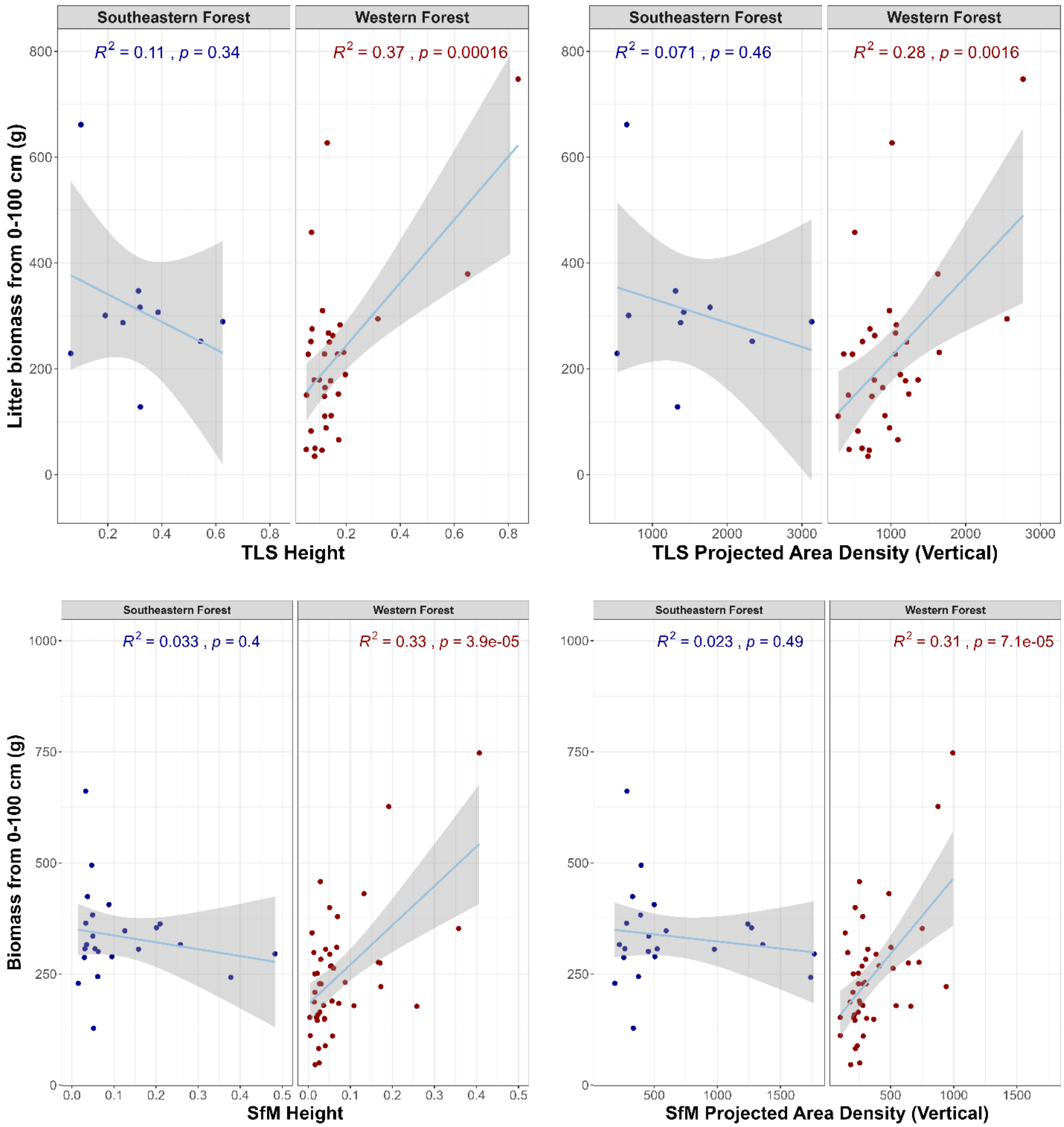

Figure 22: Forest litter biomass models based on height and PADV point cloud metrics. The majority of litter-dominated plots only contained a 0-10cm stratum.

4.3 RELATIONSHIPS BETWEEN FOREST FLOOR CHARACTERISTICS AND TREE CROWN COVER

Reliable estimates of forest floor characteristics are critically important for wildland fire emissions modeling, particularly in fire excluded forests with substantial accumulations of organic soils. In long unburned forests, accumulated duff layers present challenges not only for smoke management but also for understory diversity (Hiers et al. 2007) and post-fire tree mortality following the reintroduction of fire (Varner et al. 2007). Because duff layers are densely packed and lack air space for available oxygen, they burn mostly through smoldering combustion with lower combustion efficiency than flaming phases of combustion (Keane 2015; Finney et al. 2021). As such, deep duff accumulations can contribute to higher PM2.5 emissions that fine fuels that burn mostly within the flaming phase of combustion (Urbanski 2014; Prichard et al. 2020). In pine and oak forest types, forest litter layers and pine cones also can be major drivers of fire spread and intensity (Gabrielson et al. 2012, Varner et al. 2015). Where deep organic matter accumulations exist next to tree stems and root systems, long-duration burning can damage or kill living tissue and result in sustained damage or tree mortality (Varner et al. 2005, 2007).

For smoke management, fire and fuels planners need to estimate the amount of forest floor materials that are available to burn in planned prescribed burn operations. To date, unit-level estimates are often made through use of photo series (https://depts.washington.edu/nwfire/dps/), maps of wildland fuels (e.g., LANDFIRE), and through actual depth measurements that are converted to estimated biomass using published bulk density values. A recent study by Sánchez-López et al. (2023) created an object-based approach to predicting forest litter deposition under tree crowns. This study provides summarized depth, biomass, and bulk density values for frequently burned SE pine flatwoods and SE loblolly pine plantations and is intended to inform future development of object-based forest floor mapping in coordination with the SERDP Objects Project (RC20-1346). Because Aucilla was the only site with greater than 5 years since fire, all estimates are representative of sites that are regularly maintained by prescribed underburning. In contrast, the western pine sites represent ponderosa pine forests that have greater duff accumulations, in part due to a lack of regular prescribed burning and also due to slower decomposition rates than the SE pine sites.

The inherent variability in forest floor values poses substantial challenges in field study designs and investments in large enough samples size to inform robust statistical models (Keane 2015). Obtaining accurate forest floor measurements, including consistent depths, biomass, and bulk density values, requires a large investment in time and effort. Destructive sampling is time intensive to clear existing vegetation, systematically measure litter and duff depths, and extract forest floor layers. Laboratory analysis involves not only drying samples to obtain a dry weight biomass, but also analyzing duff material for mineral content through loss on ignition or a comparable approach.

Within the three main forest types sampled in this study, we evaluated how forest floor layers vary across bole, inside tree crown drip line, and outside drip line positions (**Tables 11, 12**). As anticipated, we found that litter and duff depth, biomass and bulk density were highly variable within and between sites with high reported standard deviations. Even with high reported variability, there were strong statistical differences across transect positions (**Tables 13-14**). Overall, SE flatwood sites generally had greater litter depth and biomass than the other two sites, and western pine litter sites generally had the highest bulk density values (**Figure 4a-c**). All measures of accumulated duff (depth, biomass and bulk density) were greatest in the western pine sites.

The SE flatwood and western pine sites both contained much greater accumulations of litter and duff next to tree boles than the inside drip line and outside drip line positions. In contrast, litter depth and biomass were not significantly different across transect positions in SE loblolly-sweetgum sites. The presence of the broadleaf deciduous tree, sweetgum, throughout loblolly pine understories likely distributed more uniform leaf litter across the sites and contributed to more even distributions of litter depth and biomass. However, accumulated duff layers were significantly greater next to tree boles than inside and outside transect positions in loblolly sweetgum forests. This could be due to incremental differences in accumulated litter, including pine needles and bark scales near tree boles, that over time contribute to greater duff accumulations.

Table 11: Litter depth (cm), biomass (cm), and bulk density (kg m^{-3}) of SE mesic pine flatwoods, SE loblolly pine-sweetgum forests, and western pine forests. SE sites are ordered by time since fire (TSF).

Site name	Position	n	Depth (cm)		Biomass (kg/m2)		Bulk density (kg/m3)	
			Mean	SD	Mean	SD	Mean	SD
SE Flatwood								
Tates Hell A	Bole	18	1.89	1.36	0.16	0.06	12.73	8.79
1-2 yr TSF	InsideDL	18	3.03	2.11	0.21	0.11	9.46	6.85
	OutsideDL	18	2.18	1.41	0.22	0.10	12.99	9.26
	All	**54**	**2.37**	**1.70**	**0.20**	**0.10**	**11.73**	**8.37**
Tates Hell B	Bole	18	4.56	2.48	0.54	0.21	14.73	8.10
2-3 yr TSF	InsideDL	17	5.62	2.66	0.44	0.14	9.85	6.12
	OutsideDL	18	3.53	1.55	0.39	0.10	12.56	4.42
	All	**53**	**4.55**	**2.39**	**0.46**	**0.17**	**12.43**	**6.58**
Fort Stewart	Bole	18	6.35	1.71	1.24	0.42	21.33	9.51
2-3 yr TSF	InsideDL	18	6.44	2.48	0.95	0.45	16.17	9.07
	OutsideDL	18	5.76	3.02	0.71	0.35	13.51	5.36
	All	**54**	**6.18**	**2.44**	**0.97**	**0.46**	**17.00**	**8.68**
Aucilla	Bole	18	7.36	1.51	1.28	0.34	17.93	5.68
>5 yr TSF	InsideDL	18	6.95	1.91	0.93	0.38	13.53	4.61
	OutsideDL	18	4.96	1.60	0.60	0.27	12.91	5.58
	All	**54**	**6.43**	**1.96**	**0.94**	**0.43**	**14.79**	**5.68**
Loblolly sweetgum								
Hitchiti B	Bole	18	2.45	0.84	0.57	0.12	26.71	12.72
1 yr TSF	InsideDL	18	2.73	0.75	0.50	0.21	18.04	5.16
	OutsideDL	18	2.85	0.93	0.50	0.21	18.87	9.22
	All	**54**	**2.68**	**0.85**	**0.52**	**0.19**	**21.21**	**10.16**
Hannah Hammock	Bole	18	3.36	0.94	0.93	0.25	28.76	8.41
1-2 yr TSF	InsideDL	18	2.87	1.12	0.50	0.21	19.32	9.79
	OutsideDL	18	4.11	1.51	0.36	0.18	8.88	2.55
	All	**54**	**3.45**	**1.30**	**0.60**	**0.32**	**18.99**	**11.08**
Hitchiti A	Bole	18	4.13	0.81	1.11	0.53	26.94	12.22
2-3 yr TSF	InsideDL	18	4.97	1.60	0.77	0.21	16.97	6.88
	OutsideDL	18	4.75	1.49	0.71	0.27	15.69	5.95
	All	**54**	**4.62**	**1.37**	**0.87**	**0.40**	**19.87**	**10.01**

Western pine								
LANL Forest	Bole	18	2.46	1.93	1.50	1.50	71.75	72.02
	InsideDL	18	2.97	1.80	1.24	0.80	44.24	25.14
	OutsideDL	18	1.59	1.18	0.39	0.24	37.66	31.38
	All	**54**	**2.34**	**1.74**	**1.04**	**1.08**	**50.43**	**47.73**
Sycan Marsh F	Bole	23	2.00	0.89	0.64	0.37	34.85	20.31
	InsideDL	24	2.11	1.05	0.56	0.45	25.15	11.09
	OutsideDL	22	1.20	0.72	0.29	0.21	30.85	32.66
	All	**69**	**1.78**	**0.98**	**0.50**	**0.39**	**30.27**	**22.76**
Methow	Bole	18	3.68	1.32	1.49	0.69	40.97	13.72
	InsideDL	18	3.17	0.93	0.80	0.27	26.66	10.59
	OutsideDL	18	2.65	1.18	0.51	0.23	20.99	9.82
	All	**54**	**3.17**	**1.21**	**0.93**	**0.61**	**29.54**	**14.12**
Lubrecht	Bole	24	2.04	1.12	0.56	0.55	28.31	20.99
	InsideDL	24	1.86	0.97	0.33	0.16	22.01	13.66
	OutsideDL	22	1.60	1.14	0.20	0.12	15.79	11.63
	All	**70**	**1.84**	**1.08**	**0.37**	**0.37**	**22.21**	**16.63**

Table 12: Duff depth (cm), biomass (cm), and bulk density (kg m^{-3}) of SE mesic pine flatwoods, SE loblolly pine-sweetgum forests, and western pine forests. SE sites are ordered by time since fire (TSF).

Site name	**Position**	**n**	**Depth (cm)**		**Biomass (kg/m2)**		**Bulk density**	
			Mean	**SD**	**Mean**	**SD**	**Mean**	**SD**
SE Flatwood								
Tates Hell A	Bole	7	0.28	0.20	0.12	0.09	44.89	28.01
	InsideDL	17	1.20	0.73	0.81	0.49	76.20	36.19
	OutsideD	17	1.16	0.86	0.73	0.62	71.17	26.70
	All	**41**	**1.03**	**0.80**	**0.66**	**0.56**	**68.77**	**32.44**
Tates Hell B	Bole	17	1.23	1.21	0.67	0.67	54.09	24.53
	InsideDL	18	1.30	0.65	0.62	0.36	50.31	30.48
	OutsideD	18	1.20	0.91	0.71	0.62	65.89	34.77
	All	**53**	**1.24**	**0.92**	**0.67**	**0.55**	**56.82**	**30.49**
Fort Stewart	Bole	18	0.83	1.10	0.59	0.79	75.39	31.81
	InsideDL	18	1.06	1.39	0.81	1.09	76.19	47.66
	OutsideD	18	0.84	1.08	0.41	0.68	42.52	34.13
	All	**54**	**0.91**	**1.18**	**0.60**	**0.87**	**64.37**	**40.75**
Aucilla	Bole	18	1.37	1.14	0.24	0.25	18.05	10.27
	InsideDL	18	1.04	1.18	0.14	0.16	14.78	6.89
	OutsideD	18	0.27	0.52	0.04	0.12	17.58	18.67
	All	**54**	**0.89**	**1.08**	**0.14**	**0.20**	**16.72**	**10.38**
Loblolly sweetgum								
Hitchiti B	Bole	18	1.93	1.25	1.41	1.48	72.59	42.76
	InsideDL	18	1.40	0.83	0.57	0.37	43.74	18.24
	OutsideD	18	1.02	0.78	0.54	0.52	52.64	25.86
	All	**54**	**1.45**	**1.03**	**0.84**	**1.00**	**56.32**	**32.49**
Hannah Hammock	Bole	18	1.31	1.34	0.77	0.75	68.14	27.79
	InsideDL	18	1.00	0.70	0.52	0.50	53.88	27.19
	OutsideD	18	0.87	0.46	0.33	0.28	41.34	29.57

	All	**54**	**1.06**	**0.91**	**0.54**	**0.56**	**54.19**	**29.76**
Hitchiti A	Bole	17	1.58	0.82	0.89	0.46	67.08	42.51
	InsideDL	18	1.51	0.62	0.76	0.47	51.14	24.38
	OutsideD	18	1.12	0.43	0.62	0.39	57.58	24.91
	All	**53**	**1.40**	**0.66**	**0.76**	**0.45**	**58.44**	**31.57**
				Western pine				
LANL Forest	Bole	18	2.24	3.19	1.77	2.61	83.60	42.87
	InsideDL	18	2.15	1.57	1.67	1.39	76.98	28.88
	OutsideD	18	0.59	0.69	0.32	0.43	53.97	31.33
	All	**54**	**1.66**	**2.19**	**1.25**	**1.82**	**72.61**	**36.08**
Sycan Marsh F	Bole	21	3.27	1.65	3.38	2.23	100.09	49.67
	InsideDL	17	2.83	1.97	3.48	2.64	124.41	49.40
	OutsideD	21	1.29	2.08	0.50	0.56	94.63	127.03
	All	**59**	**2.44**	**2.07**	**2.39**	**2.40**	**105.53**	**83.21**
Methow	Bole	16	3.61	1.28	3.96	1.72	119.61	60.53
	InsideDL	16	2.96	1.46	2.91	1.35	104.94	27.60
	OutsideD	17	1.52	0.91	1.62	1.25	124.22	103.22
	All	**49**	**2.67**	**1.50**	**2.80**	**1.72**	**116.42**	**70.74**
Lubrecht	Bole	21	2.30	1.41	2.27	2.09	88.63	45.73
	InsideDL	19	1.88	0.94	1.57	0.94	85.85	30.24
	OutsideD	20	1.64	1.21	1.16	1.18	71.05	41.67
	All	**60**	**1.95**	**1.22**	**1.67**	**1.56**	**81.89**	**40.10**

Table 13: Statistical differences in litter depth (cm), biomass (kg/m2) and bulk density (kg/m3) across transect position (next to tree bole - bole, inside crown drip line – inside, and outside crown dripline - outside) for SE flatwood, SE loblolly sweetgum, and western pine sites.

Forest Type	Comparison	Depth (cm) p-value	Biomass (kg/m2) p value	Bulk density (kg/m3) p value
SE flatwood	Inside vs bole	0.5336	0.0583	0.0015
	Outside vs bole	0.0867	0.00051	0.0093
	Outside vs Inside	0.0046	0.0949	0.8390
SE loblolly sweetgum	Inside vs bole	0.7286	$p < 0.0001$	<0.0001
	Outside vs bole	0.0811	$p < 0.0001$	<0.0001
	Outside vs Inside	0.3421	0.5326	0.0885
Western pine	Inside vs bole	0.9916	0.0096	0.0170
	Outside vs bole	0.0010	<0.0001	0.0028
	Outside vs Inside	0.00015	0.0018	0.8133

Table 14: Statistical differences in duff depth (cm), biomass (kg/m2) and bulk density (kg/m3) across transect position (bole, inside, and outside crown dripline) for SE flatwood, SE loblolly sweetgum, and western pine sites.

Forest Type	Comparison	Depth (cm) p-value	Biomass (kg/m^2) p value	Bulk density (kg/m^3) p value
SE flatwood	Inside vs bole	0.8192	0.4357	0.4613
	Outside vs bole	0.5844	0.9901	0.7817
	Outside vs Inside	0.2222	0.4863	0.8502
SE loblolly sweetgum	Inside vs bole	0.2155	0.0068	0.0057
	Outside vs bole	0.0019	0.0003	0.0093
	Outside vs Inside	0.1744	0.6460	0.9862
Western pine	Inside vs bole	0.3191	0.2913	0.9630
	Outside vs bole	0.0000	<0.0001	0.0194
	Outside vs Inside	0.0001	<0.0001	0.0107

Table 15: Simple linear models of forest floor (litter and duff) biomass relationships. All models are significant at $p < 0.0001$.

	Litter (R^2)	Duff (R^2)
All plots		
SE loblolly sweetgum	0.18	0.62
Bole	0.30002	0.6026
Inside	0.2925	0.5229
Outside	0.269	0.4831
SE flatwood	0.46	0.66
Bole	0.4284	0.4284
Inside	0.2188	0.2188
Outside	0.4263	0.6855
Western pine	0.47	0.74
Bole	0.53	0.6291
Inside	0.3395	0.6708
Outside	0.2594	0.4892

Although our study design did not support statistical models of forest floor characteristics with time since fire on SE flatwood and SE loblolly-sweetgum sites, litter depths tended to be higher on sites with greater time since fire. However, there were no apparent differences in duff accumulations on sites with increasing time since fire (**Figure 4**). Because SE sites are all part of active prescribed burning programs, the only site that represents a long-unburned forest is the SE Flatwood Aucilla site. Even though litter accumulations were higher than other SE sites, duff depth was comparable to other sites, while duff bulk density was exceptionally low. Across the 3 forest types, accumulated duff layers were greatest in western pine forest sites. This difference is likely due to longer time since fire in ponderosa pine forests along with slower decomposition rates compared to those supported in the humid forests of the southeastern US.

In addition to providing general estimates of depth, biomass and bulk density, study findings can also be used to inform how distributions of litter and duff vary with position relative to tree crowns. As such, these findings may be used to predict forest floor accumulations relative to their position within and outside of tree crowns. With increased availability of stem and crown mapping based on lidar metrics from ALS or TLS, estimates of forest floor accumulations may increasingly be made through mapping of tree crown positions and predictive modeling of litter biomass in relationship to tree crowns. Our study found particularly strong statistical differences in duff depth and biomass between bole, inside midpoints beneath tree crowns, and outside tree crowns. To date, predictive models are being developed to inform how litter accumulates beneath tree crowns. Our findings along with other related studies, suggest that similar models can be created to predict accumulated duff layers as well.

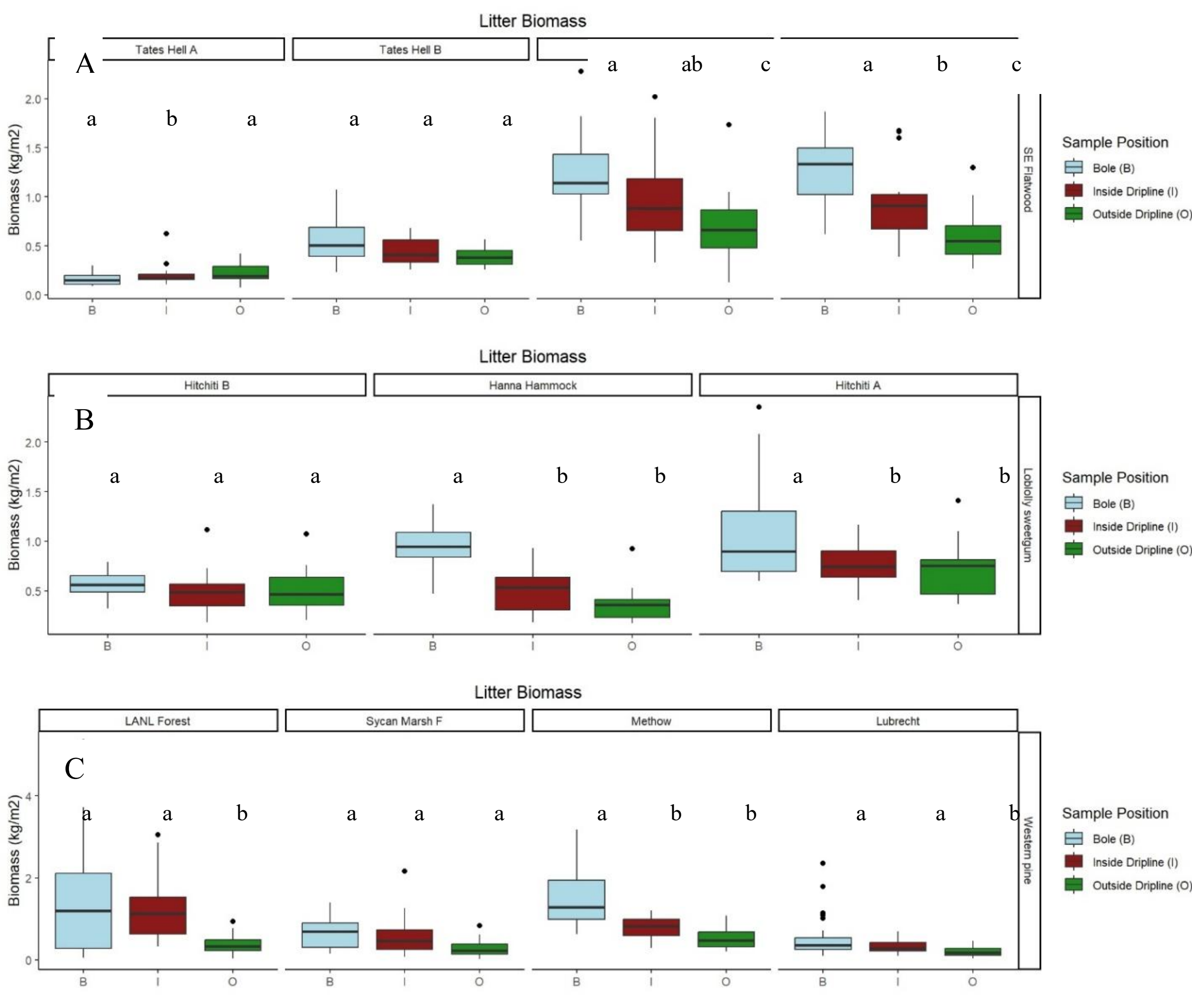

Figure 23: Biomass of litter layers across bole (B), inside (I) and outside (O) crown positions for A) SE mesic pine flatwoods, B) SE loblolly-sweetgum forests, and C) western pine forests. Significant differences between transect positions are noted (a, b, c).

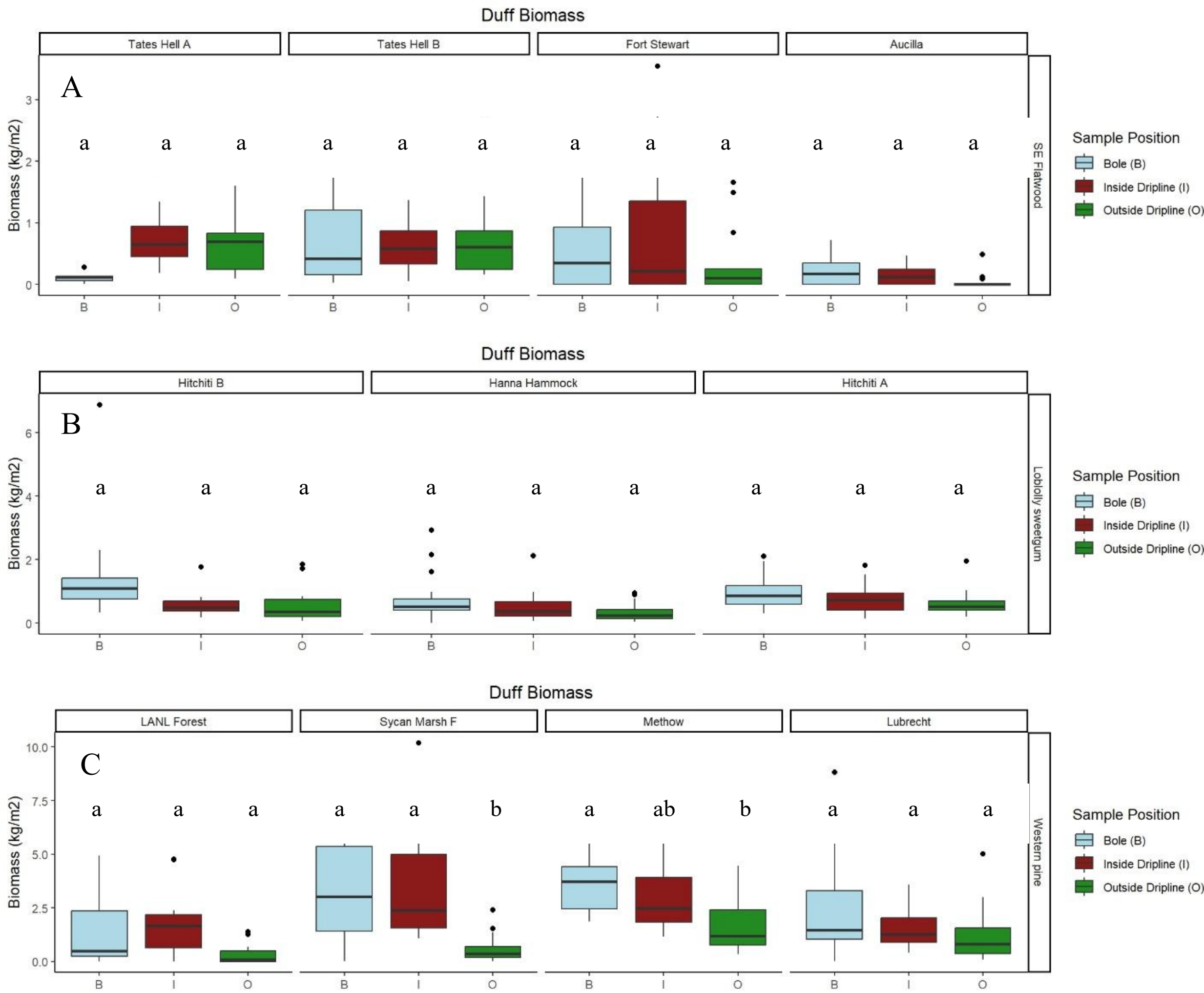

Figure 24: Biomass of duff layers across bole (B), inside (I) and outside (O) crown positions for A) SE mesic pine flatwoods, B) SE loblolly-sweetgum forests, and C) western pine forests. Significant differences between transect positions are noted (a, b, c).

4.4 INTRINSIC FUEL PROPERTIES LIBRARY

The objective of creating the Intrinsic Fuel Properties Library (IFPL) was to provide a central repository of fuel properties that can be used to refine fuel characterization for wildland fire behavior modeling. Computational fluid dynamics models of fire behavior rely on 3D grids of wildland fuel structure, composition, and properties. In this task, we compiled literature and created an online database that is the first of its kind. The IFPL currently supports values specific to North America but was designed to be expandable. Recent advances in remote sensing approaches, including ALS, TLS, and SfM photogrammetry, are changing how wildland fuels can be characterized and mapped as multi-scaled representations of fuel structure and composition. Computational fluid dynamics (CFD) models such as FIRETEC (Linn et al. 2002) and WFDS (Mell et al. 2007) require 3D inputs of wildland fuels and are capable of modeling fire behavior, smoke production, and informing wildland fire risk assessments. Similarly, Finney (2021) is developing a 1D model of fire behavior that is based on particle-based consumption and involves much higher precision and resolution than operational fire models.

Prior to this project, published literature on fuelbed and fuel particle properties existed, but a consistent library of values with uniform units and fuel typing was not available. Fuelbeds are defined as fuel complexes in wildland fuel environments and are generally represented in layers (also called strata) such tree canopies, shrub layers, grasses, downed wood, litter and duff (**Table 10**). Fuel particles are defined as the finest scale of fuel characterization and include leaves, needles, grass blades, palm fronds, and downed wood or wood fragments. Particle properties are organized into three main categories including mineral content and char fraction, heat content, particle density, and surface-area-to-volume ratio (**Table 17**).

The 3D Fuels project is focused on characterizing wildland fuels in southeastern US pine and western ponderosa pine forests. As such, we prioritized our literature review and compilation of records using these vegetation types. From there, we expanded our scope to include the following North American vegetation types in our literature review as well as international records with the majority coming from Australia, Europe and Brazil. The IFPL dataset was compiled in a relational database that supports a text file (csv format) export supported within an online repository and documented field definitions (Table 3). A common set of fuel types by fuelbed and fuel particle property was developed to standardize data labels and search queries. We also entered native units from published papers and then standardized conversion to standard metric units. An intermediate version of the database can be accessed as Excel workbook with the database export (IFP DB), references, source pdfs, and a data dictionary (Open Science Framework, DOI 10.17605/OSF.IO/WXEPJ). Following data entry and an extensive quality control/assurance review, we created a webtool that allows users to query the database by fuel type and region.

To date, the database includes 159 sources with a total of 8,308 records. Data coverage varies by intrinsic fuel properties with the most entries for bulk density/specific gravity (3,229) followed by heat of combustion/heat content (1,540), ash fraction (1,030), and surface-area-to-volume ratio (634). The database supports 1454 fuelbed records (e.g., bulk density, porosity) and 6209 fuel particle records (e.g., particle density, surface-area-to-volume ratio) from North America.

The IFPL can be accessed at: https://depts.washington.edu/fera/3dfuels/ifpl. The main screen has two tabs, including Fuelbed Layer Properties and Fuel Particle Properties. The IFPL opens with Fuelbed Layer Properties and displays summaries of all supported fuelbed layer values by fuel type and forest floor material (**Appendix A2**). To date, only North American records are available for query. In addition to summarized values by search criteria, the IFPL also offers tabular (csv) downloads of individual records and source citations for each search.

The IFPL is intended to be an expandable library of intrinsic fuel properties with a defined data type structure that facilitates consistent input and unit assignment for source records. To date, we have focused on published records within North America, but our base dataset contains records from Eurasia, Australia and South America and could be expanded to serve as an international reference library. The objective of the IFPL is to provide both fuelbed and fuel particle properties for attribution in fire behavior and smoke modeling. Because summary values are taken from disparate sources, we recommend that users carefully review values and any potential inconsistencies they represent as inputs for fire behavior and smoke models.

Table 16. Fuelbed and particle properties in the IFPL, including metric units and definitions. Fuelbed properties represent the fuelbed layers (e.g., litter and duff layers or shrub or canopy stratum properties). Fuel particle properties represent individual fuel particles such as leaves, needles, cones and downed wood.

Variable	Abbreviation	Standard symbol	Standard unit	Definition
Fuelbed properties				
Bulk density	BD	ρ_b	kg m^{-3}	Mass per unit volume of vegetation or fuel, including interstitial air space (e.g., in-situ litter or duff).
Fuel loading / available fuel loading	FL	m_f	kg m^{-2}	Dry weight biomass per unit area; can also be expressed as the dry weight biomass available for combustion (not including live tree stems, for example).
Fuelbed depth or height of fuel layer	FD	Δ	m or cm	Height of forest or shrubland canopy layer; depth of surface or ground fuel layer (e.g., litter or duff depth)
Packing ratio	PR	B	Dimensionless (0-1)	The fraction of a known volume occupied by fuel particles -- calculated as the bulk density divided by the particle density.
Porosity	POR	Λ	Dimensionless (0-1)	The proportion of the bulk volume occupied by fine gaps.
Particle properties				
Heat of combustion	HOC	H_c	J kg^{-1}	The amount of heat released per unit mass or unit volume of a particle when the particle is completely burned
Mineral content	MC	%	Percent	Fraction of completely consumed fuel that is ash, reflecting mineral content, which is defined as the percentage of fuel particles composed of minerals. This property includes silica free ash content values.
Char fraction	CF	%	Percent	Remaining mass of a fuel particle after incomplete combustion (black ash).

Variable	Abbreviation	Standard symbol	Standard unit	Definition
Particle density [F W]	PD	ρ_p	g/cm3	Mass per volume of fuel element (leaf, fine branch, stem). Termed mass-to-volume-ratio in FIRETEC.
Specific gravity	SG		Ratio	The ratio of fuel density to the density of water.
Surface-area-to-volume ratio [F W]	SAV	σ	m^2/m^{-3} or cm^2/cm^{-3}	Ratio of fuel surface area to volume.

4.5 QSM MODELS OF COMMON SHRUBS OF THE SOUTHEASTERN US

Our study assessed the accuracy of TLS data in reconstructing architectural traits for common shrub species of the southeastern US (**Table 17**). We tested high density (QSM_H) and low density (QSM_L) TLS point cloud datasets to model ten architecturally different shrubs. We demonstrated that with the *TreeQSM* algorithm, we could reconstruct the overall architecture of the shrubs using both high and low point cloud density datasets. The derived heights from both approaches produced a high coefficient of determination. However, the QSM_H method could detect branches with better accuracy than the QSM_L method (**Table 18**). In addition, our analysis showed accurate reconstruction for larger diameters (>5 mm), while more work is needed for modeling smaller diameters. Furthermore, the complexity of the shrub (i.e., more branches, more compact, higher bifurcation, smaller diameter branches, etc.) affects the accuracy of the 3-D architectural model (**Figure 25**).

In general, we noted trade-offs between TLS point-cloud density, the complexity of the shrub, model input parameters, and processing time. For example, the more detailed the input data, the longer the preparation and processing time; however, this does produce more precise results. Therefore, the desired resolution of the 3D models, and the complexity of the shrubs scanned, should be considered in designing the experimental setup to generate the appropriate point cloud density. Other trade-offs may include TLS technology available, project budget and timeline, as well as project significance.

Further research into optimizing QSM algorithms for understory vegetation is still needed, especially for complex architectures. Future work should include fine-tuning input parameters and evaluating other parameters, such as volume estimations. A key focus of future research should also include improving QSM modeling to account for and better resolve uncertainties from TLS occlusion. Feasibility testing of leaf modeling and models derived from in-situ TLS data is also needed. In addition, future studies could include scaling up from single shrub level to multiple shrub or plot level studies. Despite these future research needs, the methodology used in this study already demonstrates the generally high accuracy of shrub models generated using existing TLS instrumentation. QSM shrub reconstructions are nondestructive, versatile representations of plant architecture. Many fields, including forestry, agriculture, ecology, silviculture, and fire behavior, would benefit from these detailed 3D shrub models.

Table 17. Summary of shrub characteristics and calculated traits in the QSM study, including branch diameter range (min to max), shrub form, highest branching order (BOh), and shrub complexity (Sc).

Shrub ID	Shrub Common Name *(Scientific Name)*	Height (cm)	Branch Diameter Range (mm)	Shrub Form	*BOh*	*Sc*
1	winterberry holly *(Ilex verticillate)*	121	1-29	Columnar	5	0.27
2	highbush blueberry *(Vaccinium corymbosum)*	54	2-7	Irregular	4	0.14
3	alder-leaved buckthorn *(Rhamnus alnifolia)*	64	2-15	Vase-like	6	0.92
4	azalea *(Rhododendron klondyke)*	95	4-27	Vase-like	3	0.00
5	Lodense privet *(Ligustrum vulgare)*	43	3-8	Columnar	4	0.53
6	'rosebud' azalea *(Rhododendron rosebud)*	36	2-5	Rounded	2	0.06
7	southern arrowwood *(Viburnum dentatum)*	57	0.5-32	Rounded	6	0.32
8	barberry 'concorde' *(Berberis thunbergii)*	40	3-10	Rounded	3	0.2
9	meserve holly *(Ilex x Meserveae)*	62	3-24	Vase-like	6	1.00
10	sky pencil *(Ilex crenata)*	71	3-15	Columnar	4	0.32

Table 18. Percentage of manually measured branches detected by low density (L) and high density (H) point clouds.

Model	Reference Branch Count	Average QSM branch Count	Average Std. dev	% branches detected
QSM_H (correct)	1347	1059.33	12.98	78.64
QSM_L (correct)	1347	748.50	21.46	55.57
QSM_H (error_included)	1347	1203.00	10.50	89.31
QSM_L (error_included)	1347	1098.00	18.60	81.51

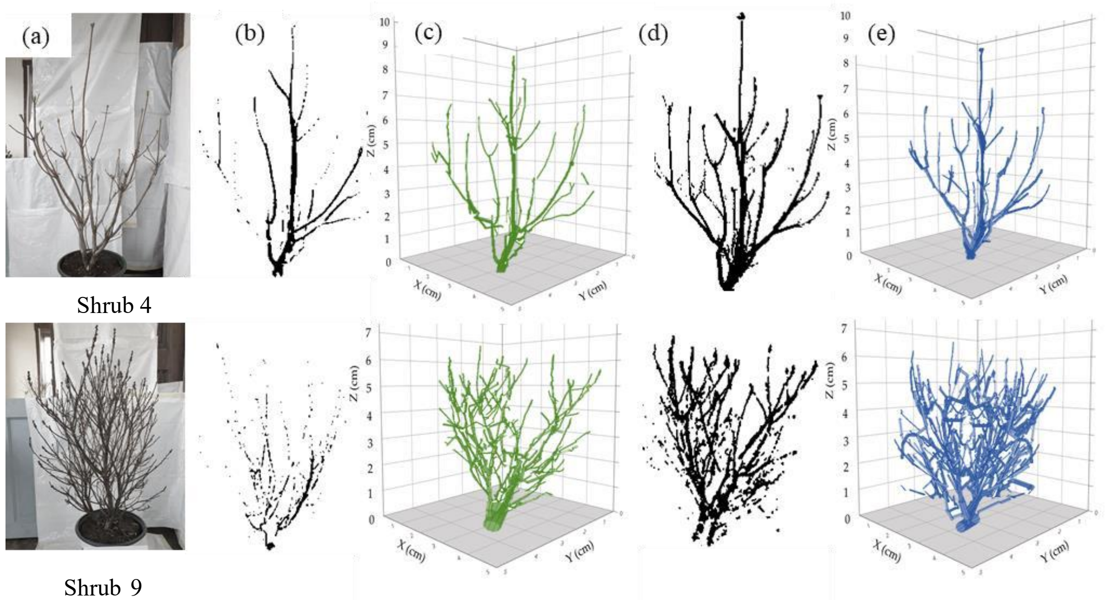

Figure 25. Examples of shrub representation as point clouds and QSM models. Top row: shrub 4, the shrub with the lowest complexity (Sc). Bottom row: shrub 9, the shrub with the highest complexity. (a) photo of shrub (b) low-resolution TLS point cloud. (c) Reconstructed QSM_L using TreeQSM. (d) High-resolution TLS point cloud and (e) reconstructed QSM_H using TreeQSM .

Finding 1: *Low and high density point clouds both had strong linear relationships with shrub height and branch detection.*

Both QSM_L and QSM_H calculated shrub heights showed a strong linear fit with the measured shrub heights (**Figure 26**). QSM_L had an R2 of 0.98, an RMSE of 5.18 cm and an MAE of 4.43 cm. Except for shrub 3, there were only slight variations between iterations. The QSM_H had a marginally higher R^2 of 0.99, and lower RMSE and MAE of 3.20 cm and 2.40 cm, respectively. When all the identified branches are included in the total branch count, including the incorrectly labeled branches (e.g., QSM_H(error_included)), not surprisingly, the total number of branches increased, and these increased number of branch estimates are closer to the measured number (**Table 21**). The erroneously modeled branches inflated branch detection percentages by nearly 11% and 26% for QSM_H and QSM_L, respectively.

For the QSM_L, the prediction of branch diameter had an R^2 was 0.94 with RMSE of 0.79 mm and MAE of 0.61 mm. The regression results for the QSM_H had a slightly lower R^2 of 0.91 and higher RMSE and MAE than the QSM_L. Both sets of models underestimated branch diameter. The standard errors of the models indicate that the QSM_L models had extensive ranges of modeled values for the same branch. For diameters smaller than 5mm, the *TreeQSM* models generally overestimated the branches, with both the QSM_L and QSM_H models exhibiting relatively low R^2 values of 0.44 and 0.37, respectively, and high standard errors. In contrast, branch diameters larger than 5 mm were predicted much more accurately.

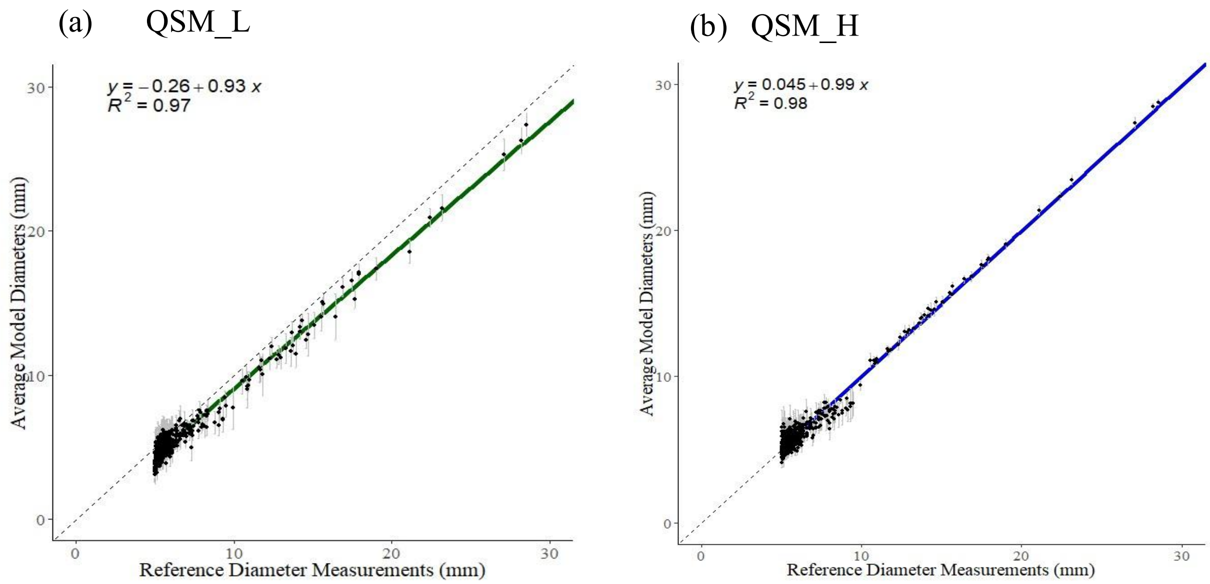

Figure 26. **Linear regression of modeled vs measured shrub branch diameter for branches > 5 mm in diameter for QSM_L (a) and QSM_H (b).**

For QSM_L, 13% of detected branches were overestimated (0.6 mm thicker on average) and diameters larger than 5 mm were underestimated by 9% (1.12 mm thinner on average. Notwithstanding that the QSM_H had a higher branch count, it performed better for branch diameter classes larger than 5 mm, with an average percentage error of only 2.6%. For branches larger than 10 mm, the QSM_H diameters were only slightly overestimated. Furthermore, the range in diameter predictions for any one branch was generally smaller for QSM_H than for QSM_L.

Finding 2: *Low-density point clouds are adequate for shrubs with simple architecture, but high density point clouds are likely required for shrubs with complex architecture.*

The final objective of this study was to determine whether architectural traits influence the accuracy of the models. We classified shrubs into one of four categories of shrub complexity (*Sc*): Low= $Sc \leq 0.25$, Medium = *Sc* between 0.25 and 0.5, High = *Sc* larger than 0.5 and less than 0.75 and very high = $Sc \geq 0.75$. As the shrub's complexity increases, the percentage of branches detected decreases for both modeling methods. However, this change in accuracy for the QSM_L method is greater than for the QSM_H method. Overall, the QSM_H maintains a high level of accuracy (above 75%), which remains relatively constant as the shrub complexity increases. We found that the QSM_L method accurately detected branches in low-complexity shrubs (72.69%); however, the accuracy of branches detected for highly complex shrubs fell to 56.47%. For example, of the 117 branches of medium complex shrubs, 81 branches were undetected by QSM_H, while for the most complex shrubs with 685 branches, QSM_H did not detect approximately 150 branches. Rounded crown-shaped shrubs had more branches detected with both QSM_H and QSM_L methods, 83% and 68%, respectively. Similarly, the columnar-shaped shrubs had the least number of branches detected in both QSM methods. The maximum difference in branch detection between the various shrubs forms was approximately 12% for QSM_H and 16% for QSM_L.

Table 19. Coefficient of determination results comparing manually measured diameters to modeled diameters for QSM_H by complexity and by shrub form.

Shrub Complexity	Branch diameter prediction vs. model R^2	Shrub Form	Branch diameter prediction vs. model R^2
Low	0.97	Columnar	0.90
Medium	0.94	Rounded	0.92
High	0.87	Vase-like	0.92
Very high	0.84	Irregular	0.63

The qualitative evaluation of the QSM models indicates that while the models successfully captured the overall shrub form, incorrectly modeled or occluded branches were more common with the low density TLS data. In general, the quality of TLS data varies with the type of TLS instrument used and also its characteristics, scan setup and layout, co-registration and the processing of the point cloud (Disney et al. 2018, Wang et al. 2020). We kept the model input parameters (patch diameter and ball radius) consistent for all the shrubs over the multiple model runs for each shrub, after having optimized them based on initial experiments with the shrubs. It is important to note that changing these parameters would likely change the resulting QSM models. The absolute and relative error by diameter class gives insight regarding which diameters are estimated accurately and where the QSM may need improvement. The QSM_L had a relatively high percentage of errors for all diameter classes, whereas the primary source in the QSM_H resulted from the '0-5 mm' diameter class. Both methods overestimated the smallest diameter class.

We found that shrub architectural form and complexity have a notable effect on model accuracy metrics such as the percentage of branches detected. As suspected, accuracy decreased as complexity increased for QSM_L. We observed a gradual decline in R^2 as the shrubs' complexity (*Sc*) value increased. However, for the QSM_H method, the percentage of branches detected for low complexity shrubs initially declined (approximately 10%), then stabilized at 75% as shrub complexity increased. Although the portion of branches detected remains relatively constant, we noted that the count of branches that were not detected nevertheless increased as shrub complexity increased. The decrease in branch detection is conceivably due to intricate branching patterns causing occlusion of the internal architecture of the shrub as well as small twigs not captured by the TLS point cloud. Our research highlights a strong relationship between the TLS input data and the *TreeQSM* results and offers a promising approach for future QSM of shrub architecture.

4.6 RELATIONSHIP BETWEEN TLS REFLECTANCE AND LITTER FUEL MOISTURE

In this laboratory based study, we quantified changes in fuel moisture using active sensor laser pulses at set distances from two 1550 nm lidar units. Beyond the determination that lidar intensity returns can be used to estimate fuel moisture levels, we also determined that time-of-flight and a phase shift lidar units can both effectively measure changes in moisture in litter fuel beds. These findings corroborate studies that have used lidar to determine material characteristics using the intensity of the return values (Di Biase et al. 2021; Zahiri et al. 2021). They are also in close agreement with studies that utilized dual band TLS point clouds to determine live leaf moisture content (Elsherif et al. 2018; Gaulton et al. 2013; Junttila et al. 2016). However, this study provides an important new perspective on using a single wavelength TLS unit to determine moisture content of wildland fuels. While we limited our study to common forest litter types, this is an important step in utilizing an active sensor to relate spectral qualities of wildland fuels with fuel moisture while also capturing 3D positional information.

The purpose of this study was to explore the relationships between different metrics derivable from TLS scans and known fuel moisture levels of samples in a laboratory setting. Our initial results are promising for a field application to estimate fuel moisture of forest litter from TLS intensity returns. Our results with high levels of significance and high coefficients of determination show that model development for field applications is possible. A variable model with distance from scanner incorporated will be necessary to provide reliable results. Further, most lidar datasets do not have calibrated intensity values, and the intensity values generally are relativized to a range of minimum and maximum intensity values returned within a scan. This inherently makes comparison between scans difficult. There are also numerous environmental factors that can influence lidar return values such as temperature, and humidity (Li et al. 2021; Strand et al. 2003). We performed our experiment in a controlled laboratory environment where we could be reasonably certain that no external factors would impact intensity return values between scans on different days.

Finding 1: *Measured fuel moisture contents, reflectance values, and modelled relationships*

Sample moisture content ranged from 0% (oven dried weight) to 300% (fully saturated). Red oak leaves and the fabric mesh had the highest saturated moisture content and weighed 3 times the dried sample weight. Maximum moisture content for conifer needle litter ranged between 160% to 200%. Fully saturated pine boards reached approximately 65% moisture content. Sample reflectance values at 1550 nm ranged from 0.1 when fully saturated to 0.6 when oven dried (**Figure 27**). The highest variance between sample moisture content was generally observed at ~1450 nm but a large spread of moisture values was also observed around 1550 nm. Regression analysis showed that sample reflectance at 1550 nm had a significant negative relationship ($p < 0.05$) with measured fuel moisture (**Figure 28**). The rate of the decrease, variance of the points, and shape of the relationship changed depending on the sample material.

Reflectance at 1550 nm as recorded by the spectrometer was strongly correlated with the intensity values from the TLS units. Model fit differed among sample types, with the lowest coefficient of determination for pine boards. This was likely due to the heterogenous reflectance, an artifact of the wood grain and knots. Aside from the pine boards, there was also a clear tendency for the more compact samples to have a higher coefficient of determination (e.g., Douglas-fir needles and the fabric mesh). Ponderosa pine, longleaf pine, and southern red oak had relatively low packing ratios with large amounts of air space within the samples. This structure also provided a more varied surface for reflected lidar pulses compared to the more homogenous surface of a compact sample. Variance in the relationship between the spectrometer readings and the intensity returns from the TLS units were similar between the FARO and REIGL units.

Finding 2: *Modeled relationships were strong overall but weak within the range of prescribed burning operations*

We evaluated a range of metrics that can be derived from lidar pulse intensity. Of the 7 metrics evaluated, mean intensity per sample and standard deviation of intensity values per sample produced the most robust models. Broken stick linear regression models had high coefficients of determination, but relationships were strongest when samples had a moisture content greater than 100%. At these moisture content levels, the strong relationship was likely only due to surface water evaporation. Changes in intensity values were much smaller once surface water evaporated and moisture was primarily intercellular. This result suggests lidar-based fuel moisture sensing will not be reliable in informing decisions based on fuel moisture content less than 30%, which is typically required for prescribed burn planning (Pollet and Brown, 2007; Wade, 2013). However, lidar-based measurements could be helpful in remote stations that detect when live and dead fuel moistures are curing and potentially available for wildfires.

Finding 3: *We found consistent relationships between phase shift (FARO) and time of flight (RIEGL) instruments. Relationships between TLS reflectance and fuel moistures were robust across a range of tested sampling angles and distances, but the RIEGL performed better at greater distances from the scanner.*

We also evaluated if angle of incidence and distance from scanner influenced lidar intensity returns and how results differed between PS and TOF sensors. While a strong relationship was found between laser pulse return intensity and fuel moisture, the relationship deteriorated with distance from the scanner. This result was consistent between PS and TOF scanners. Coefficients of the relationship between intensity and moisture also changed as distance increased (**Table 20**). The TOF scanner maintained a stronger relationship as distance increased while the PS scanner only had a strong relationship at close ranges. The mean of lidar intensity values had the strongest correlation with fuel moisture for the RIEGL data and performed well for the FARO data.

For this study we were interested if TLS can be used in the field, where variability is inherent in the ground surface. The angle of incidence of each lidar pulse is determined not only by the orientation of the sample relative to the ground, but also the distance of each sample from the scanner. With a single exception of fully saturated pine boards located 3 m from the FARO scanner, there was no significant difference between the regression coefficient with samples at 45^{o} compared to samples at 0^{o} relative to the ground.

Correlations between reflectance and fuel moisture were comparable between the FARO and RIEGL units. However, beyond a distance of 3 m, the RIEGL unit performed much better than the FARO at modeling fuel moisture. While the relationship deteriorated with distance for the RIEGL, the rate of deterioration was much less than that of the FARO. Deterioration was related to the distance, the angle of incidence, and the footprint size. The coefficient of determination for final broken stick models ranged from 0.98 for the southern red oak and fabric mesh samples at 3m distance to 0.07 for long leaf pine at 12 m. With few exceptions, regression models of reflectance values from the TOF REIGL had stronger model fits than that of the PS FARO, especially at the further distances (**Table 19**).

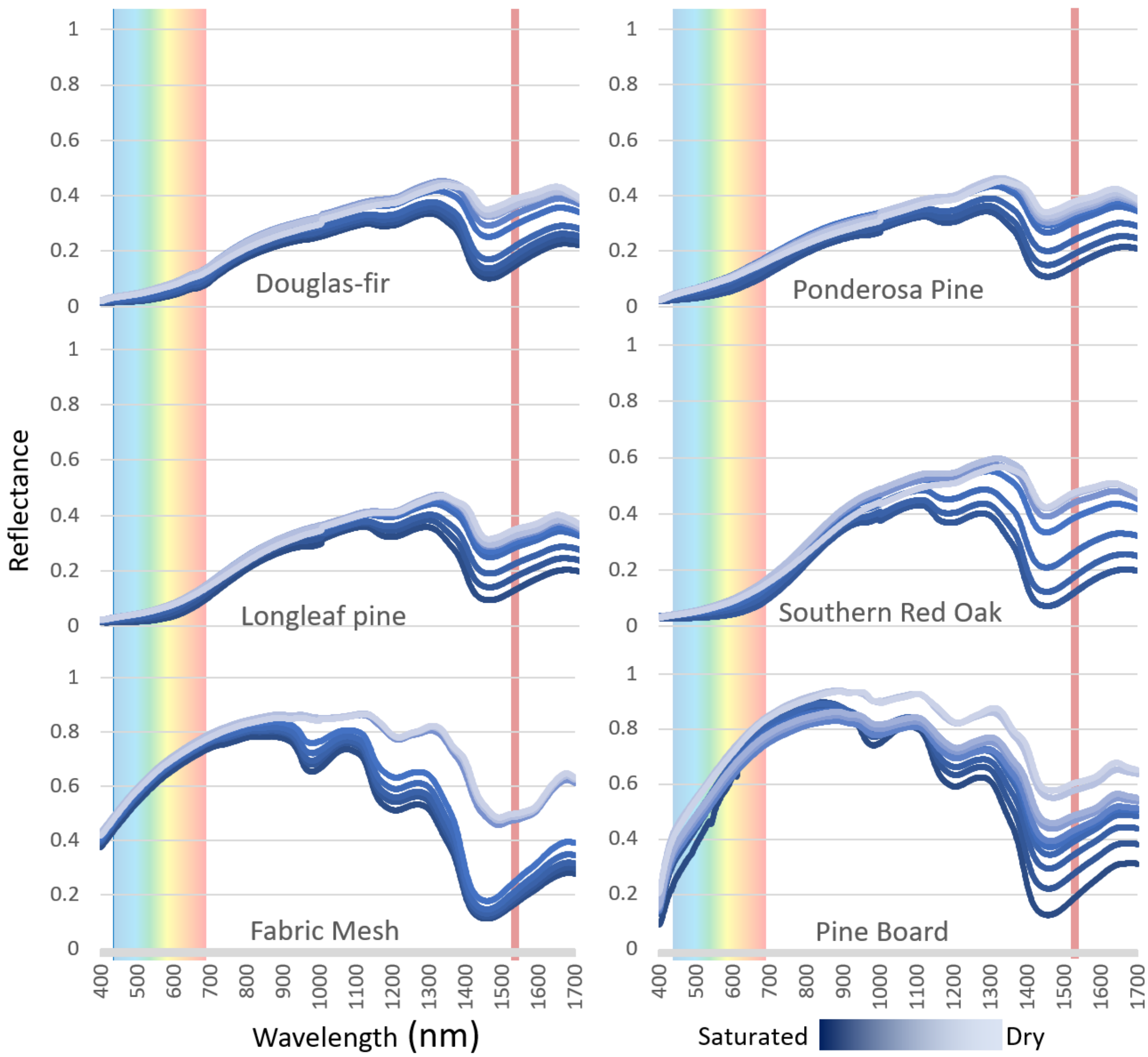

Figure 27. Mean reflectance values by sample material and saturation level. The dark blue line represents samples at full saturation, with the color lightening to light blue for the final oven dried reflectance values. The red line at 1550 nm represents the wavelength of the TLS units used for this experiment.

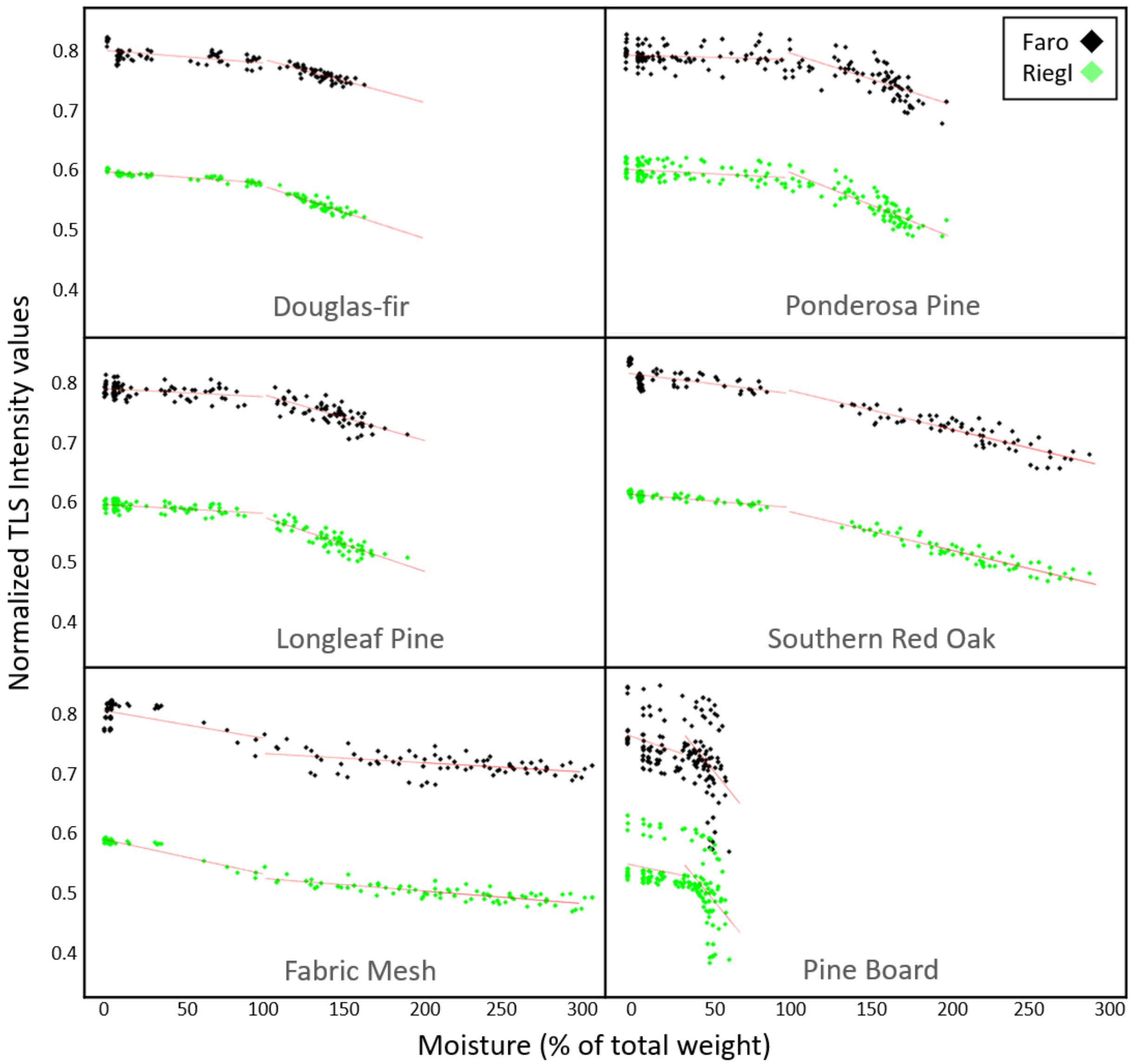

Figure 28. Mean normalized intensity values of the samples placed at 3 m from FARO and RIEGL scanners. Regression lines from a broken stick linear regression model are added. The selected break location was 100% for all sample materials except pine board where the break was located at 40%.

Table 20. **Coefficient of determination values for multiple linear regression models across sample types.** FM0, 45, and 90 indicate the sample angle relative to the ground.

Mean and SD		DF R^2	PP R^2	LLP R^2	SRO R^2	FM0 R^2	FM45 R^2	FM90 R^2	PB0 R^2	PB45 R^2	PB90 R^2
FARO	ALL	0.65	0.40	0.28	0.83	0.66	0.84	0.88	0.25	0.44	0.49
RIEGL	ALL	0.86	0.56	0.69	0.95	0.92	0.94	0.92	0.32	0.54	0.50
FARO	3M	0.94	0.78	0.86	0.95	0.91	0.96	0.96	0.43	0.59	0.52
RIEGL	3M	0.95	0.76	0.90	0.98	0.96	0.98	0.98	0.46	0.65	0.61
FARO	6M	0.81	0.55	0.68	0.94	0.87	0.94	0.95	0.34	0.58	0.60
RIEGL	6M	0.92	0.60	0.79	0.97	0.94	0.97	0.98	0.38	0.58	0.63
FARO	9M	0.62	0.45	0.19	0.91	0.66	0.86	0.84	0.25	0.47	0.45
RIEGL	9M	0.83	0.51	0.72	0.96	0.93	0.97	0.97	0.30	0.55	0.67
FARO	12M	0.54	0.37	0.07	0.85	0.66	0.89	0.86	0.17	0.44	0.44
RIEGL	12M	0.88	0.49	0.68	0.93	0.92	0.97	0.97	0.26	0.50	0.67

Finding 4: *Implications for field-based TLS fuel moisture monitoring*

The purpose of this study was to explore the relationships between different metrics derivable from TLS scans and known fuel moisture levels of samples in a laboratory setting. Our initial results are promising for a field application to estimate fuel moisture of forest litter from TLS intensity returns. We performed our experiment in a controlled laboratory environment where we could be reasonably certain that no external factors would impact intensity return values between scans on different days. The next potential step for this application of TLS is to take the scanners into the field for real world data collection. This study provides the background and regression analysis parameters for application to field collected data. To operationalize lidar scanning to quantify fuel moisture levels beyond fine scale moisture mapping from a stationary location use of UAS or mobile lidar units may be possible. In particular, a UAS-based lidar unit sampling at 1550 nm wavelengths could cover a much larger area with a more consistent distance from ground than a stationary tripod mounted TLS.

Applications beyond fuel moisture mapping are numerous. A UAS-based lidar unit could be used for detection and verification of wetland below canopy by isolating only the ground returns and determining locations of inundated soils and vegetation. While ALS has been used to detect inundated areas under canopy, a UAS-based approach would allow for the intentional selection of lidar sensor using 1550 nm wavelength as well as greater temporal resolution of resampling. Any query where detection of ground moisture is important could take advantage of the benefits of using an active sensor over a passive sensor spectroradiometer.

Because of weak relationships with lower fuel moisture values, TLS may not be useful for helping to inform decisions about wildland fire behavior, but it can be useful to determine moisture gradients, seasonal shifts in fuel availability for combustion, and the detection of areas with high moisture and water content such as seeps and small wetlands. To further evaluate this method, field studies are needed to measure TLS coupled with field measurements of ground moisture to verify the ability of TLS to quantify fuel moisture outside of a laboratory environment.

5.0 CONCLUSIONS AND IMPLICATIONS FOR FUTURE RESEARCH

As a precursor to a comprehensive system that can characterize wildland fuels in 3D for operational decision support, our project produced a 3D repository of voxel fuels, intrinsic fuel properties and quantitative modeling scripts that partition point cloud data into voxels and create 3D input for existing and custom applications. Based on our work on quantitative modeling, intrinsic fuel properties and model sensitivity analysis, the 3D Fuels project lays the groundwork for an eventual application, called FuelsCraft, that will integrate and parse hierarchically sampled 3D Fuels data using machine learning (AI) for next-generation fire behavior and effects modeling (ESTCP Project RC23-7779). Our hierarchical approach to 3D fuel characterization, with a focus on both surface and canopy fuels, facilitates the production of fine-scale fuel meshes for physics-based models and coarser meshes to be used in current and future operational models for prescribed burning. As an intermediate step towards a fully integrated 3D Fuels modeling framework, we anticipate that results from this project will contribute to the development of 3D fuels modeling that can augment current functionality in FUELS3D and STANDFIRE and increase their applicability for operational use.

Prescribed burning programs commonly target frequent understory burning to maintain fire-adapted understory vegetation and structure in southeastern western US pine forests. Although prescribed fire managers are aware of how spatial complexity of fuel types, status (live/dead), and fuel moisture influence patterns of fire spread, duration, and intensity, available maps of understory fuels are often not of sufficient resolution and accuracy to guide prescriptions. For example, LANDFIRE provides a reasonable starting point for forest type and disturbance history of large fires or other disturbances, but understory fuel characterization is generally imprecise and in need of site-specific customization. Under extreme fire weather and behavior, including wind-driven fire spread and large fire size and growth, thresholds to burning are low and fine-scale patterns of surface fuels are eclipsed by large-scale fire behavior (Werth et al. 2011). However, under milder burning conditions (low wind, surface fires), under which prescribed burns and managed wildfires are conducted, the structure and composition of surface fuels are critical to fire spread, duration, and intensity (Hiers et al. 2009, 2020, Rowell et al. 2022). Operational models of fire behavior that are used in wildland fire management planning would greatly benefit from improved characterization of understory fuel complexes for decision support under increasingly complex weather and burning environments.

Due to issues with canopy occlusion and their inherently high spatial and temporal variability, understory fuels often are poorly characterized using airborne remote sensing platforms (Gale et al. 2021). For wildland fire behavior and effects modeling, this presents an ongoing challenge. Understory fuels, which are generally termed surface fuels in wildland fire behavior modeling, are the primary driver of fire spread and energy transfer (Rothermel 1972, Keane 2015, Finney et al. 2021). Even when forest canopies are burned in crown fire events, fire behavior is generally still dependent on the fire intensity, duration and spread of surface fuels. As such, the spatial configuration and composition of surface fuels are critical components of wildland fire behavior and effects but are often greatly oversimplified in models due to a lack of spatially resolved data.

A promising development in operational fire behavior modeling is the transition from full computational fluid dynamics modeling of fire behavior and combustion to more operational applications such as QUIC-fire, which implements FIRETEC on a coarser grid with rapid computations and WFDS-levelset, which spreads fire based on gridded terrain, fuels and wind inputs (Bova et al. 2015). Both implementations can use the full physics-based modes to produce calibrated fire spread and intensity and then model fire progression on coarser fuel meshes and over large landscapes. Another key deliverable will be a data archive of 3D fuels and consumption that can be used as evaluation datasets to inform operational prescribed burn programs on DoD installations.

The 3D Fuels datasets and modeling steps will be used to generate inputs to CFD models and 3D fuel characterization. These will be used to develop new operational models of fire behavior, smoke and other fire effects (Hoffman et al. 2018, O'Brien et al. 2018). A key advantage of our 3D fuel modeling approach is that voxel fuels were treated as scalable building blocks and the process of partitioning point cloud data into voxel fuel inputs can be widely applied to other fuel types and complexes. In this project, we were focused on some of the most commonly burned fuel types on DoD lands. We intentionally selected geographically distinct vegetation that has similar structures (e.g., southern pine and ponderosa pine forest understories). Through sampling of parallel fuel structures, we can evaluate how the process of 3D fuel characterization at the voxel level can be applied to structurally similar vegetation and fuels and customized to the fuel properties that may vary by species (e.g., S:V, bulk density) and fuel conditions that vary by geographic region and day-of-burn conditions (e.g., fuel moisture). A preliminary example of this is some predictive fuel mapping that was conducted at Blackwater River State Forest as part of a coordinated FIREX-AQ and 3D Fuels campaign (**Figure 29**).

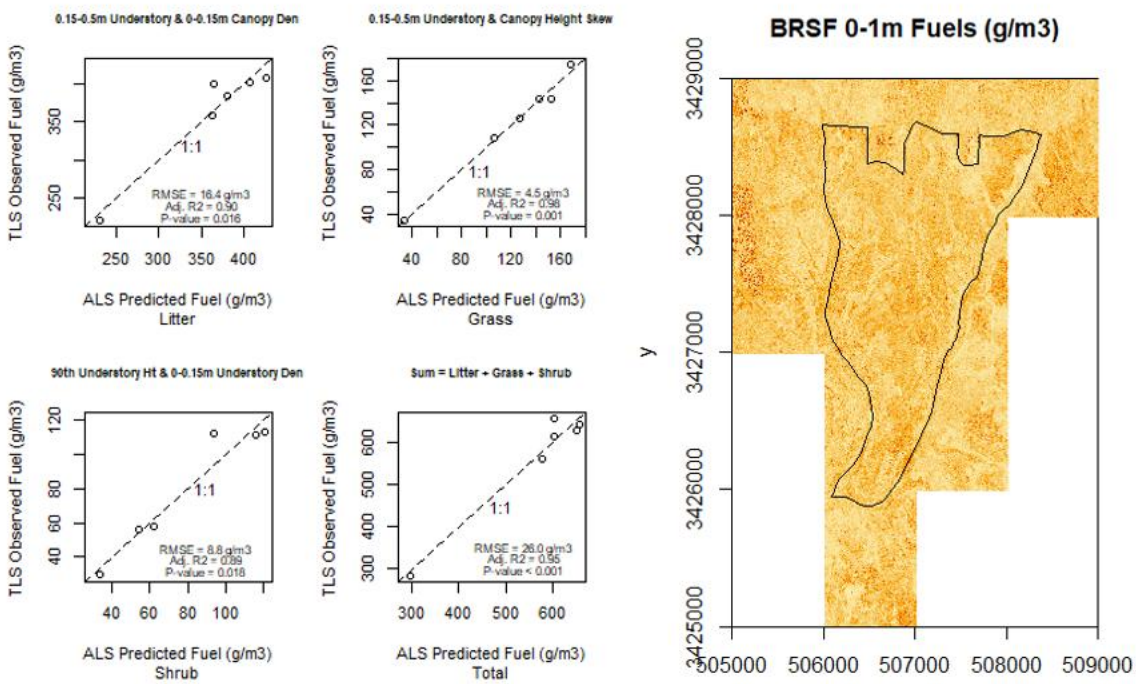

Figure 29: Predicted surface fuel bulk density (g/m3) based on ALS canopy metrics for the Blackwater River State Forest site.

Our work was guided by four research questions, which have been addressed by this project but remain highly relevant to subsequent research being conducted by SERDP and ESTCP-funded fire science projects.

1) ***What are the appropriate sampling resolutions of wildland fuels to model fire behavior and consumption, ranging from full physics-based modeling applications to operational models of fire behavior and consumption?***

This question was foundational to the 3D Fuels hierarchical sampling design and is being actively explored by others in the field of wildland fuel characterization (e.g., Maxwell et al. 2023). In addition to sampling fine-scale fuels data within 0.5x0.5x1.0 m voxel plots, subsampled into 10x10x10cm voxels for occupied volume and 50x50x10 cm strata for bulk density sampling, we also produced high resolution scans of surface fuels at the scale of 5x5m sampling plots and also at unit-wide synoptic scanning. In addition to surface fuel characterization within our hierarchical sampling design, we also calculated canopy metrics for all forested sites to facilitate unit-scale mapping of canopy and surface fuels.

To specifically address these question, we partnered with Russ Parsons (coI) and a modeling team, including Jesse Johnson, Eric Borke (MS student) and Anthony Marcozzi (MS student) with the University of Montana Computer Science department. Two complementary studies were supported as part of the Closing Gaps project to perform model sensitivity analyses of fuel types and resolutions with the physics-based model WFDS. Together, these studies demonstrate that coarse grid resolutions are sufficient to represent observed fire behavior at the scale of an experimental burn (Borke 2023) and tree seedlings (Marcozzi et al. 2023). Further sensitivity analyses are planned within the FuelsCraft project.

2) ***What are the critical fuelbeds and physical fuel properties required to advance physics-based fire behavior, smoke, and fire effects models for operational use on DoD installations? Specifically, is fine-scale heterogeneity in surface fuels critical to mapping and quantifying fuel consumption in sites commonly burned on DoD lands?***

Through detailed field sampling and comparison with point cloud metrics, we contributed to a systematic classification of major fuel types in southeastern mesic flatwoods, southeastern loblolly-sweetgum forests, western ponderosa pine/mixed conifer forests, and western grasslands. The fuel typing (**Table 3**) was developed in coordination with work that is ongoing by Louise Loudermilk and others on related SERDP and ESTCP projects. Through our work on the FuelsCraft project and active collaborations with Russ Parsons (SERDP Closing Gaps Project), Andy Hudak (SERDP Objects Project) and other wildland fire scientists and modelers, we will continue to examine where and when fine-scale surface fuel characterization is critical for predictions of wildland fire behavior and consumption.

3) ***How can we most efficiently and accurately create gridded, 3D maps of surface fuel properties based on the integration of remotely sensed imagery and fuel properties informed from field-based and laboratory measurements?***

Through active and ongoing collaborations, the 3D fuels project contributed to development of object-based fuel classification and landscape mapping that have moved from image and field data collection to a coordinated system that will produce realistic fuelbeds for wildland fire behavior modeling. Specifically, the 3D Fuels project has transitioned into the development of FuelsCraft, which will allow users to create and modify synthetic fuelbeds of highly realistic canopy and surface fuels predicted from coordinated imagery, including synoptic ALS and TLS datasets, informed by fine-scale remote sensing and field measurements (Rowell et al. 2016, Rowell 2017). The recently funded ESTCP FuelsCraft and FastFuels are codeveloping FuelsCraft to create an onramp of realistic canopy and surface fuels for use in FastFuels and QUIC-Fire. This work is ongoing with the SERDP Objects Project led by Andy Hudak (PI), and past collaborations with the SERDP Closing Gaps Project inspired the latest ESTCP project on FuelsCraft.

4) ***What are the tradeoffs between input precision, model fidelity, and time to collect and integrate 3D datasets?***

The 3D fuels project was designed to create a novel hierarchical dataset of coordinated remote sensing and field measurements. The 3D fuels project likely oversampled the heterogeneity of surface fuelbeds to help inform uncertainty in wildland fuel mapping and as inputs to wildland fire behavior and effects modeling. Our investment in field-based estimates of surface fuel biomass and bulk density was considerable and realistic only within a funded research campaign. For model sensitivity analysis funded through the 3D fuels project, we partnered with Russ Parsons (coI) and a modeling team, including Jesse Johnson, Eric Borke (MS student) and Anthony Marcozzi (MS student) with the University of Montana Computer Science department.

Two complementary studies were supported to perform model sensitivity analyses of fuel types and resolutions with the physics-based model FDS. Together, these studies demonstrate that coarse grid resolutions are sufficient to represent observed fire behavior at the scale of an experimental burn (Borke 2023) and tree seedlings (Marcozzi et al. 2023). Our work with FuelsCraft will allow us to generate synthetic fuelbeds to be used in iterative modeling of how sensitive models such as QUIC-fire and FDS are to the resolution and precision of wildland fuel characteristics. Rowell and others led a SERDP-funded limited scope project on this topic (RC19-1329 Influence of Fuel Heterogeneity and a Novel Fuel Rendering Technique on Fire Spread Predictions). In that work, they highlighted the current limitations of QUIC-fire to relatively coarse grid sizes (2m).

Summary of Major Deliverables and Findings

1) 3D Fuels Data Repository

Through the creation of the 3D Fuels repository and supporting processing and analysis methods, the overall goal of our project was met. Specifically, the primary objective of this project was to advance our understanding of 3D fuel characterization and provide evaluation datasets that will advance physics-based fire behavior, smoke and other fire effects models for operational use at scales relevant to Department of Defense (DoD) land managers. Our hierarchical sampling design yielded detailed information on the structure and composition of canopy and surface fuels across southeastern pine, western pine and western grassland sites. The 3D Fuels repository is currently being archived with the SERDP-funded Wildland Fire Science Initiative data repository (https://wfsi-data.org).

2) Predictive models of biomass based on TLS and photogrammetry point cloud metrics

In this study, we evaluated predictive models of surface fuel biomass based on TLS- and photogrammetry point-cloud metrics. In addition to TLS scanning, we presented a novel, video-based approach for rapid data collection that demonstrates potential across multiple domains, and presented a suite of metrics that can be used to summarize point cloud models. Application of this technique has the potential to provide managers with an accessible option for inexpensive data collection and can lay the groundwork for rapid collection of input datasets to train landscape-scale fuel models. Videos collected from a handheld GoPro camera produced SfM point clouds with reliable representations of fuel height and structure across our sites that had somewhat better performance than our TLS approach, likely due to differences in scanning approaches. Specifically, TLS images were acquired from 4 high-resolution scans on the outside edges of 5x5 m plots whereas videos for the close-range SfM photogrammetry were collected less than 1m above each 0.5x0.5x1 m voxel plot.

3) Relationship of forest floor bulk density to tree crowns

As part of our larger effort to characterize the 3D structure and biomass of forest types common to prescribed burning programs in the southeastern and western US, study sites included southeastern pine flatwoods, loblolly-sweetgum plantations, and western ponderosa pine and mixed conifer forests. Our main objective was to evaluate if tree crowns, in combination with other site variables such as forest type and time since disturbance, can be used to inform local predictions of forest floor cover, depth and biomass. Within the three main forest types sampled in this study, we evaluated how forest floor layers vary across bole, inside tree crown drip line, and outside drip line positions. As anticipated, we found that litter and duff depth, biomass and bulk density were highly variable within and between sites with high reported standard deviations. Even with high reported variability, there were strong statistical differences across transect positions. These field-based observations offer valuable model evaluation data and will be used by the SERDP-funded Objects team for this purpose.

4) Development of the Intrinsic Fuel Properties Library

The Intrinsic Fuel Properties Library (IFPL) provides a central repository of fuel properties that can be used to refine fuel characterization for wildland fire behavior modeling. The IFPL currently supports values specific to North America but was designed to be expandable. Recent advances in remote sensing approaches are changing how wildland fuels can be characterized and mapped as multi-scaled, 3D representations of fuel structure and composition and as inputs to CFD models such as FIRETEC and FDS. Prior to this project, published literature on fuelbed and fuel particle properties existed, but a consistent library of values with uniform units and fuel typing did not exist. To date, the database includes 159 sources with a total of 8,308 records. The database supports 1454 fuelbed records (e.g., bulk density, porosity) and 6209 fuel particle records (e.g., particle density, surface-area-to-volume ratio) from North America. The IFPL can be accessed at: https://depts.washington.edu/fera/3dfuels/ifpl.

5) Quantitative structural models of shrub species that are common southeastern US shrub species

We modeled the shrub architecture of ten architecturally different shrubs at low and high point cloud densities. As a reference, we manually measured the shrub's architectural parameters and compared them to the QSM-derived parameters. The QSMs derived from both the low-density point clouds (QSM_L), and the high-density point clouds (QSM_H), showed a high agreement with reference shrub height measurements, with R^2 values of 0.98 and 0.99, respectively. QSM_H correctly modeled an average of 80% of branches, while QSM_L correctly modeled 56% of the branches. The accuracy of the models was similar across growth forms, but was strongly affected by architectural complexity and branch diameter size. The results of this study illustrate the potential of non-destructive lidar approaches for quantifying shrub architectural traits and provide guidance for where high-resolution point clouds may be required to capture complex shrub architecture.

6) Relationship between TLS reflectance and litter fuel moisture

The purpose of this study was to explore the relationships between different metrics derivable from TLS scans and known fuel moisture levels of samples in a laboratory setting. Our initial results are promising for a field application to estimate fuel moisture of forest litter from TLS intensity returns. Because of weak relationships with lower fuel moisture values, TLS may not be useful for helping to inform decisions about wildland fire behavior, but it can be useful to determine moisture gradients, seasonal shifts in fuel availability for combustion, and the detection of areas with high moisture and water content such as seeps and small wetlands.

Modeled relationships between TLS reflectance and litter fuel moisture had high coefficients of determination, but relationships were strongest when samples had a moisture content greater than 100%. At these moisture content levels, the strong relationship was likely only due to surface water evaporation. Changes in intensity values were much smaller once surface water evaporated and moisture was primarily intercellular. This result suggests lidar-based fuel moisture sensing will not be reliable in informing decisions based on fuel moisture content less than 30%, which is typically required for prescribed burn planning (Pollet and Brown, 2007; Wade, 2013). However, lidar-based measurements could be helpful in remote weather stations that detect when live and dead fuel moistures are curing and potentially available for wildfires. Correlations between reflectance and fuel moisture were comparable between the FARO and RIEGL units. However, beyond a distance of 3 m, the RIEGL unit performed much better than the FARO at modeling fuel moisture.

6.0 LITERATURE CITED

Anderson, H.E. 1982. Aids to determining fuel models for estimating fire behavior. GTR-INT-122. USDA Forest Service Intermountain Forest and Range Experiment Station, Ogden, UT.

Atchley, A.L., Linn, R., Jonko, A., Hoffman, C.M., Hyman, J.D., Pimont, F., Sieg, C. and Middleton, R.S. 2021. Effects of fuel spatial distribution on wildland fire behaviour. International Journal of Wildland Fire 30: 179-189.

Banwell, E.M. and J.M. Varner. 2014. Structure and composition of forest floor fuels in long-unburned Jeffrey pine-white fir forests of the Lake Tahoe Basin, USA. International Journal of Wildland Fire 23: 363–72.

Batchelor, J.L., Wilson, T.M., Olsen, M.J., Ripple, W.J. 2022. New structural complexity metrics for forests from single terrestrial lidar scans. Remote Sensing 15: 145.

Batchelor, J.L. 2023. Fine-scale remote sensing of forest structure and condition. PhD dissertation. University of Washington, Seattle.

Bester, M. S. 2022. The Burning Bush: Linking LiDAR-derived Shrub Architecture to Flammability. PhD dissertation. West Virginia University.

Borke, E.M. 2023. Assessing the impact of parallel burnout fires on flank rate of spread. MS Thesis. University of Montana.

Brown, S., 2002. Measuring carbon in forests: current status and future challenges. Environmental Pollution. 116, 363–372.

Bova, A.S., Mell, W.E., and Hoffman, C.M. 2015. A comparison of level set and marker methods for the simulation of wildland fire front propagation. International Journal of Wildland Fire 25: 229-241.

Bright, B.C., Hudak, A.T., Meddens, A.J, Hawbaker, T.J., Briggs, J.S., Kennedy, R.E. 2017. Prediction of forest canopy and surface fuels from lidar and satellite time series data in a bark beetle-affected forest. Forests 8: 322.

Bright, B.C., Loudermilk, E.L., Pokswinski, S.M., Hudak, A.T., O'Brien, J.J. 2016. Introducing close-range photogrammetry for characterizing forest understory plant diversity and surface fuel structure at fine scales. Canadian Journal of Remote Sensing 42: 460-472.

Brown, J.K. and Bevins, C.D. 1986. Surface fuel loadings and predicted fire behavior for vegetation types in the northern Rocky Mountains. USDA Forest Service, Intermountain Research Station, Research Note INT-358,

Calders, K., Adams, J., Armston, J., Bartholomeus, H., Bauwens, S., Bentley, L.P., Chave, J., Danson, F.M., Demol, M., Disney, M., Gaulton, R., Krishna Moorthy, S.M., Levick, S.R., Saarinen, N., Schaaf, C., Stovall, A., Terryn, L., Wilkes, P., Verbeeck, H., 2020. Terrestrial laser scanning in forest ecology: Expanding the horizon. Remote Sens. Environ. 251: 112102.

Calders, K., Newnham, G., Burt, A., Murphy, S., Raumonen, P., Herold, M., Culvenor, D., Avitabile, V., Disney, M., Armston, J., Kaasalainen, M., 2015. Nondestructive estimates of above-ground biomass using terrestrial laser scanning. Methods in Ecology and Evolution 6: 198-208.

Calders, K., Origo, N., Burt, A., Disney, M., Nightingale, J., Raumonen, P., Åkerblom, M., Malhi, Y., Lewis, P. 2018. Realistic forest stand reconstruction from terrestrial LiDAR for radiative transfer modelling. Remote Sensing 10: 933.

Chave, J., Andalo, C., Brown, S., Cairns, M.A., Chambers, J.Q., Eamus, D., Fölster, H., Fromard, F., Higuchi, N., Kira, T., Lescure, J.-P., Nelson, B.W., Ogawa, H., Puig, H., Riéra, B., Yamakura, T. 2005. Tree allometry and improved estimation of carbon stocks and balance in tropical forests. Oecologia 145, 87–99. https://doi.org/10.1007/s00442-005-0100-x

Cova, G., Rowell, E., Prichard, S.J. 2023. Evaluating close-range photogrammetry for 3D understory fuel characterization and biomass prediction in pine forests. Remote Sensing 15:4837.

Cooper, S.D., Roy, D.P., Schaaf, C.B., Paynter, I. 2017. Examination of the potential of terrestrial laser scanning and structure-from-motion photogrammetry for rapid nondestructive field measurement of grass biomass. Remote Sensing 9: 531.

Danson, F.M., Gaulton, R., Armitage, R.P., Disney, M., Gunawan, O., Lewis, P., Pearson, G., Ramirez, A.F., 2014. Developing a dual-wavelength full-waveform terrestrial laser scanner to characterize forest canopy structure. Agric. For. Meteorol. 198, 7–14.

Di Biase, V., Hanssen, R.F., Vos, S.E., 2021. Sensitivity of near-infrared permanent laser scanning intensity for retrieving soil moisture on a coastal beach: calibration procedure using in situ Data. Remote Sensing 13: 1645

DiMario, A.A., Kane, J.M., Jules, E.S. 2018. Characterizing forest floor fuels surrounding large sugar pine (*Pinus lambertiana*) in the Klamath Mountains, California. Northwest Science 92: 181–90.

Disney, M. I., Boni Vicari, M., Burt, A., Calders, K., Lewis, S. L., Raumonen, P., & Wilkes, P. 2018. Weighing trees with lasers: Advances, challenges and opportunities. Interface Focus 8: 20170048.

Dickman, L.T., Jonko, A.K., Linn, R.R., et al. 2022. Tansley review: Integrating plant physiology into simulation of fire behavior and efffects. New Phytologist 238: 952-970.

Donager, J.J., Sánchez Meador, A.J., Blackburn, R.C. 2021. Adjudicating perspectives on forest structure: how do airborne, terrestrial, and mobile lidar-derived estimates compare? Remote Sensing 13(12): 2297.

Elsherif, A., Gaulton, R., Shenkin, A., Malhi, Y., Mills, J., 2019. Three dimensional mapping of forest canopy equivalent water thickness using dual-wavelength terrestrial laser scanning. Agriculture and Forest Meteorology 276: 107627.

Falk, D., Miller, C., McKenzie, D., Black, A. 2007 Cross-scale analysis of fire regimes. Ecosystems 10: 809-823.

Finney, M.A., Cohen, J.D., Grenfell, I.C., and Yedinak, K.M. 2010. An examination of fire spread thresholds in discontinuous fuel beds. International Journal of Wildland Fire 19: 163-170.

Finney, M.A., McAllister, S.S., Grumstrup, T.P., Forthofer, J.M. 2021. Wildland Fire Behavior: dynamics, principles and processes. CSIRO Publishing, Australia.

Furman, J. 2018. Next generation fire modeling for advanced wildland fire training. Fire Management Today 78: 48-53.

Gabrielson, A.T., Larson, A.J., Lutz, J.A., Reardon, J.J. 2012. Biomass and burning characteristics of sugar pine cones. Fire Ecology 8: 58-70.

Gale, M.G., Cary, G.J., Van Dijk, A.I.J.M., Yebra, M. 2021. Forest fire fuel through the lens of remote sensing: review of approaches, challenges and future directions in the remote sensing of Biotic determinants of fire behaviour. Remote Sensing of Environment 255: 112282.

Gaulton, R., Danson, F.M., Ramirez, F.A., Gunawan, O. 2013. The potential of dual-wavelength laser scanning for estimating vegetation moisture content. Remote Sensing of the Environment 132: 32–39

Greaves, H.E., Vierling, L.A., Eitel, J.U.H., Boelman, N.T., Magney, T.S., Prager, C.M., Griffin, K.L. 2015. Estimating aboveground biomass and leaf area of low-stature Arctic shrubs with terrestrial LiDAR. Remote Sensing of Environment 164: 26-35.

Greaves, H.E., Vierling, L.A., Eitel, J.U.H., Boelman, N.T., Magney, T.S., Prager, C.M., Griffin, K.L. 2017. Applying terrestrial lidar for evaluation and calibration of airborne lidar-derived shrub biomass estimates in Arctic tundra. Remote Sensing Letters 8: 175-184.

Hancock, S., Gaulton, R., Danson, F.M. 2017. Angular reflectance of leaves with a dual-wavelength terrestrial lidar and its implications for leaf-bark separation and leaf moisture estimation. IEEE Transactions on Geoscience and Remote Sensing 55: 3084–3090.

Hawley, C.M., Loudermilk, E.L., Rowell, E.M., Pokswinski, S. 2018. A novel approach to fuel biomass sampling for 3D fuel characterization. MethodsX 5: 1597–1604.

Heinsch, F.A. and Andrews, P.L. 2010. BehavePlus fire modeling system, version 5.0: design and features. GTR-RMRS-249. USDA Forest Service Rocky Mountain Research Station, Fort Collins, CO.

Hiers, J. K., O'Brien, J.J., Will, R.E., Mitchell, R.J. 2007. Forest floor depth mediates understory vigor in xeric *Pinus palustris* ecosystems. Ecological Applications 17: 806-814.

Hiers, J.K., O'Brien, J.J., Mitchell, R.J., Grego, J.M., Loudermilk, E.L. 2009. The wildland fuel cell concept: an approach to characterize fine-scale variation in fuels and fire in frequently burned longleaf pine forests. International Journal of Wildland Fire 18: 315-325.

Hiers, J.K., O'Brien, J.J., Varner, J.M., Butler, B.W., et al. 2020. Prescribed fire science: the case for a refined research agenda. Fire Ecology 16: 11.

Hiers, J.K., O'Brien, J.J., Mitchell, R.J., Grego, J.M., Loudermilk, E.L. 2009. The wildland fuel cell concept: an approach to characterize fine-scale variation in fuels and fire in frequently burned longleaf pine forests. International Journal of Wildland Fire 18: 315-325.

Hille, M.G., and Stephens, S.L. 2005. Mixed conifer forest duff consumption during prescribed fires: tree crown impacts. Forest Science 51: 417–424.

Hoffman, C.M., Linn, R., Parsons, R., Sieg, C., Winterkamp, J. 2015. Modeling spatial and temporal dynamics of wind flow and potential fire behavior following a mountain pine beetle outbreak in a lodgepole pine forest. Agricultural and Forest Meteorology 204: 79-93.

Hoffman, C.M., Sieg, C.H., Linn, R., Mell, W., Parsons, R.A., Ziegler, J.P., Hiers, J.K. 2018. Advancing the science of wildland fire dynamics using process-based models. Fire 1:32.

Hood, S.M., Crotteau, J.S., Cleveland C.C. 2024. Long-term efficacy of fuel reduction and restoration treatments in Northern Rockies dry forests. Ecological Applications: e2940.

Hosoi, F. and Omasa, K. 2012. Estimation of vertical plant area density profiles in a rice canopy at different growth stages by high-resolution portable scanning LIDAR with a lightweight mirror. ISPRS Journal of Photogrammetry and Remote Sensing 74: 11-19.

Hudak, A.T., Kato, A. Bright, B.C., Loudermilk, E.L., Ottmar, R.D., Hawley, C., Prichard, S.J., Rowell, E.M., Restaino, J., Axe, T., Hayakawa, Y. 2020. Towards spatially explicit estimation of pre- and post-fire fuels and fuel consumption from traditional and point cloud measurements. Journal of Forestry 66: 428-442.

Hutchings, G., Gattiker, J., Scherting, B., and Linn, R.R. 2024. Wildland fire mid-story: A generative modeling approach for representative fuels. Environmental Modelling & Software 171: 105877.

Janoutová, R., Homolová, L., Novotný, J., Navrátilová, B., Pikl, M., Malenovský, Z. 2021. Detailed reconstruction of trees from terrestrial laser scans for remote sensing and radiative transfer modelling applications. In Silico Plants 3: diab026.

Jin, J., De Sloover, L., Verbeurgt, J., Stal, C., Deruyter, G., Montreuil, A.-L., De Maeyer, P., De Wulf, A., 2020. Measuring surface moisture on a sandy beach based on corrected intensity data of a mobile terrestrial LiDAR. Remote Sensing 12: 209.

Junttila, S., Vastaranta, M., Liang, X., Kaartinen, H., Kukko, A., Kaasalainen, S., Holopainen, M., Hyyppä, H., Hyyppä, J. 2017. Measuring leaf water content with dual-wavelength intensity data from terrestrial laser scanners. Remote Sensing 9: 8.

Keane, R.E. 2015. Wildland Fuel Fundamentals and Applications. Springer.

Keane, R.E., Herynk, J.M., Toney, C., Urbanski, S.P., Lutes, D.C., Ottmar, R.D. 2013. Evaluating the performance and mapping of three fuel classification systems using Forest Inventory and Analysis surface fuel measurements. Forest Ecology and Management 305: 248-263.

Kreye, J.K., J.M. Varner, and C.J. Dugaw. 2014. Spatial and temporal variability of forest floor duff characteristics in long-unburned *Pinus palustris* forests." Canadian Journal of Forest Research 44: 1477–86.

Liang, X., Kankare, V., Hyyppa, J., et al. 2016. Terrestrial laser scanning in forest inventories. ISPRS Journal of Photogrammetry and Remote Sensing 115: 63-77.

Linn, R., Reisner, J., Coleman, J.J., Winterkamp, J. 2002. Studying wildfire behavior using FIRETEC. International Journal of Wildland Fire 11: 233-246.

Linn, R.R. and Cunningham, P. 2005. Numerical simulations of grass fires using a coupled atmosphere-fire model: basic fire behavior and dependence on wind speed. Journal of Geophysical Research: Atmospheres 110 (D13).

Linn, R.R., Goodrick, S.L., Brambilla, S.L., Brown, S. M.J., Middleton, R.S., O'Brien, J.J., Hiers, J.K. 2020. QUIC-fire: a fast-running simulation tool for prescribed fire planning. Environmental Modelling and Software 125: 104616.

Linn R.R., Winterkamp J., Colman J.J., Edminster C., Bailey J.D. 2005. Modeling interactions between fire and atmosphere in discrete element fuel beds. International Journal of Wildland Fire 14: 37-48.

Loudermilk, E.L., Achtemeier, G.L., O'Brien, J.J., Hiers, J.K., Hornsby, B.S. 2014. High-resolution observations of combustion in heterogeneous surface fuels. International Journal of Wildland Fire 23: 1016-1026.

Loudermilk, E.L., Hiers, J.K., O'Brien, J., Mitchell, R.J., Singhania, A., Fernandez, J.C., Cropper, W.P. Jr., Slatton, K.C. 2009. Ground-based LIDAR: a novel approach to quantify fine-scale fuelbed characteristics. International Journal of Wildland Fire 18: 676-685.

Loudermilk, E.L., O'Brien, J.J., Goodrick, S.L., Linn, R.R., Skowronski, N.S., Hiers, J.K. 2022. Vegetation's influence on fire behavior goes beyond just being fuel. Fire Ecology 18: 1–10.

Loudermilk, E.L., Pokswinski, S., Hawley, C.M., Maxwell, A., Gallagher, MR., Skowronski, N.S., Hudak, A.T., Hoffman, C., Hiers, J.K. 2023. Terrestrial laser scan metrics predict surface vegetation biomass and consumption in a frequently burned southeastern US ecosystem. Fire 6: 151.

Maxwell, A., Gallagher, M.R., Minicuci, N., and Bester, M. 2023. Impact of reference data sampling density for estimating plot-level average shrub heights using terrestrial laser scanning data. Fire 6:98.

Marcozzi, A.A., Johnson, J.V., Parsons, R.A., Flanary, S.J., Seielstad, C.A. and Downs, J.Z. 2023. Fire 6, 394.
Mell W., Jenkins M.A., Gould J., Cheney P. 2007. A physics-based approach to modeling grassland fires. International Journal of Wildland Fire 16: 1-22.
Mitchell, R.J., Hiers, J.K., O'Brien, J.J., Jack, S.B., Engstrom, R.T. 2006. Silviculture that sustains: the nexus between silviculture, frequent prescribed fire, and conservation of biodiversity in longleaf pine forests of the southeastern United States. Canadian Journal of Forest Research 36: 2724-2736.
Mueller, E.V., Skowronski, N.S., Clark, K.L., Gallagher, M.R., Mell, W.E., Simeoni, A., Hadden, R.M. 2021. Detailed physical modeling of wildland fire dynamics at field scale-An experimentally informed evaluation. Fire Safety Journal 120:103051.
Mueller, E., Mell, W., Simeoni, A. 2014. Large eddy simulation of forest canopy flow for wildland fuel modeling. Canadian Journal of Forest Research 44: 1534-1544.
O'Brien, J., Hiers, J., Varner, J., Hoffman, C., Dickinson, M., Michaletz, S., Loudermilk, E., Butler, B. 2018. Advances in mechanistic approaches to quantifying biophysical fire effects. Current Forestry Reports 4: 161–177.
Olsoy P., Glenn N., Clark P., Derryberry D. 2014. Aboveground total and green biomass of dryland shrub derived from terrestrial laser scanning. Journal of Photogrammetry and Remote Sensing 88: 166-173.
Ottmar R.D., Sandberg D.V., Riccardi C.L., Prichard S.J. 2007. An overview of the Fuel Characteristic Classification System – quantifying, classifying and creating fuelbeds for resource planning. Canadian Journal of Forest Research 37: 2383–2393.
Parsons, R., Mell, W.E., McCauley, P. 2011. Linking 3D spatial models of fuels and fire: effects of spatial heterogeneity on fire behavior. Ecological Modelling 222: 679-691.
Parsons, R.A., Pimont, F., Wells, L., Cohn, G., Jolly, W.M., de Coligny, F., Rigolot, E., Dupuy, J-L., Mell, W., Linn, R.R. 2018. Modeling thinning effects on fire with STANDFIRE. Annals of Forest Science 75: 1-11
Parsons, R.A., Wells, L., Pimont, F., Jolly, M., Linn, R., Mell, W. 2017. STANDFIRE: an IFT-DSS module for spatially explicit 3D fuel treatment analysis. Joint Fire Science Program Final Report Project 12-1-03-30. https://www.firescience.gov/projects/12-1-03-30/project/12-1-03-30_final_report.pdf.
Piermattei, L., Karel, W., Wang, D., Wieser, M., Mokroš, M., Surový, P., Hollaus, M. 2019. Terrestrial structure from motion photogrammetry for deriving forest inventory data. Remote Sensing 11: 950.
Pimont, F., Dupuy, J.-L., Linn, R.R., Dupont, S. 2011. Impact of tree canopy structure on wind-flows and fire propagation simulated with FIRETEC. Annals Forest Science 68: 523-530.
Pimont, F., Parsons, R., Rigolot, E., De Coligny, F.R., Dupuy, J.-L. Dreyfus, P., Linn, R. 2016. Modeling fuels and fire effects in 3D: model description and applications. Environmental Modelling and Software 80: 225-240.
Ponomarev, O.A., Zakir'ianov, F.K., Terpugov, E.L., Fesenko, E.E., 2001. Absorption of infrared radiation by a thin water layer. Biofizika 46, 402–407.
Prichard, S.J., Keane, R., Rowell, E., Hudak, A., Loudermilk, E.A., et al. 2022. US Forest Service National Smoke Assessment: Fuels and Consumption. Springer.
Prichard, S.J., Kennedy, M.C., Andreu, A.G., Eagle, P.C., French, N.H., Billmire, M. 2019a. Next-generation biomass mapping for regional emissions and carbon inventories: incorporating uncertainty in wildland fuel characterization. Journal of Geophysical Research: Biogeosciences 124: 3699-3716.

Prichard, S., Larkin, N.S., Ottmar, R., French, N.H. Prichard, S., Larkin, N.S., Ottmar, R., French, N.H.F., Baker, K., Brown, T., Clements, C., Dickinson, M., Hudak, A., Kochanski, A., Linn, R., Liu, Y., Potter, B., Mell, W., Tanzer, D., Urbanski, S., Watts, A. 2019b. The Fire and Smoke Model Evaluation Experiment—A Plan for Integrated, Large Fire–Atmosphere Field Campaigns. Atmosphere: 10: 66.

Raj, T., Hashim, F.H., Huddin, A.B., Ibrahim, M.F., Hussain, A. 2020. A survey on LiDAR scanning mechanisms. Electronics 9: 741.

Raumonen, P., Kaasalainen, M., Åkerblom, M., Kaasalainen, S., Kaartinen, H., Vastaranta, M., Holopainen, M., Disney, M., Lewis, P. 2013. Fast automatic precision tree models from Terrestrial Laser Scanner Data. Remote Sensing 5: 491–520

Raumonen, P. and Åkerblom, M. 2022. InverseTampere/TreeQSM: Version 2.4.1 (2.4.1). Zenodo. https://doi.org/10.5281/zenodo.6539580

Ritter, S.M., Hoffman, C.M., Battaglia, M.A., Stevens-Rumann, C.S., Mell, W.E. 2020. Fine-scale fire patterns mediate forest structure in frequent-fire ecosystems. 11: e03177

Rocha K.D., Silva C.A., Cosenza D.N., Mohan M., Klauberg C., Schlickmann M.B., Xia J., Leite R.V., Almeida D.R., Atkins J.W., et al. 2023. Crown-level structure and fuel load characterization from airborne and terrestrial laser scanning in a longleaf pine (*Pinus palustris* Mill.) forest ecosystem. Remote Sensing 15:1002.

Rothermel, R.C. 1972. A mathematical model for predicting fire spread in wildland fuels. Res. Pap. INT-115. Ogden, UT: U.S. Department of Agriculture, Forest Service, Intermountain Forest and Range Experiment Station. 40 p.

Ross, C.W., Loudermilk L., O'Brien, J.J., Flanagan, S.A., McDaniel, J., Aubrey, D.P., Lowe, T., Hiers, J.K., Skowronski, N.S. Lidar-derived estimates of forest structure in response to fire frequency. Fire Ecology 20: 44.

Rowell, E. 2017. Virtualization of fuelbeds: building the next generation of fuels data for multiple-scale fire modeling and ecological analysis. Doctoral Dissertation, University of Montana.

Rowell, E., Loudermilk, E.L., Hawley, C., Pokwinski, S., Seielstad, Queen, L., O'Brien, J.J., Hudak, A.T., Goodrick, S., Hiers, J.K. 2020. Coupling terrestrial laser scanning with 3D fuel biomass sampling for advancing wildland fuels characterization. Forest Ecology and Management 462: 117945.

Rowell, E., Loudermilk, E.L., Seielstad, C., O'Brien, J.J. 2016. Using simulated 3D surface fuelbeds and terrestrial laser scan data to develop inputs to fire behavior models. Canadian Journal of Remote Sensing 00: 1-17.

Rowell, E., Prichard, S.J., Varner, M.J. and Shearman, T.M. 2022. Re-envisioning fire and vegetation feedbacks. In: S. Goodrick and K. Speer Wildland Fire Dynamics. Cambridge Univ. Press.

Rowell, E.M., Seielstad, C.A., Ottmar, R.D., 2015. Development and validation of fuel height models for terrestrial lidar–RxCADRE 2012. International Journal of Wildland Fire 25: 38–47.

Sánchez-López, N., Hudak, A.T., Boschetti, L., Silva, C.A., Bright, B.C., Loudermilk E.L. 2023. A spatially explicit model of litter accumulation in fire maintained longleaf pine forest ecosystems of the southeastern USA. In Viegas, D.X. and Ribeiro, L.M (eds) Advances in Forest Fire Research 2022, CiTUA. pp 1383-1389.

Sandberg, D.V., Riccardi, C.L., Schaaf, M.D. 2007. Reformulation of Rothermel's wildland fire behavior model for heterogeneous fuelbeds. Canadian Journal of Forest Research 37: 2438-2455.

Scott, J.H. and Burgan, R.E. 2005. Standard fire behavior fuel models: a comprehensive set for use with Rothermel's surface fire spread model. GTR-RMRS-153. USDA Forest Service Rocky Mountain Research Station, Fort Collins, CO.

Skowronski, N.S., Clark, K.L., Duveneck, M. 2011. Three-dimensional canopy fuel loading predicted using upward and downward sensing LiDAR systems. Remote Sensing of Environment 115: 703-714.

Silva, C.A., Hudak, A.T., Vierling, L.A., Loudermilk, E.L., O'Brien, J.J., Hiers, J.K., Jack, S.B., Gonzalez-Benecke, C., Lee, H., Falkowski, M.J., Khosravipour, A. 2016. Imputation of individual longleaf pine (*Pinus palustris* Mill.) tree attributes from field and LiDAR data. Canadian Journal of Remote Sensing 42: 554-573.

Silva, C.A., Hudak, A.T., Vierlin, L.A., Valbuena, R. et al. 2021. TreeTop: a shiny-based application for extracting forest information from LiDAR data for ecologists and conservationists. Methods in Ecology and Evolution. https://doi.org/10.1111/2041-210X.13830.

Suchocki, C. and Katzer, J., 2018. Terrestrial laser scanning harnessed for moisture detection in building materials – Problems and limitations. Automation in Construction 94: 127–134.

Urbanski, S. 2014. Wildland fire emissions, carbon, and climate: emissions factors. Forest Ecology and Management 317: 51-60.

US Department of Defense. 2014. SERDP Fire Science Strategy. US Department of Defense Strategic Environmental Research and Development Program Resource Conservation and Climate Change Division. https://climateandsecurity.org/wp-content/uploads/2020/01/serdp_fire-science-strategy.pdf

Van Wagner, C.E. 1977. Conditions for the start and spread of crown fire. Canadian Journal of Forest Research 7: 23-34.

Varner, J.M., Gordon, D.R., Putz, F.E., Hiers, J.K. 2005. Restoring fire to long-unburned Pinus palustris ecosystems: novel fire effects and consequences for long-unburned ecosystems. Restoration Ecology 13: 536-544.

Varner, J.M., Hiers, J.K., Ottmar, R.D., Gordon, D.R., Putz, F.E., Wade,, D.D. 2007. Overstory tree mortality resulting from reintroducing fire to long-unburned longleaf pine forests: the importance of duff moisture. Canadian Journal of Forest Research 37: 1349-1358.

Varner, J.M., Kane, J.M., Kreye, J.K., Engber, E. 2015. The flammability of forest and woodland litter: a synthesis. Current Forestry Reports 1: 91-99.

Wallace, L, Gupta, V., Reinke, K., and Jones, S. 2016. An assessment of pre- and post-fire near surface fuel hazard in an Australian dry sclerophyll forest using point cloud data captured using a terrestrial laser scanner. Remote Sensing 8:679.

Wallace, L., Hillman, S., Reinke, K., Hally, B., 2017. Non-destructive estimation of above-ground surface and near-surface biomass using 3D terrestrial remote sensing techniques. Methods in Ecology and Evolution 8: 1607–1616.

Wallace, L., Hillman, S., Hally, B., Taneja, R., White, A., McGlade, J. 2022. Terrestrial laser scanning: An operational tool for fuel hazard mapping? Fire 5: 85.

Wallace, L., Lucieer, A., Watson, C.S. 2014. Evaluating tree detection and segmentation routines on very high resolution UAV LiDAR data. IEEE Transactions on Geoscience and Remote Sensing 52: 7619-7628.

Wang, D., Momo Takoudjou, S., & Casella, E. 2020. LeWoS: A universal leaf-wood classification method to facilitate the 3D modelling of large tropical trees using terrestrial LiDAR. Methods in Ecology and Evolution 11: 376–389.

Werth, P.A., Potter, B.E., Clements, C.B., Finney, M.A., Goodrick, S.L., Alexander, M.E., Cruz, M.G., Forthofer, J.A., McAllister, S.S. 2011. Synthesis of knowledge of extreme fire behavior: volume I for fire managers. PNW-GTR-854. USDA Forest Service Pacific Northwest Research Station, Portland, OR.

Yedinak, K.M., Strand, E.K., Hiers, J.K., and Varner, J.M. 2018. Embracing complexity to advance the science of wildland fire behavior. Fire 1:20.

Zahiri, Z., Laefer, D.F., Gowen, A. 2021. Characterizing building materials using multispectral imagery and LiDAR intensity data. Journal of Building Engineering 44: 102603.

APPENDIX A: SUPPORTING DATA

A1 ARCGIS ONLINE WEBSITE

Geospatial records of 3D Fuels unit, 5x5 m plot and voxel plot locations are archived on this ArcGIS online site. Once all 3D Fuels datasets are available on the WFSI repository, we will update this site to link to publicly available datasets.

A2 INTRINSIC FUEL PROPERTIES LIBRARY

The intrinsic fuel property is an online repository of physical properties of wildland fuels, organized in two tabs (https://depts.washington.edu/fera/3dfuels/ifpl/). Fuel layer properties include properties of wildland fuelbed layers such as bulk density and depth of litter and duff layers or the packing ratio and porosity of shrub or canopy fuels. Fuel particle properties include the intrinsic fuel properties of individual fuel particles such as leaves, needles, wood particles, and tree cones.

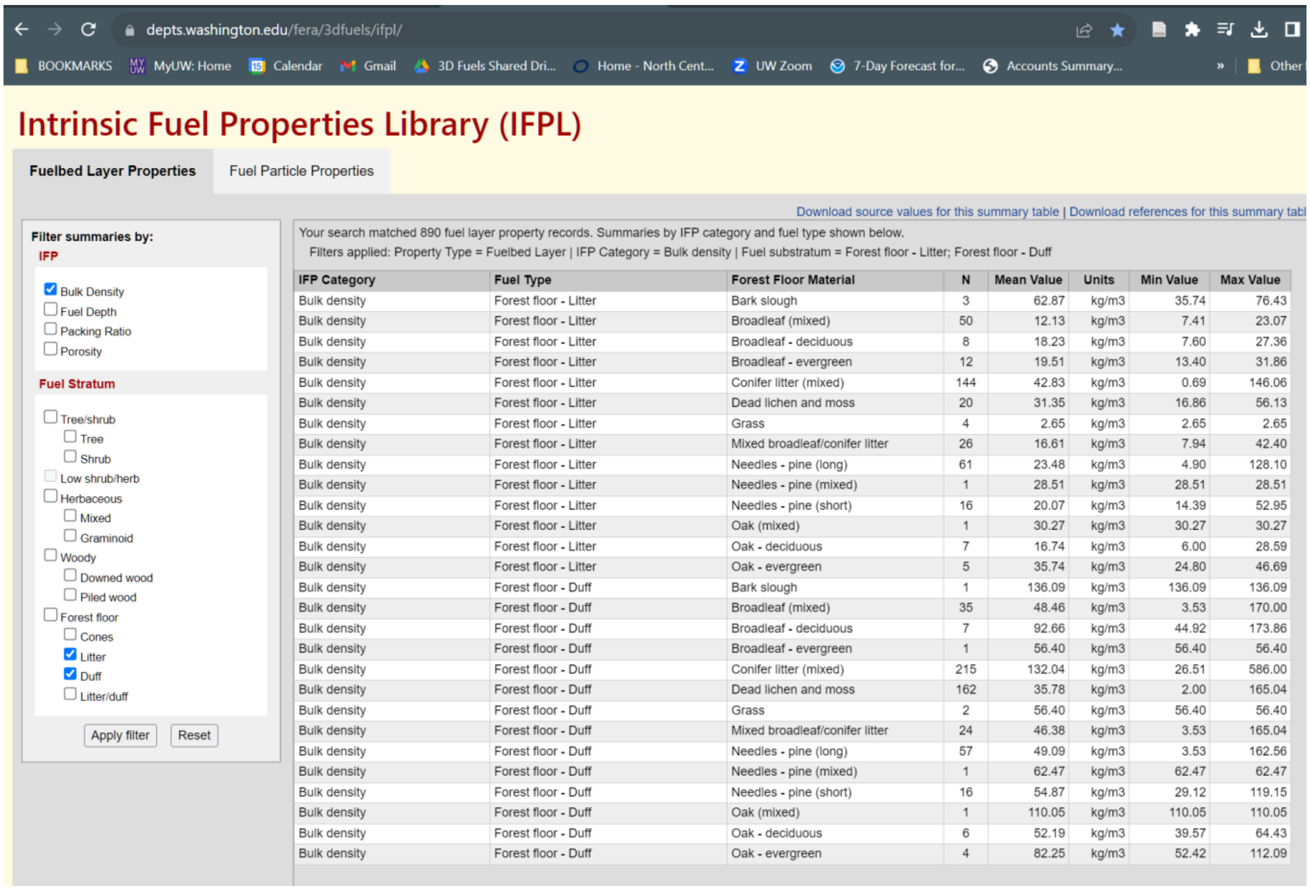

IFP Category	Fuel Type	Forest Floor Material	N	Mean Value	Units	Min Value	Max Value
Bulk density	Forest floor - Litter	Bark slough	3	62.87	kg/m3	35.74	76.43
Bulk density	Forest floor - Litter	Broadleaf (mixed)	50	12.13	kg/m3	7.41	23.07
Bulk density	Forest floor - Litter	Broadleaf - deciduous	8	18.23	kg/m3	7.60	27.36
Bulk density	Forest floor - Litter	Broadleaf - evergreen	12	19.51	kg/m3	13.40	31.86
Bulk density	Forest floor - Litter	Conifer litter (mixed)	144	42.83	kg/m3	0.69	146.06
Bulk density	Forest floor - Litter	Dead lichen and moss	20	31.35	kg/m3	16.86	56.13
Bulk density	Forest floor - Litter	Grass	4	2.65	kg/m3	2.65	2.65
Bulk density	Forest floor - Litter	Mixed broadleaf/conifer litter	26	16.61	kg/m3	7.94	42.40
Bulk density	Forest floor - Litter	Needles - pine (long)	61	23.48	kg/m3	4.90	128.10
Bulk density	Forest floor - Litter	Needles - pine (mixed)	1	28.51	kg/m3	28.51	28.51
Bulk density	Forest floor - Litter	Needles - pine (short)	16	20.07	kg/m3	14.39	52.95
Bulk density	Forest floor - Litter	Oak (mixed)	1	30.27	kg/m3	30.27	30.27
Bulk density	Forest floor - Litter	Oak - deciduous	7	16.74	kg/m3	6.00	28.59
Bulk density	Forest floor - Litter	Oak - evergreen	5	35.74	kg/m3	24.80	46.69
Bulk density	Forest floor - Duff	Bark slough	1	136.09	kg/m3	136.09	136.09
Bulk density	Forest floor - Duff	Broadleaf (mixed)	35	48.46	kg/m3	3.53	170.00
Bulk density	Forest floor - Duff	Broadleaf - deciduous	7	92.66	kg/m3	44.92	173.86
Bulk density	Forest floor - Duff	Broadleaf - evergreen	1	56.40	kg/m3	56.40	56.40
Bulk density	Forest floor - Duff	Conifer litter (mixed)	215	132.04	kg/m3	26.51	586.00
Bulk density	Forest floor - Duff	Dead lichen and moss	162	35.78	kg/m3	2.00	165.04
Bulk density	Forest floor - Duff	Grass	2	56.40	kg/m3	56.40	56.40
Bulk density	Forest floor - Duff	Mixed broadleaf/conifer litter	24	46.38	kg/m3	3.53	165.04
Bulk density	Forest floor - Duff	Needles - pine (long)	57	49.09	kg/m3	3.53	162.56
Bulk density	Forest floor - Duff	Needles - pine (mixed)	1	62.47	kg/m3	62.47	62.47
Bulk density	Forest floor - Duff	Needles - pine (short)	16	54.87	kg/m3	29.12	119.15
Bulk density	Forest floor - Duff	Oak (mixed)	1	110.05	kg/m3	110.05	110.05
Bulk density	Forest floor - Duff	Oak - deciduous	6	52.19	kg/m3	39.57	64.43
Bulk density	Forest floor - Duff	Oak - evergreen	4	82.25	kg/m3	52.42	112.09

Figure A2.1 Sample screen of the Intrinsic Fuel Properties Library with filtered results for litter and duff bulk density values, summarized by fuel type and forest floor material. Source records can be then downloaded using the top-right link "download source values for this summary table." Source references can be downloaded using the other top-right link, "download references for this summary table."

A3. SUMMARY TABLES OF BIOMASS BY FUEL TYPE FOR EACH 3D FUEL SITE.

Table A3.1. Dry weight biomass by fuel type for SE mesic pine flatwood sites, including mean, standard deviation (SD), minimum (min) and maximum (max) values, number of plots by fuel type (N), and total per site (Total). Mean voxel plot biomass (g) for each site is listed under site name.

Unit	TSF	Fuel type	Mean	SD	Min	Max	N	Total
Tates Hell A	1-2 yr	Live shrub	27.6	20.2	9.7	73.8	17	45
Mean biomass		Standing dead shrub	5.2	5.7	0.5	25.0	32	45
278 g		Vines	1.3	1.7	0.2	4.4	6	45
		Forb	0.2		0.2	0.2	1	45
		Grass	2.1	4.8	0.0	19.6	17	45
		FWD	22.6	20.6	5.5	84.1	24	45
		Litter	74.5	34.4	23.6	143.9	14	45
		Moss/lichen	0.0		0.0	0.0	1	45
		Duff	123.2	87.1	18.5	458.5	30	45
		Other	1.7	2.7	0.0	7.5	9	45
Osceola	1-2 yr	Live shrub	16.4	8.1	0.8	31.0	29	40
Mean biomass		Standing dead shrub	5.4	4.7	0.6	18.7	22	40
363 g		Vines	0.8	0.7	0.0	2.9	28	40
		Forb	1.3	2.7	0.0	13.7	30	40
		Grass	10.1	11.4	0.1	39.2	25	40
		FWD	29.9	33.6	0.7	153.8	34	40
		Litter	152.0	63.6	54.1	280.1	24	40
		Moss/lichen	0.1	0.1	0.1	0.2	12	40
		Duff	17.6	14.9	1.2	67.1	40	40
		Other	0.2	0.2	0.0	0.6	8	40
Blackwater	2 yr	Live shrub	11.5	5.8	1.8	17.1	9	18
Mean biomass		Standing dead shrub	3.1	2.7	0.4	6.4	4	18
201 g		Vines	0.6	0.6	0.1	2.1	11	18
		Forb	4.4	5.0	0.0	13.6	11	18
		Grass	44.1	33.3	7.6	110.5	16	18
		FWD	9.8	9.7	0.3	34.2	14	18
		Litter	71.9	35.5	28.3	134.5	10	18
		Moss/lichen	0.1	0.1	0.0	0.1	3	18
		Other	0.1	0.1	0.0	0.2	3	18
Fort Stewart	2-3 yr	Live shrub	5.0	5.4	0.1	20.4	17	45
Mean biomass		Standing dead shrub	0.9	0.7	0.1	2.0	9	45
425 g		Vines	0.9	1.2	0.0	4.3	13	45
		Forb	4.5	4.3	0.1	18.8	39	45
		Grass	45.7	52.9	1.0	132.9	12	45
		FWD	32.9	57.1	0.3	335.4	41	45
		CWD	332.4	261.0	147.9	517.0	2	45
		Litter	165.6	81.8	36.0	350.0	26	45
		Moss/lichen	1.9	1.8	0.3	4.6	5	45
		Duff	150.5	139.6	1.7	400.4	10	45
		Other	0.2	0.0	0.2	0.3	2	45

Unit	TSF	Fuel type	Mean	SD	Min	Max	N	Total
Tates Hell B	2-3 yr	Live shrub	14.0	15.0	0.0	46.4	23	45
Mean biomass		Standing dead shrub	1.7	2.6	0.0	11.0	24	45
493 g		Vines	0.4	0.1	0.3	0.4	2	45
		Forb	3.5	4.0	0.0	13.4	26	45
		Grass	38.3	56.0	0.0	176.8	35	45
		FWD	42.5	43.5	0.5	187.5	33	45
		Litter	137.4	46.1	64.6	244.6	28	45
		Moss/lichen	1.0	0.8	0.0	1.8	4	45
		Duff	194.3	135.5	4.4	659.9	39	45
		Other	1.9	3.3	0.1	7.7	5	45
Aucilla	> 5 yr	Shrub	6.2	7.8	0.4	38.2	32	45
Mean biomass		Woody standing dead	17.2		17.2	17.2	1	45
336 g		Vines	1.9	3.7	0.0	18.0	32	45
		Forb	4.0	3.7	0.2	12.0	8	45
		Grass	10.0	20.0	0.0	106.4	37	45
		FWD	41.5	74.3	0.1	314.7	28	45
		Litter	160.8	77.9	39.3	357.6	32	45
		Moss/lichen	1.2	1.4	0.2	4.3	16	45
		Duff	112.3	94.1	25.9	317.4	13	45
		Other	0.9	1.4	0.0	3.4	6	45

Table A3.2. Dry weight biomass by fuel type for SE loblolly pine-sweetgum sites, including mean, standard deviation (SD), minimum (min) and maximum (max) values, number of plots by fuel type (N), and total per site (Total). Mean voxel plot biomass (g) for each site is listed under site name.

Unit	TSF	Major Category	Mean	SD	Min	Max	N	Total
Hannah Hammock	1-2 yr	Shrub	3.8	3.6	0.0	13.4	29.0	45
Mean biomass		Woody standing dead	3.5	4.2	1.1	12.1	6.0	45
286.3		Vines	14.7	14.8	0.4	64.5	42.0	45
		Forb	23.9	27.2	1.9	110.9	40.0	45
		Grass	17.2	24.1	0.1	103.1	38.0	45
		FWD	18.7	19.5	0.8	92.8	34.0	45
		Litter	67.3	30.4	12.5	160.9	28.0	45
		Duff	75.3	83.1	19.6	379.6	27.0	45
		Other	0.5	0.6	0.1	0.9	2.0	45
Hitchiti B	1-2 yr	Live Shrub	53.7	244.9	0.1	1302.2	28.0	45
Mean biomass		Shrub standing dead	5.9	4.1	0.2	16.2	18.0	45
448.3		Vines	11.7	7.4	0.2	33.0	43.0	45
		Forb	4.0	3.9	0.2	18.7	39.0	45
		Grass	12.0	15.4	0.2	64.2	30.0	45
		FWD	44.2	51.4	3.4	261.5	36.0	45
		CWD	347.2	200.3	205.6	488.8	2.0	45
		Litter	149.5	49.1	44.7	256.3	31.0	45
		Moss/lichen	0.2	0.3	0.0	0.9	15.0	45

Unit	TSF	Major Category	Mean	SD	Min	Max	N	Total
		Duff	135.5	91.3	20.4	519.1	44.0	45
		Other	0.2	0.1	0.1	0.3	7.0	45
Hitchiti A	2-3 yr	Live shrub	11.2	15.0	0.5	69.7	27.0	45
Mean biomass		Standing dead shrub	1.5	1.8	0.0	3.8	4.0	45
509.1		Vines	6.9	8.2	0.2	44.3	35.0	45
		Forb	1.9	3.6	0.1	18.4	33.0	45
		Grass	21.6	22.0	1.9	85.7	25.0	45
		FWD	47.5	60.9	4.2	270.6	35.0	45
		Litter	225.7	107.8	88.1	476.4	18.0	45
		Moss/lichen	0.2	0.1	0.0	0.3	6.0	45
		Duff	164.9	221.7	6.9	1499.2	43.0	45
		Other	1.1	2.2	0.1	7.8	11.0	45

Table A3.3. Dry weight biomass by fuel type for western ponderosa pine forest sites, including mean, standard deviation (SD), minimum (min) and maximum (max) values, number of plots by fuel type (N), and total per site (Total). Mean voxel plot biomass (g) for each site is listed under site name.

Unit		Major Category	Mean	SD	Min	Max	N	Total
Lubrecht		Live shrub	31.4	40.8	0.3	138.0	36	45
Mean biomass		Standing dead shrub	4.3	3.6	0.1	10.5	11	45
435 g		Forb	4.6	3.5	0.1	17.6	43	45
		Grass	16.5	14.0	0.3	49.6	45	45
		FWD	115.4	155.8	5.7	583.7	38	45
		CWD	62.4	87.3	0.7	124.2	2	45
		Litter	134.3	87.5	11.1	374.1	35	45
		Moss/lichen	5.9	6.8	0.1	25.3	34	45
		Duff	131.8	154.3	0.4	965.0	42	45
		Other	4.2	4.8	0.2	17.5	13	45
LANL Forest		Live shrub	3.2	2.8	0.1	7.4	10	45
Mean biomass		Standing dead shrub	21.5	17.0	3.3	46.5	5	45
500 g		Forb	1.2	2.2	0.0	8.4	17	45
		Grass	11.8	16.6	0.2	60.5	38	45
		FWD	90.5	163.9	0.6	906.0	36	45
		CWD	137.4		137.4	137.4	1	45
		Litter	197.0	216.6	7.2	1091.6	34	45
		Duff	198.8	206.7	29.0	918.8	33	45
		Other	2.4	4.0	0.0	10.6	11	45
Sycan Forest		Live shrub	2.7	3.2	0.1	8.6	12	23
Mean biomass		Standing dead shrub	2.4	2.7	0.0	6.5	5	23
682 g		Forb	0.6	0.7	0.0	2.3	19	23
		Grass	1.0	1.2	0.0	3.9	18	23
		FWD	99.9	93.2	0.4	293.5	12	23
		CWD	3669.0		3669.0	3669.0	1	23
		Litter	153.2	109.5	11.0	371.2	17	23

Unit	Major Category	Mean	SD	Min	Max	N	Total
	Moss/lichen	0.2	0.2	0.0	0.6	8	23
	Duff	286.4	249.0	7.7	828.0	15	23
	Other	4.7	10.7	0.1	28.9	7	23
Sycan Forest 2A	Live shrub	14.2	29.3	0.0	86.8	15	23
Mean biomass	Standing dead shrub	18.8	23.5	3.3	45.8	3	23
879 g	Forb	0.5	0.6	0.0	1.6	5	23
	Grass	11.3	15.0	0.2	56.1	22	23
	FWD	84.6	131.8	1.7	442.4	11	23
	CWD	241.5		241.5	241.5	1	23
	Litter	163.0	67.4	76.3	283.5	16	23
	Moss/lichen	1.8	2.4	0.0	6.9	10	23
	Duff	714.1	2022.1	64.0	9009.7	19	23
	Other	7.5	10.9	0.3	23.5	7	23
Methow	Live shrub	29.5	49.8	0.2	183.9	27	45
Mean biomass	Standing dead shrub	126.8		126.8	126.8	1	45
951 g	Forb	7.9	17.6	0.1	103.7	36	45
	Grass	33.6	58.9	0.2	307.1	35	45
	FWD	47.1	58.8	1.7	225.7	29	45
	Litter	180.8	106.5	6.4	399.4	37	45
	Moss/lichen	0.6	0.8	0.0	2.7	23	45
	Duff	719.1	446.3	76.8	1902.0	36	45
	Other	3.6	6.7	0.1	25.4	15	45

Table A3.4. Dry weight biomass by fuel type for grassland sites, including mean, standard deviation (SD), minimum (min) and maximum (max) values, number of plots by fuel type (N), and total per site (Total). Mean voxel plot biomass (g) for each site is listed under site name.

Unit	Major Category	Mean	SD	Min	Max	N	Total
Sycan Grassland	Live shrub	149.77	211.38	0.3	299.23	2	23
Mean biomass	Standing dead shrub	16.22	21.7	0.87	31.56	2	23
87 g	Forb	6.45	5.05	0.76	19.05	22	23
	Grass	33.81	22.42	7.6	102.17	18	23
	FWD	5.97	11.31	0.16	28.63	6	23
	Litter	1.81		1.81	1.81	1	23
	Moss/lichen	17.97	38.55	0.25	157.22	18	23
	Other	3.47	4.76	0.09	14.37	9	23
Glacial Heritage	Live shrub	2.25	6.47	0.01	30.29	21	45
Mean biomass	Standing dead shrub	0.86		0.86	0.86	1	45
122 g	Forb	5.79	4.8	0.07	21.85	35	45
	Grass	82.17	26.7	43.18	159.65	44	45
	FWD	5.9	6.09	0.13	31.04	41	45
	Litter	17.05	52.23	0.02	238.17	21	45
	Moss/lichen	40.12	36.07	1	154.07	40	45
	Duff	35.15	15	12.71	53.28	9	45

Unit	Major Category	Mean	SD	Min	Max	N	Total
	Other	0.3		0.3	0.3	1	45
LANL Grassland	Live shrub	15.64	27.08	0.02	111.46	25	45
Mean biomass	Standing dead shrub	2.66		2.66	2.66	1	45
305 g	Forb	12.54	12.58	0.02	58.82	44	45
	Grass	29.83	21.76	1.69	77.27	44	45
	FWD	10.57	16.62	0.03	54.78	26	45
	Litter	33.42	41.48	0.24	140.4	36	45
	Duff	141.21	68.53	85.3	226.17	4	45
	Other	1.68	4.77	0.01	21.1	20	45
Tenalquot	Live shrub	72.46	108.91	0.04	364.46	26	45
Mean biomass	Standing dead shrub	1.23	0.45	0.91	1.54	2	45
170 g	Forb	5.96	5.32	0.12	21.26	35	45
	Grass	57.55	28.98	0.04	134.44	42	45
	FWD	33.26	95.73	0.06	451.6	22	45
	Litter	50.57	87.47	0.02	368.51	28	45
	Moss/lichen	93.5	75.14	0.17	299.08	39	45
	Duff	204.47	162.05	24.74	426.4	6	45
	Other	0.55		0.55	0.55	1	45

A4. SUMMARY OF MODEL SENSITIVITY ANALYSES CONDUCTED IN COLLABORATION WITH THE SERDP-FUNDED CLOSING GAPS PROJECT (RC20-1025).

1) *Borke, E.M. 2023. Assessing the impact of parallel burnout fires on flank rate of spread. MS Thesis. University of Montana.*
   In this study, a grassland within Sycan Marsh Preserve was parameterized within the WFDS and compared to observed rates of spread from a prescribed burn in 2017 that predated our sampling campaign. Simulated rates of spread were evaluated across a range of domain sizes and mesh resolutions with voxel sizes ranging from 0.25m to 2m (**Table 1**). Within these simple grass fuels, coarser voxel sizes were sufficient to represent rates of spread.

Table A4.1. Simulated domain locations and grid resolutions, adapted from Borke 2023.

Fuel area				
# Meshes	*x*-domain	*y*-domain	*z*-domain	Voxel size
16	[0, 100]	[0, 100]	[0, 4]	0.25m
4	[-25, 125]	[-25, 125]	[4, 8]	0.5m
1	[-25, 125]	[-25, 125]	[8, 18]	1m
1	[-25, 125]	[-25, 125]	[18, 58]	2m
25-m buffer				
	x x *y* domain		z-domain	Voxel size
5	[-25, 125] x [-25, 125] \ [0, 100] x [0, 100]		[0, 4]	0.5m
Wind development area				
2	[-25, 125]	[-75, -25]	[0, 6]	0.5m
	[-25, 125]	[-75, -25]	[6, 18]	1m
	[-25, 125]	[-75, -25]	[18, 58]	2m

2) *Marcozzi, A. 2022. Sensitivity of lidar derived fuel cells to fire modeling at laboratory scales. MS Thesis. University of Montana.*

   Published as:
   Marcozzi, A.A., Johnson, J.V., Parsons, R.A., Flanary, S.J., Seielstad, C.A. and Downs, J.Z. 2023. Fire 6, 394. https://doi.org/10.3390/fire6100394.

   In this study, terrestrial laser scan datasets were represented in heterogeneous fuel cells and evaluated within WFDS. A series of laboratory experiments were conducted to burn and record mass loss rate of Engelmann spruce (*Picea engelmannii*) and ponderosa pine (*Pinus ponderosa*) seedlings under different fuel moisture and temperature environments. Tree seedlings were scanned with a Leica BLK360 Terrestrial Laser Scanner. Point clouds were processed and then represented in voxel grids across a range of grid resolutions: 2cm, 4cm, 8cm, and 16 cm. FDS simulations were conducted using an assumption of uniform fuel moisture across all burn experiments for 16 tree seedlings.

   Model simulations of mass loss rate closely corresponded to observed mass loss rates. However, TLS sampling tended to overpredict thermally thin fuels close to sapling stems and thus biased combustion towards stem centers whereas actual patterns of combustion were concentrated away from stems. Comparisons of fuel cell resolution demonstrated that the tested cell resolutions had little impact on mass loss rate but that experimental ranges of fuel moisture and dry weight biomass strongly influenced mass loss rate. Coarser cell resolutions (16cm) were sufficient to represent mass loss rate and were computationally more efficient.

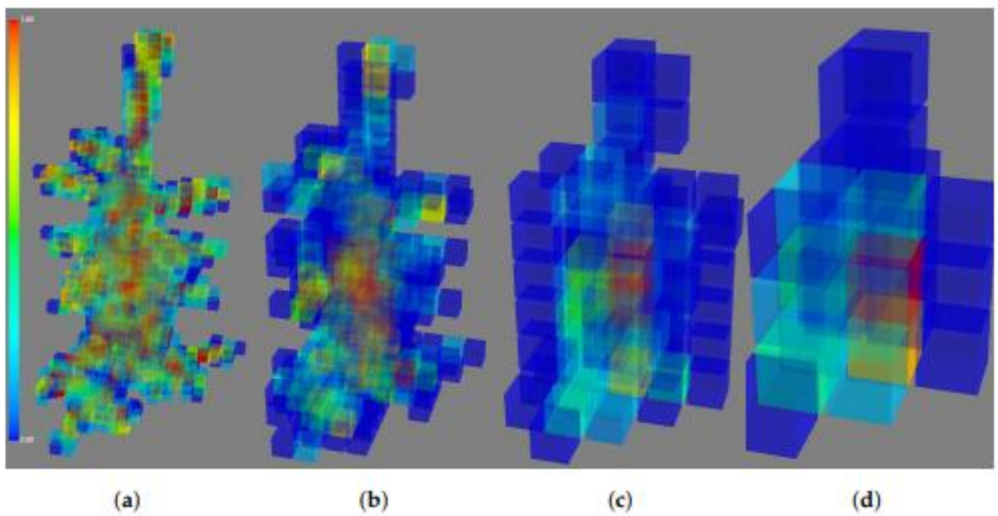

Figure A4.1. Comparison of voxelized point clouds at a) 2cm, b) 4cm, c) 8cm, and d) 16 cm resolutions. Color ramps range from 0-1 with 0 representing empty voxels and 1 representing high point cloud densities (Source: Marcozzi et al. 2023, Figure 3).

APPENDIX B: LIST OF SCIENTIFIC AND TECHNICAL PUBLICATIONS

3D Fuels Project Publications

1. Batchelor, J.L., Wilson, T.M., Olsen, M.J., Ripple, W.J. New structural complexity metrics for forests from single terrestrial lidar scans. Remote Sensing 15: 145.
2. Batchelor, J.L. 2023. Fine-scale remote sensing of forest structure and condition. PhD dissertation. University of Washington, Seattle.
3. Bester, M.S. 2022. The Burning Bush: Linking LiDAR-derived Shrub Architecture to Flammability. PhD Dissertation. West Virginia University.
4. Bester, M., McNeil, B., and Skowronski, N.S. In review. Lidar-based quantitative structure modeling of architecturally different shrubs. ASK.
5. Bester, M., McNeil, B., and Skowronski, N.S. In prep. Linking LiDAR-measured architectural traits to flammability of understory shrubs.
6. Bester, M.S., Maxwell, A.E., Gallagher, M.R., and Skowronski, N.S. 2023. Synthetic forest stands and point clouds for model selection and feature space comparison. Remote Sensing 15:4407.
7. Borke, E.M. 2023. Assessing the impact of parallel burnout fires on flank rate of spread. MS Thesis. University of Montana.
8. Batchelor, J., Rowell, E., Prichard, S., Nemans, D., Cronan, J., and Moskal, L.M. 2003. Quantifying vegetation moisture levels with terrestrial lidar scanning. Remote Sensing.
9. Cova, G., Rowell, E., Prichard, S.J. 2023. Evaluating close-range photogrammetry for 3D understory fuel characterization and biomass prediction in pine forests. Remote Sensing 15:4837.
10. Kleydson, D.R., Silva, C.A., Consenza, D.N., Mohan, M., Klauberg, C., Schlickmann, M.B., Xia, J., Leite, R.V., Almeida, D., Atkis, J.W., Cardil, A., Rowell, E., Parsons, R., Sanchez-Lopez, N., Prichard, S.J., and Hudak, A.T. 2023. Crown-level structure and fuel load characterization from airborne and terrestrial laser scanning in a longleaf pine (*Pinus palustris* Mill.) forest ecosystem. Remote Sensing 15:1002.
11. Marcozzi, A. 2022. Sensitivity of lidar derived fuel cells to fire modeling at laboratory scales. MS Thesis. University of Montana.
12. Marcozzi, A.A., Johnson, J.V., Parsons, R.A., Flanary, S.J., Seielstad, C.A. and Downs, J.Z. 2023. Fire 6, 394. https://doi.org/10.3390/fire6100394.
13. Nemens, D., Prichard, S.J.,
14. Prichard, S.J., Rowell, E., Keane, R.E, Hudak, A.T., Lutes, D, and Loudermilk, E.L. 2022. Chapter 4: Wildland fuel characterization across space and time. In: French, N., Pruett, R., Lobata, T. Fire, Smoke and Health. American Geophysical Union, Wiley Press.
15. Rocha K.D., Silva C.A., Cosenza D.N., Mohan M., Klauberg C., Schlickmann M.B., Xia J., Leite R.V., Almeida D.R., Atkins J.W., et al. 2023. Crown-level structure and fuel load characterization from airborne and terrestrial laser scanning in a longleaf pine (*Pinus palustris* Mill.) forest ecosystem. Remote Sensing 15:1002.
16. Rowell, E., Prichard, S.J., Varner, M.J. and Shearman, T.M. 2022. Re-envisioning fire and vegetation feedbacks. *In*: S. Goodrick and K. Speer Wildland Fire Dynamics. Cambridge University Press.

17. Prichard, S.J., Keane, R., Rowell, E., Hudak, A., Loudermilk, E.A., Lutes, D., Chappell, L, Hornsby, B., Hall, J., Ottmar, R.D. 2022. US Forest Service National Smoke Assessment: Fuels and Consumption. Springer.
18. Prichard, S.J., Nemens, D., Rowell, E., Hudak, A., Thoreson, J., Sanchez, N., and Eagle, P. In prep. Forest floor properties in open pine forests of the southeastern and western United States. Fire Ecology.
19. Nemens, D., Prichard, S.J., Rowell, E., Bright, B., Hudak, A., Eagle, P., Cronan, J., Skowronski, N., Loudermilk, E., Silva, C. In prep. Hierarchically scaled remote sensing and field dataset for three-dimensional wildland fuel characterization. Fire Ecology